UNIVERSITY OF CINCINNATI

Date: 31-Mar-2010

I, Joon Sub Shim **,**

hereby submit this original work as part of the requirements for the degree of:

Doctor of Philosophy

in Electrical Engineering

It is entitled:

Self-Assembled Carbon Nanotube as an Optical Immunosensor for Point-of-Care Clinical Diagnostics

Student Signature: Joon Sub Shim

This work and its defense approved by:

Committee Chair: Chong Ahn, PhD
Chong Ahn, PhD

Vesselin Shanov, PhD
Vesselin Shanov, PhD

Marc Cahay, PhD
Marc Cahay, PhD

Mark Schulz, PhD
Mark Schulz, PhD

Jason Heikenfeld, PhD
Jason Heikenfeld, PhD

Self-Assembled Carbon Nanotube as an Optical Immunosensor for Point-of-Care Clinical Diagnostics

A dissertation submitted to the

Graduate School
of the University of Cincinnati

In partial fulfillment of the
Requirements for the degree of

DOCTOR OF PHILOSOPHY

In the Department of Electrical and Computer Engineering
of the College of Engineering

By

Joon Sub Shim

B.S., Double Major (Department of Mechanical Engineering
& Department of Electrical Engineering),
Korea Advanced Institute of Science & Technology, Korea, 2004

Committee Chairman
Dr. Chong H. Ahn

Committee Members
Dr. Marc Cahay
Dr. Jason Heikenfeld
Dr. Vesselin Shanov
Dr. Mark J. Schulz

ABSTRACT

In this research, a new method for the self-assembly of carbon nanotubes (CNTs) using magnetic capturing and fluidic alignment has been developed and characterized. In this new method, the residual iron (Fe) catalyst at one end of the CNT was utilized as a self-assembly driver to attract and locate the CNT using magnetic forces, while the assembled CNT was aligned by the shear force induced from the fluid flow through the assembly channel. The self-assembly principles and procedures were successfully developed and the electrical properties of the assembled multi-walled carbon nanotube (MWNT) and single-walled carbon nanotube (SWNT) were fully characterized. The new assembly method developed in this work shows its feasibility for the precise self-assembly of parallel CNTs for electronic devices and nano-biosensors.

In order to prepare the electrodes for the assembly of CNTs, a self-aligned nano-scale gap between multiple metal layers has been fabricated using a technique of controlled undercut and metallization and has been applied to the massive assembly of the individual CNT. The new method enables conventional optical lithography to fabricate nanogap electrodes and self-aligned patterns with nano-scale precision. The self-aligned Ni pattern on the nanogap electrode provides an assembly spot where the residual Fe catalyst at the end of the CNT is magnetically captured. The captured CNT is aligned parallel to the flow direction by fluidic shear force. The combined forces of magnetic attraction and fluidic alignment achieve the massive self-assembly of CNTs at target positions. Single walled nanotubes (SWNTs) were successfully assembled between the nanogap electrodes and their electrical responses were fully characterized, showing stable current-voltage (I-V) responses.

As an application of the CNT-assembled electrode to a functional device, an on-chip optical immunosensor using CNTs with a photovoltaic polymer coating has been proposed, developed, characterized and applied for the detection of a cardiac biomarker in this work. An individual CNT was assembled on a titanium (Ti) electrode and coated with a photovoltaic polymer, and then insulated with Parylene. Under an incident light, the photovoltaic polymer generated electrons that changed the conductivity of the CNT. The on-chip chemiluminescent immunoassay was directly performed on the CNT photodetector for the detection of Cardiac Troponin T (cTnT) with a concentration of 12 pg/ml, which envisaged a new optical immunosensor using the self-assembled CNT for point-of-care (POC) clinical diagnostics.

In conclusion, a new self-assembly of CNTs using magnetic capturing and fluidic alignment has been designed, developed and characterized in this work for addressing the difficulty of CNT assembly at the target position between two electrodes with a nanogap. The electrodes with a nanogap were also newly developed using a technique of controlled undercut and metallization and then fully characterized as assembly beds for the self-assembled CNT. Finally, the new assembly methods and devices have been successfully applied to the new optical immunosensor with high sensitivity for POC clinical diagnostics.

ACKNOWLEDGMENT

Above all, I would like to express all my thanks to the Lord God, my heavenly father. He encouraged me when I was frustrated, showed me a direction when I lost my way, empowered me to overcome every difficulty, gave me wisdom to solve the problems, and blessed me to achieve my goals of research until this moment. During my Ph. D. study, I have come to understand the true meaning of his word: “The fear of the Lord is the beginning of wisdom, and knowledge of the Holy One is understanding. (Proverbs 9:10)”

I want to express my sincere appreciation to my advisor, Dr. Chong Ahn. He gave me valuable lessons throughout my study toward Ph. D. degree. He guided me to grab the right direction to achieve my final goals, discussed problems with valuable comments, and supported all the materials for my experiments. Furthermore, he inspired me to become a better person as well as an excellent researcher. As a faithful Christian, his energetic activity with a ceaseless passion impressed me to have a strong desire to become a successful person like him, serving and truly loving the God and neighbors. He will be my mentor and role-model during my life time.

Also, I would like to thank my committee members, Dr. Mark Schulz, Dr. Vesselin Shanov, Dr. Marc Cahay, Dr. Jason Heikenfeld. They gave me valuable comments and guidance to finish my dissertation. Because of their efforts, my dissertation was improved a lot. Especially, I would like to give my special thanks to Dr. Mark Schulz and Dr. Vesselin Shanov for their generous supply of high-quality carbon nanotubes. Their support allows me to testify my rough idea and to finally accomplish my Ph. D. study.

Additionally, I wish to appreciate many people who enable me to accomplish this work. First, I would like to thank Dr. Yeo-Heung Yun for his wonderful collaboration and valuable discussions. He synthesized carbon nanotube for my researches and gave me helpful comments to solve the challenging issues. Also, I appreciate staff members in engineering research center (ERC), Dr. Robert Jones, Jeff Simkins, and Ronald Flenniken. They gave me a training to use excellent equipments in ERC cleanroom, maintained the system with high performance, discussed with me about technical issues. In addition, I am very grateful to the members of BioMEMS and Microsystems Lab. My senior members of Dr. Jungyoup Han, Dr. Jaephil Do, Dr. Junhai Kai, Dr. Rong Rong, Dr. Sehwan Lee, Dr Soohyun Lee, Dr. Chunyan Lee, Dr. Zhiwei Zou, Dr. Matthew Estes, Dr. Michael Rust and Dr. Pei-Ming Wu. They gave me a valuable training and instructions to learn the excellent technologies of BioMEMS Lab in UC. Also, I appreciate all other friends at the group, Dr. Andrew Browne, Kang Kug Lee, Wooseok Jung. We spent long time at the Lab with a great collaboration. Additionally, I appreciate my friends in Power Mission Baptist Church. Their prayers and encouragements helped me to overcome every obstacle and to have a wonderful time in Cincinnati.

Finally, I would like to deeply appreciate my family. My parents and little brother in Korea always supported and encouraged my study. I cannot think of my accomplishments without their help. Also, I want to express my heartfelt thanks to my wife, Yun Jeong, and my daughter, Yebin. They are the sources of my happiness and pleasure, giving me the hope and the confidence to achieve my Ph. D. study.

Table of Contents

List of Figures

containing CNTs is guided to the Ni pattern by a PDMS microchannel; (c) Fe catalyst at the end of CNT is magnetically attracted to the Ni pattern; and (d) CNT is aligned parallel to the flow direction.

Figure 2.3 SEM images of (a) residual Fe catalyst at the end of MWNT and (b) individually assembled MWNT at the edge of 200 nm wide Ni pattern by magnetically attracting the residual Fe catalyst.

Figure 2.4 Fabrication procedures of Ni patterns on Au/Ti electrodes and PDMS microchannel: (a) PMMA spin coating on SiO_2/Si substrate; (b) E-beam Lithography; (c) Au/Ti deposition; (d) Lift-off; (e) 2nd PMMA spin coating; (f) E-beam Lithography and Ni deposition; (g) 2nd Lift-off; and (h) PDMS microchannel covering

Figure 2.5 Procedures to filter out metal impurities: (a) Place on the magnet to magnetically separate the metal impurities; (b) Pipette the separated bundles of CNT from metal impurities; and (c) Full dispersion of CNT bundles in solution

Figure 2.6 ESEM image of dispersed CNT in the solution of 0.5 wt% Tween 20 in DI water.

Figure 2.7 (a) Assembled MWNTs without filtration and (b) with filtration for the removal of metal impurities.

Figure 2.8 Assembled MWNT: (a) SEM image and (b) I-V curve for the aligned MWNT on Au/Ti electrode. The linear electrical response for MWNT shows stable ohmic contact. After annealing, the resistance of individually assembled MWNT on Au/Ti electrodes was reduced from 39 kΩ to 29 kΩ.

Figure 5.5 The sequences of chemiluminescent immunoassay inside the microchannel: (a) Immobilizing 1st antibody on the surface of the parylene coated CNT photodetector; (b) Capturing target protein (cTnT) from the sample; (c) Immobilizing the HRP conjugated 2nd antibody on cTnT; and (d) Chemiluminescent reaction with the substrate solution by the enzyme of HRP.

Figure 5.6 (a) I-V curve from bare CNT and PmPV and (b) Conductivity change for CNT coated with PmPV under the incident light.

Figure 5.7 (a) Drain-source current change according to the intensity of incident light and (b) Characterization of V_{ds} for maximum output.

List of Acronyms and Symbols

CNT	Carbon Nanotube
Fe	Iron
Ni	Nickel
SWNT	Single Wall Nanotube
MWNT	Multi Wall Nanotube
C_k	Chiral Vector
DEP	Dielectrophoretic Force
POCT	Point-Of-Care Testing
NIL	Nano Imprint Lithography
FET	Field Effect Transistor
1D	1-Dimensional
2D	2-Dimensional
cTnT	Cardiac Troponin T
CVD	Chemical Vapor Deposition
PECVD	Plasma-Enhanced Chemical Vapor Deposition
Co	Cobalt
ESEM	Environmental Scanning Electron Microscopy
SEM	Scanning Electron Microscope
Au	Gold
Ti	Titanium

PDMS	Poly(dimethylsiloxane)
F	Force
m	Magnetic momentum
B	Magnetic field
μ	Viscosity
u	Flow velocity
l	Length
r	Radius
HRTEM	High Resolution Transmission Electron Microscopy
J	diffusion flux
D	Diffusion coefficient
Φ	Concentration
x	Diffusion length
RTP	Rapid Thermal Process
PEG	Polyethylene glycol
PEI	Polyethylenimine
ELISA	Enzyme-Linked Immunosorbent Assay
HRP	Horseradish Peroxidase
PmPV	Poly(m-phenylenevinylene-co-2,5-dioctoxy-p-phenylenevinylene)
PBS	Protein Blocking Solution
E-Beam	Electron Beam

CHAPTER 1

INTRODUCTION

The objective of this research is to develop a new optical immunosensor for detecting cardiac biomarkers using a carbon nanotube (CNT) that is precisely assembled on a self-aligned multilayer electrode with a nano-scale gap. Since the discovery of CNTs in 1991 by Dr. Iijima, CNTs have been investigated and utilized for various applications because of their unique electrical properties. However, their practical implementation as a functional nanodevice is still considered as one of the difficult and challenging task due to the difficulties of nano-scale manipulation. Thus, currently there is a great demand for the development of new techniques for the precise manipulation, alignment, and assembly of CNTs.

In this research, the unique residual iron (Fe) catalyst located at the end of CNTs is magnetically captured at the edge of the nickel (Ni) nanopattern; then, the captured CNT is aligned parallel to the flow direction. For this self-assembly of the CNT, a novel fabrication technique is developed to achieve a functional nanogap electrode through low-cost procedures. This new fabrication method allows optical lithography to self-align a Ni pattern on the nanogap electrode with nano-scale precision. Finally, as an application of the CNT-assembled device, a photodetector was realized by coating the self-assembled CNT with a photovoltaic polymer, which generates charges under the irradiation of light. Using this CNT-based photodetector, an on-chip optical immunosensor was developed for the highly selective and sensitive detection of a cardiac biomarker.

The proposed nanofabrication method for implementing the functional CNT-assembled device is fully processed with mass-producible techniques. Also, this technique can be extended to the assembly of other functional nano-materials such as

various types of nanowires and nanoparticles. As a result, the techniques developed in this research will facilitate the implementation of practical devices assembled with nano-materials, including CNTs.

1.1 INTRODUCTION TO CARBON NANOTUBES

There are two types of CNTs, which are classified by the number of walls: a single wall nanotube (SWNT) and a multi wall nanotube (MWNT). As shown in Figure 1.1 (a), a SWNT has a rolled structure made of a single-layer graphene sheet, which has a honeycomb-shaped crystal lattice of sp^2 bonded carbon atoms [1, 2]. There are both metallic and semiconducting SWNTs; their electrical properties are decided by the chiral direction of the rolled graphene. As defined in Figure 1.1 (b), the chiral vector (C_k) is represented as

$$C_k = n\vec{a}_1 + m\vec{a}_2 \qquad \text{Eq (1)}$$

, where $\vec{a}_1$ and $\vec{a}_2$ are the unit vector in a graphene sheet, and n and m are the chiral direction [3]. When n-m=3k where k is an integer, the SWNT has a metallic property. Otherwise, the SWNT has a semiconducting property.

There has been tremendous attention on this carbon nano-structure because of its excellent properties. First, CNTs have outstanding mechanical strength, with a young's modulus of 1.4 TPa [4, 5] and tensile strength of 50 GPa [4, 6]. In the case of steel, they are 200 GPa and 1~2 GPa, respectively. In spite of an extremely narrow diameter of 1 ~ 20 nm, this strong structure of CNTs enables a robust implementation of a nanosystem compared to the other nano-materials. Also, the thermal conductivity of CNTs is higher than a diamond's, which was previously known as the best thermal conductor. The

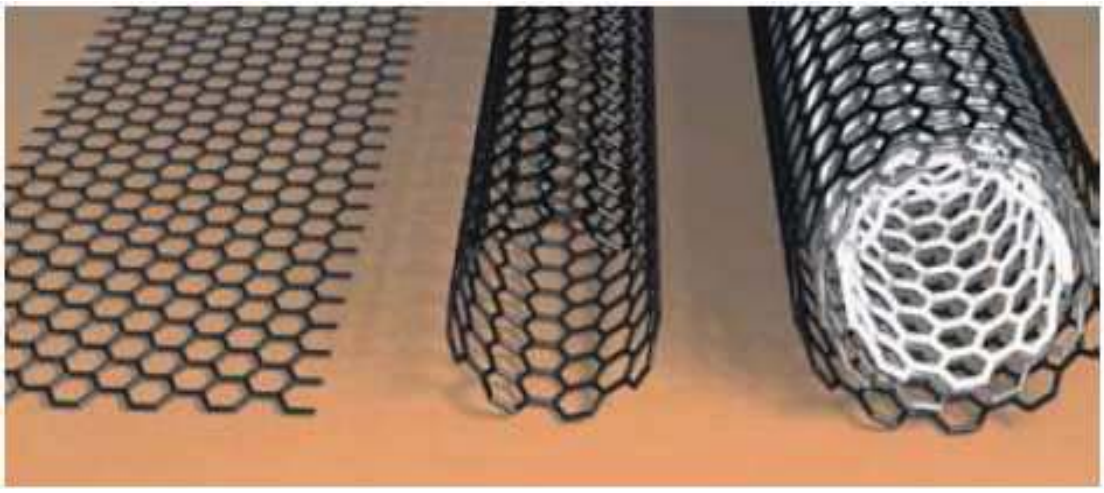

(a)

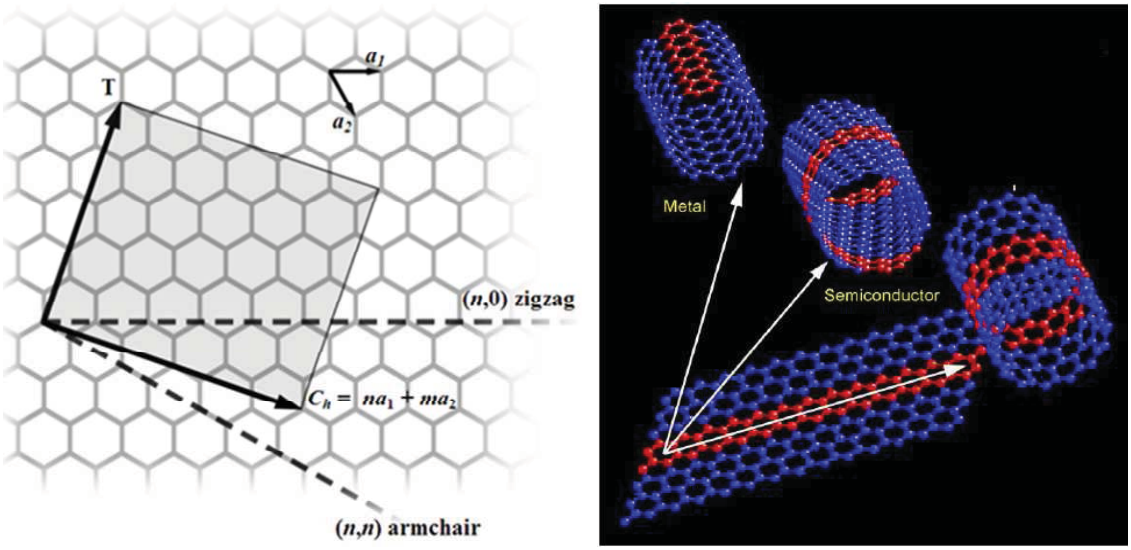

(b)

Figure 1.1 Various types of carbon nanotube: (a) Structure of graphene sheet, single wall nanotube and multi wall nanotube [1] and (b) Different chirality of single wall nanotube. The chirality decides the metallic or semiconducting property of single wall nanotube [2].

thermal conductivity of CNTs is 3,000 W/m·K [7], whereas the conductivity of a diamond is 900~2,300 W/m·K. The high thermal conductivity of CNTs can be utilized to dissipate the heat from ultra-small electronic circuitry.

In terms of electrical properties, CNTs are an ideal material for overcoming current limitations in electronic devices. The major advantage of their superior electrical properties results from a quasi-ballistic transport of electrons through CNT [8, 9]. The ballistic transport implies that electrons can freely move through the conductor without scattering. At room temperature, there is no material to enable the ballistic transport. However, in case of CNTs, the quasi-ballistic transport of electrons is possible, which results in CNTs having a long mean free path. For example, copper has 10's of nm at room temperature, whereas CNTs have at least 1 μm of mean free path [10]. Also, the quasi-ballistic transport in CNTs allows a small loss of energy during the movement of electrons. Therefore, when a current flows through a CNT, very little heat is generated, which enables the CNT to carry a high density of current without an electrical breakdown [11]. Also, due to the absence of scattering, electrons are extremely mobile and can move through CNTs quickly [12], which is an essential property for implementing high frequency electronic devices with low noise [13, 14].

In particular, semiconducting CNTs have proved to have tremendous potential as a sensing component due to their structural advantages [15-17]. When a CNT is assembled between two electrodes, the extremely narrow current path is largely affected by the interruption of target molecules, changing the current level flowing through the CNT. Specifically, as shown in Figure 1.2, the compatible size of a CNT with bio-molecules, such as DNA and proteins, results in these molecules completely surrounding

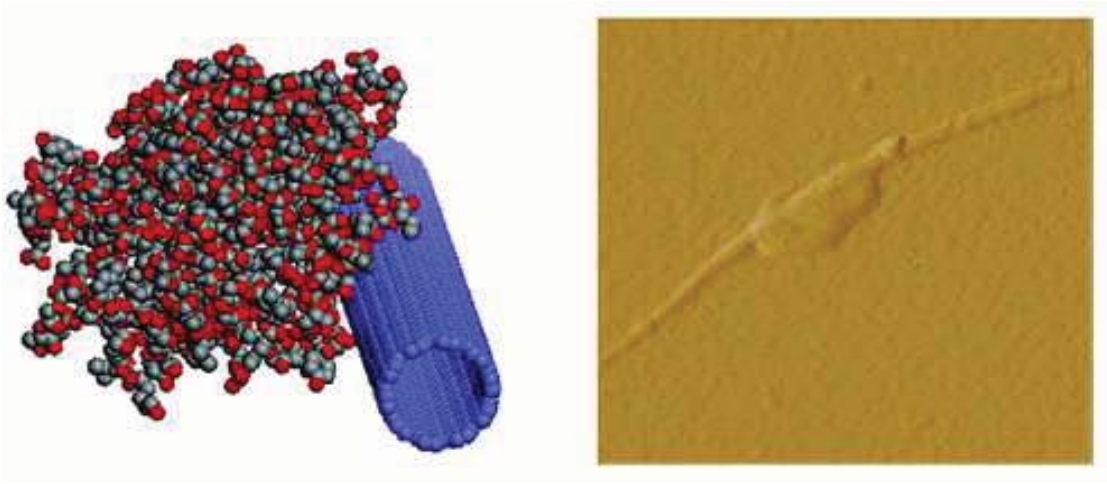

(a) (b)

Figure 1.2 Protein immobilization on the surface of CNT: (a) Schematic model [20] and (b) AFM image of protein binding on SWNT [18].

the CNT. For this reason, significant signal change could be attained despite the small number of target molecules. Thus, the compatible size enables the CNT to be applied to various biosensors for detecting cells [18], proteins [19, 20] and DNA [21] with high sensitivity [22]. In addition, all of the atoms in the SWNT contact the outside environment, so small variations in the surrounding media can directly affect the signal passing through the SWNT, resulting in a large change in the electrical conductivity. Thus, the application of the CNT-assembled device to biosensors is a very effective way of exploiting the full potential of the unique material structure of the CNT.

1.2 RESEARCH MOTIVATION

The superior functionality of CNTs has made them one of the strongest candidates for use as a biosensor, which usually requires an extremely high sensitivity for the low detection limit of small biomolecules. The point-of-care testing (POCT) biosensors, used

for clinical diagnostics near the site of patient care, usually require high sensitivity and should be implemented in a micro/nano fluidic platform for a hand-held small system. Also, the sensor is implemented on a disposable platform that prevents contamination of the device by multiple uses. Thus, the realization of highly sensitive and specific POCT biosensors has been considered a very desirable yet challenging task.

The individual CNT is an excellent material for the realization of a POCT biosensor, because it is not only excellent as a sensing component, but also cheap and of a small size suitable for integration with the POCT device. Thus, the CNT-based biosensor fabricated using mass-producible technique at a low cost can provide highly accurate and reliable detection of biomarkers for point-of-care (POC) clinical diagnostics.

In this respect, the motivation of this research is to develop a CNT biosensor to implement a highly accurate immunosensor integrated with a POCT device for the clinical diagnosis of cardiac disease To achieve this goal, a new, mass-producible nano-assembly technique needs to be developed for the self-assembly of CNTs. Also, to achieve low-cost production, the electrodes for CNT assembly have to be fabricated with inexpensive equipment, without complex and expensive procedures. Finally, a new detection method is required to realize the CNT biosensor with high selectivity and sensitivity.

1.3 PREVIOUS WORK

As shown in Figure 1.3, there have been various attempts to assemble CNTs such as utilizing chemical templates [23-25], magnetic force [26, 27], direct growth on an electrode [28-30], and dielectrophoretic force (DEP) [31-33]. Among these techniques,

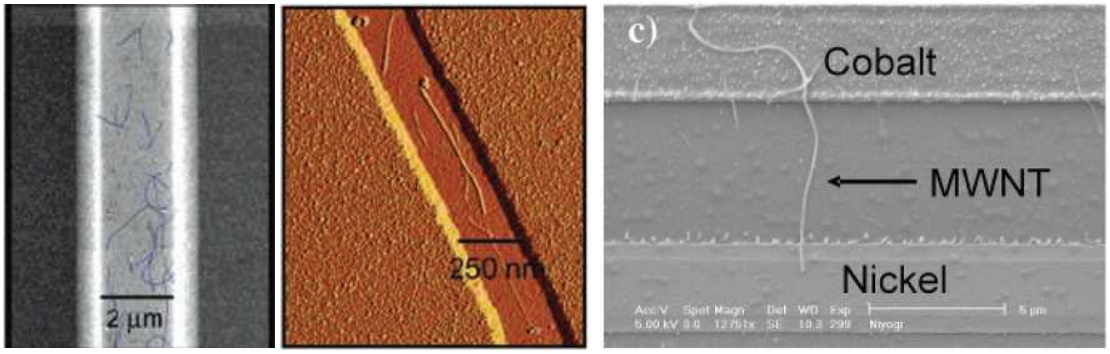

(a) (b)

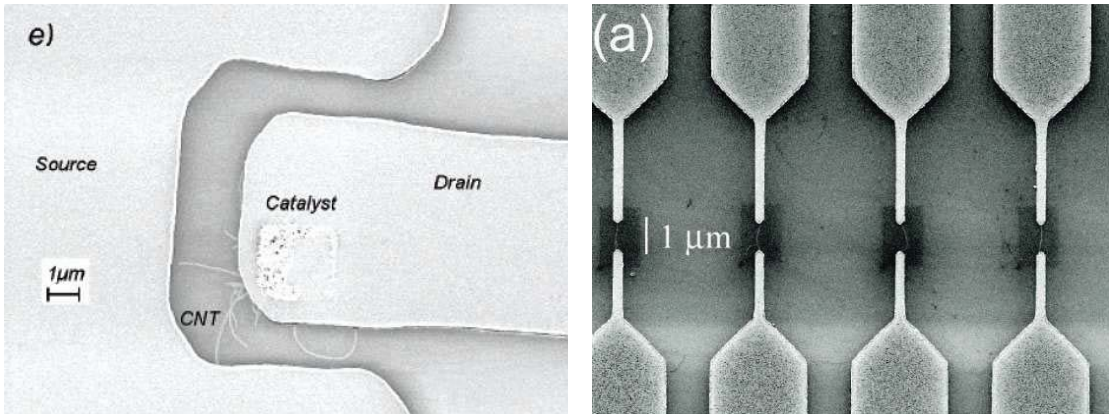

(c) (d)

Figure 1.3 Previous works for the assembly of carbon nanotube: (a) Chemical template assisted assembly [25]; (b) Magnetic assembly after Ni coating on MWNT [27]; (c) Direct growth on the electrode [29]; and (d) Dielectrophoretic (DEP) assembly [33].

functionalizing CNTs to chemically bind at a target position is suitable as a mass producible technique, but the chemical template method requires the surface treatment of the CNT, resulting in the change of its electrical properties. Also, while the previous magnetic method was successful in capturing nanotubes, it was not able to demonstrate accurate alignment, and the additional Ni deposition on the CNT results in metal

contamination. Furthermore, growing nanotubes directly on a microelectrode by a CVD process requires a high temperature process, which would affect previous fabrication steps; additionally, it is difficult to control the number of CNTs grown on the electrodes.

Currently, nanotube alignment by DEP force has been widely investigated and utilized to make nano component devices. Because the DEP method can massively align the nanotubes on the electrode with high yield and reproducibility, the method has been extensively investigated to optimize the conditions for the reliable assembly of CNT. However, there are several limitations for this method. First, metallic nanotubes are attracted by a much higher DEP force than semiconducting nanotubes [34, 35]. Owing to this selective attraction, a much higher percentage of assembled nanotubes by the DEP method would have a metallic property. Also, there is another concern regarding the crossing of the CNT over adjacent electrodes. Because DEP force is generated at both ends of each nanotube, nanotubes easily cross over the nearest electrode if the nanotube is longer than the gap between each electrode pair. Furthermore, in order to generate DEP force and attract the nanotube to electrodes, electrical potential should be applied by the electrodes. So, the electrodes assembled with a CNT should be connected to an external voltage supply, which increases fabrication complexity.

In addition to the assembly of nanotubes, the fabrication of a nano-gap between electrodes is also a challenging issue for implementing nanotube-assembled devices. Because the sonication process for dispersing nanotubes in solution results in the mechanical breaking of nanotubes, the length of individual nanotubes could be reduced to the sub-micron scale [36-38]. In order to ensure the successful contact of the sub-micron

length nanotubes over the electrodes, the nano-scale gap between the electrodes is very desirable for the CNT-assembled devices.

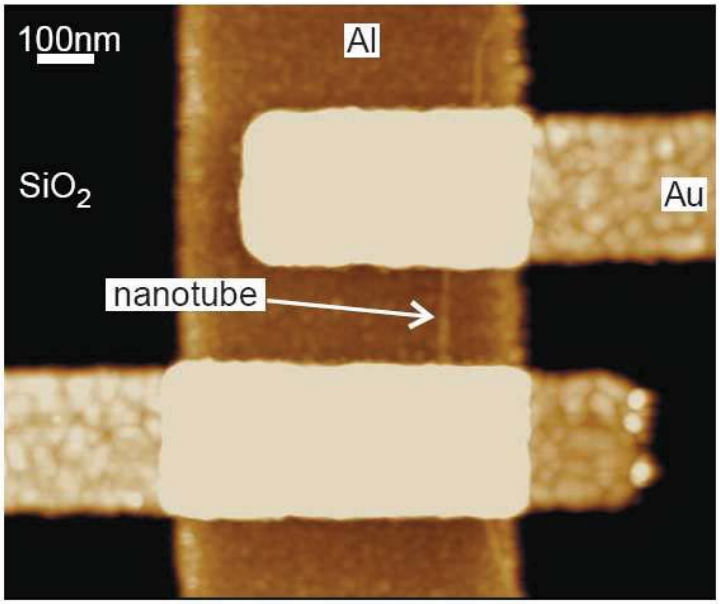

(a)

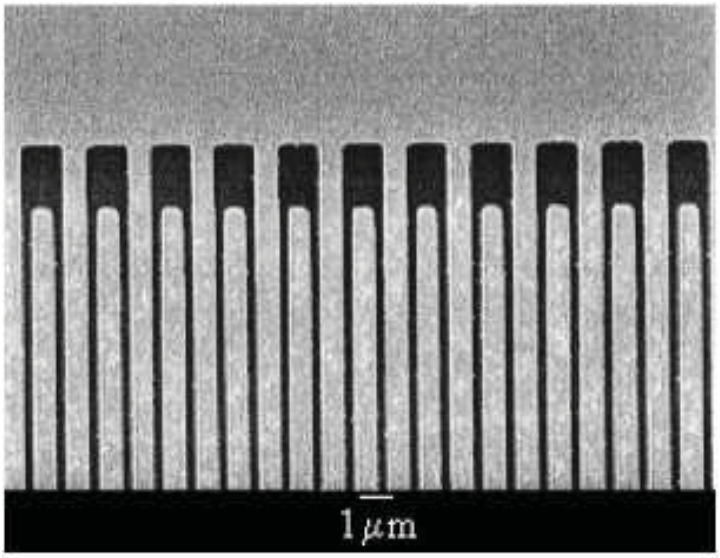

(b)

Figure 1.4 Nanogap electrode fabrication: (a) by E-beam lithography [40] and (b) by deep UV lithography [44].

For the implementation of a CNT-assembled device, electron beam (e-beam) lithography is widely used to make the electrode on the CNT because of its high precision and reliability [39-42]. In many works, however, manual searches for nano-components with long processing times have been performed, and thereby it is not effective techniques for realizing the nano-material assembled devices to commercial products. As a mass-producible technique, optical lithography has played a key role during the development of microfabrication technology because of its advantages in rapid, reproducible, uniform, cost-effective and precise processes. For a nano-scale fabrication using optical lithography, advanced techniques with alternative light sources such as deep UV [43, 44] and X-ray [45] have achieved the patterning of sub-micron features. In spite of these advances, nano-scale patterning is still difficult to fabricate with such lithography due to the high cost of equipment set-up, mask fabrication, light source and photoresist for X-ray or deep UV lithography [46]. Moreover, the alignment of multiple metal layers with nano scale precision is considered as one of the most difficult tasks in optical lithography. Recently, nano imprint lithography (NIL) has been extensively explored and has successfully achieved sub-100 nm patterns [47]. However, NIL has also suffered from a low yield in large area fabrication and a difficulty in alignment for multilayer processes [46]. As a result, the new nano-fabrication technique is required, which is compatible with the conventional lithography with low cost materials and overcomes the difficulty of alignment in nano-scale resolution.

As an application of CNT-assembled devices, a CNT field effect transistor (FET) is the representative structure that turns the CNT into a sensing element [22]. The transistors have been applied as an electrical sensor by measuring the charges of

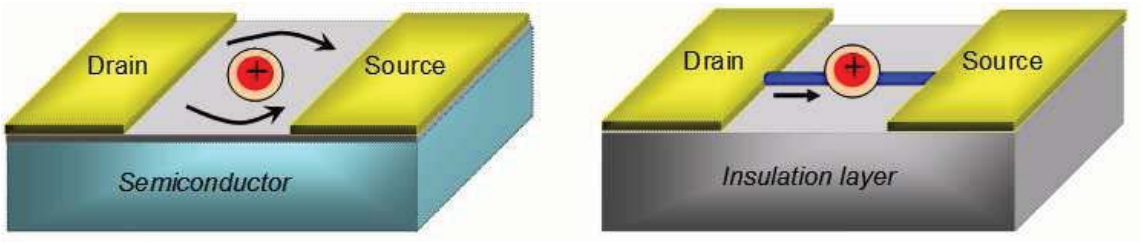

(a) (b)

Figure 1.5 Effect of surface charge on FET device with: (a) 2D thin film and (b) 1D nano-materials.

surrounding media, which provide a gate potential of FET to change the conductivity of the current channel [48, 49]. This FET-type sensor has been widely utilized because of its fast and simple measurement, the small size of the device and its easy integration with electronic circuitry [50, 51]. Recently, to enhance the sensitivity of the FET-sensors, the nanowires and the CNTs have been intensively researched as a sensing element. In these materials, because of the long cylindrical shape with a small diameter, which is called as a 1-dimensional (1D) structure, the current path is directly interfered by the change of surrounding charge as illustrated in Figure 1.5 [52-54]. However, in 2-dimensional (2D) materials that have a thin-film planar structure of typical transistors, the current can circumvent the site of the surrounding change. As a result, the FET-sensor integrated with 1D materials shows a much more sensitive response with a large signal change than the one with 2D materials.

By functionalizing the surface of CNT FET sensors, various types of sensors have been realized for the detection of proteins [17, 55], gases and vapors [16, 56, 57], and light [58]. Among these applications, the CNT FET has been successfully realized as a biosensor by exploring the extremely high sensitivity of the CNT, demonstrating the

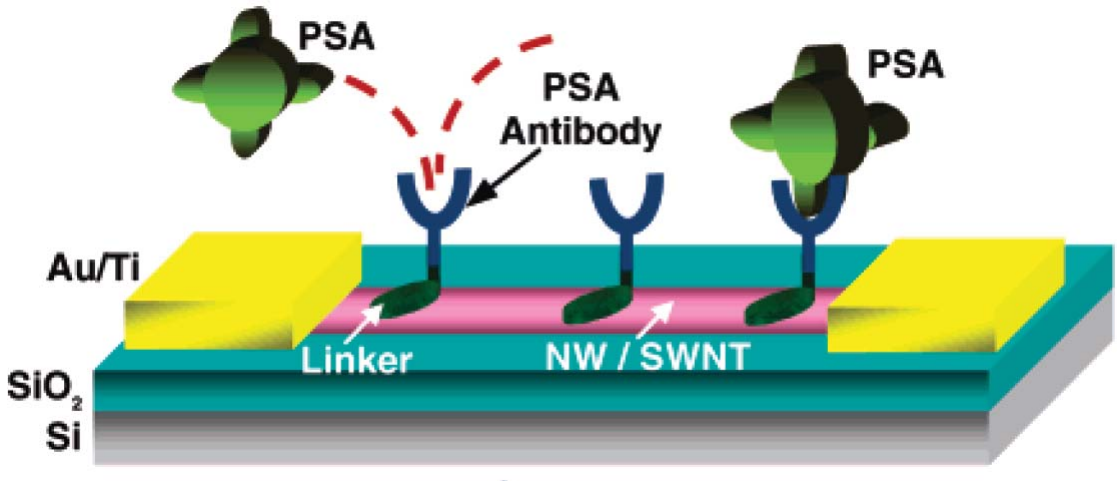

Figure 1.6 Standard structure of CNT FET type biosensor by protein immobilization on the surface of CNT [55].

simple and rapid operation by a label-free detection of biomolecules. Additionally, by directly functionalizing the CNT with antibodies [19, 55] or DNA [21, 59], the CNT has been proposed as a multi-functional element, capable of detecting various types of target molecules. For these types of sensors, however, non-specifically bound molecules on the CNT FET largely affect the signal change. To enhance the selectivity of CNT-biosensors, polymers [60, 61] and protein-blocking molecules [19, 62] have been coated on the CNT, preventing the non-specific binding of proteins. However, the ionic molecules in the sample solution still affect the output signal of the CNT-biosensors.

For the development of a selective and sensitive POCT device, optical detection is selected as a sensing principle. In optical devices, the sensing element is insulated or isolated from the sample solution and the signal is transmitted to the sensor as a light. Thus, optical sensing is much less affected by the ionic noise or the non-specifically bound molecules in the sample than the previous reported electrical measurements. However, most of currently available optical measurements need an optical reader with

separate light sources or photodiodes, which are not suitable for the hand-held POCT system. So, there is a strong demand for the development of a low-cost and highly sensitive optical or photosensitive sensor for POCT applications.

1.4 RESEARCH OBJECTIVES

The objective of this research is to develop a new self-assembly method of CNTs for implementing a functional nanobiosensor, which can be applied to the POC clinical diagnostics of cardiac disease as a demonstrative vehicle using mass-producible and cost-effective nano self-assembly methods. Also, a new chemiluminescence-based optical sensor using the CNT coated with a photovoltaic polymer has been investigated in order to attain its high selectivity as well as sensitivity. The major research is focused on: (1) the development of a new technique for the self-assembly of CNTs, which allows the mass-producible fabrication of the CNT-assembled device; (2) the development of a new electrode fabrication technique for the assembly of CNTs with a fast processing time and low-cost procedures; and (3) the development of a nano-biosensor with highly selective and sensitive detection of cardiac biomarkers for POCT clinical diagnostics as a disposable lab chip platform.

To achieve these goals, a new technique for the self-assembly of CNTs is developed by magnetically capturing the residual Fe-catalyst at the end of the CNT. The self-assembly approach allows the massive integration of CNT at the target position without any pretreatment for the assembly. Also, the new fabrication procedure is developed to achieve nano-scale self-alignment and patterning by optical lithography. This fabrication is fully processed with optical lithography for the inexpensive production

of the nano-device. Finally, an on-chip optical immunosensor is developed with the CNT-assembled device implemented by these new methods. The developed biosensor is insulated with parylene and measures the transmitted optical signal so that ions and proteins can not disturb the detection of a cardiac biomarker such as Troponin T (cTnT).

The details of this research are addressed in the following chapters:

Chapter 1 introduces this work, including the research motivation and objectives.

Chapter 2 introduces the new self-assembly technique for CNTs. The principle of fluidic and magnetic assembly of CNTs will be presented. The details of experimental procedures will be presented. Also, a new magnetic filtration method will be presented to filter out metal impurities. The electrical response will be shown for the assembled metallic MWNT and semiconducting SWNT.

Chapter 3 discusses the theoretical analysis of magnetic and fluidic force to optimize the efficiency of the CNT assembly. This analysis was performed with the magnetic simulation by MagNet and the fluidic simulation softwares by CFD-ACE+. The critical height to capture the CNT is calculated in this analysis based on the simulation result. The experimental characterization of the CNT assembly will be compared with the theoretical analysis.

Chapter 4 discusses the new fabrication technique that achieves nano-scale alignment and patterning by standard optical lithography. The detailed fabrication steps for this new technique will be announced. The characterization result to control the gap size and aligning distance will be shown. The electrical response from the assembled CNT by applying the developed assembly technique will be discussed.

Chapter 5 presents the on-chip optical immunosensor by the photovoltaic polymer coated CNT. The principle of light sensing by CNTs coated with the photovoltaic polymer will be introduced. The fabrication procedures for the CNT optical sensor will be presented. The performance of the developed CNT optical sensor will be shown. The detection result of the cardiac biomarker by the CNT immunosensor will be presented.

Chapter 6 discusses the conclusion of this research and the suggested future work to implement highly functional nano-biosensor for POCT application.

CHAPTER 2

PRECISE SELF-ASSEMBLY OF INDIVIDUAL CARBON NANOTUBE USING MAGNETIC CAPTURING AND FLUIDIC ALIGNMENT

2.1 INTRODUCTION

CNTs have been investigated and utilized for various applications since their discovery by Dr. Iijima, due to their unique electrical and material properties [63, 64]. However, the major bottleneck in current applications is the poor physical control of individual nanotubes because of the nano-scale size of CNTs [65-67]. For fabricating a reliable nanosystem integrated with CNTs, a precise assembly technique of CNTs should be developed with a mass-producible approach. Also, in order to utilize the excellent properties of the CNT, the assembly procedures should be performed at a low temperature without any preprocessing of the CNT. Additionally, the individual CNT should be integrated at the desired electrode with a high yield for both metallic and semiconducting CNTs.

In this work, we have explored a new method for the self-assembly of CNTs in the direction of fluid flow with a precise position by magnetically capturing the residual Fe catalyst. While DEP has a stronger attraction on metallic nanotubes than semiconducting nanotubes [32, 35, 68], this method is equally effective on both types of nanotubes. Also, this assembly technique does not require a pretreatment on the CNT, allowing to exploit the full functionality of pristine CNTs. Moreover, since our magnetic alignment technique uses an external magnetic field and small Ni pattern to localize the magnetic force, each electrode is not constrained by the connection to an external power source. Thus, the new assembly method provides design flexibility for the precise, parallel assembly of CNTs for a variety of applications, including CNT integrated circuits and nano-biosensors.

2.2 PRINCIPLES

The basic mechanism of the new self-assembly technique involves the use of the ferromagnetic metal catalyst that is naturally located at one end of the CNT during the synthesizing process. Various methods have been reported for the synthesis of CNTs, including arc-discharge, chemical vapor deposition (CVD), and plasma-enhanced chemical vapor deposition (PECVD) [69-71]. In these synthesis processes, metal

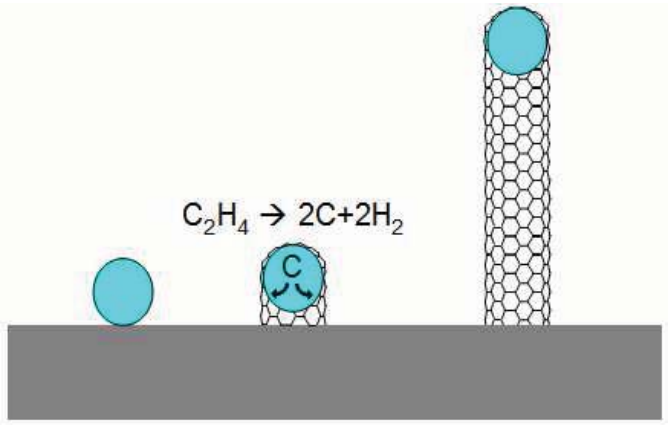

(a)

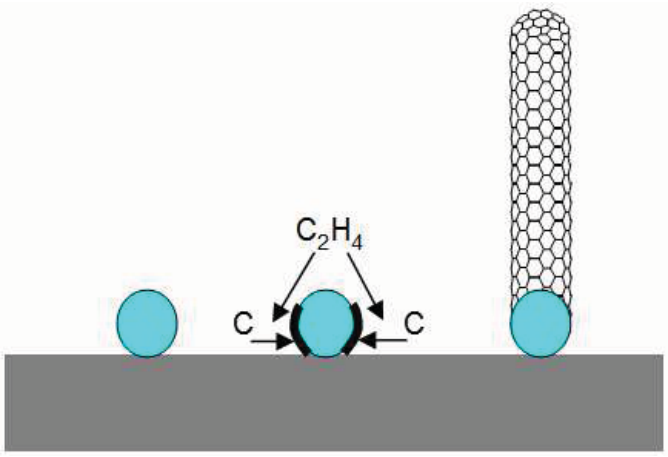

(b)

Figure 2.1 Two different growth mode in CVD synthesis of carbon nanotube: (a) Tip-growth mode and (b) root-growth mode

catalysts such as iron (Fe), nickel (Ni) and cobalt (Co) provide seeding sites for CNT growth. There are two kinds of mechanisms in CNT synthesis as shown in Figure 2.1 [72].

One of these mechanisms is called tip growth and the other is called bottom growth, according to the location of the catalyst during growth. For both growth-mechanisms, the catalyst is commonly located at one end of each CNT. Since these catalysts of Fe, Co and Ni are ferromagnetic materials, they can be magnetized in an external magnetic field. Thus, the ferromagnetic metal catalyst works as a nano-scale magnet that allows the CNTs to be manipulated for the self-assembly.

Figure 2.2 shows a schematic illustration of the assembly procedure. First, a microfluidic channel is used to guide a solution containing CNTs to the Ni pattern on a gold electrode. Next, magnetic force is produced on the Ni pattern by applying an external magnetic field, thus the metal catalyst of the CNT is attracted and positioned at the target point of self-assembly. Finally, the shear force from the liquid flowing through the microchannel aligns the CNT parallel to the flow direction [73].

In this work, the new self-assembly technique for CNTs is proposed utilizing the residual Fe catalyst at the end of the CNT. Because this approach does not require any preprocessing on the CNT, the superior functionalities of the pristine CNT can be fully exploited to implement functional nanodevices. Also, whereas the self-assembly of CNT by the DEP force has a strong selectivity on metallic CNTs, this method is equally effective for the assembly of both metallic CNT and semiconducting CNT. Furthermore, the suggested technique utilizes the external magnetic field, and the induced magnetic force is specifically generated at the nano-scale Ni pattern. So, the electrodes are not

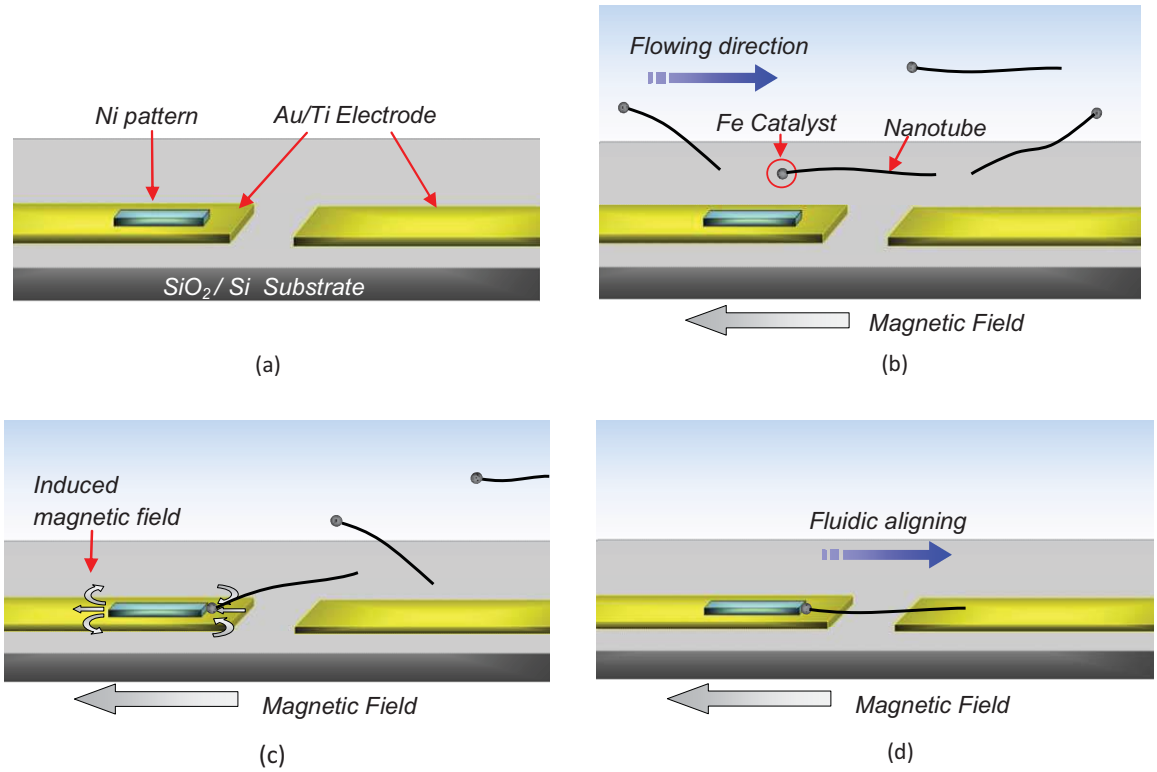

Figure 2.2 Procedure for fluidic alignment of CNT by magnetic attraction on a Ni pattern: (a) Fabrication of Ni pattern on Au/Ti electrodes; (b) solution containing CNTs is guided to the Ni pattern by a PDMS microchannel; (c) Fe catalyst at the end of CNT is magnetically attracted to the Ni pattern; and (d) CNT is aligned parallel to the flow direction.

connected to an external power source without geometrical restrictions, to concentrate the electrical field as in the DEP assembly. As a result, this new method provides a design flexibility for implementing a wide range of applications, including CNT-integrated circuits and nano-biosensors.

2.3 DESIGN AND FABRICATION

2.3.1 Synthesis of CNTs

A thermal CVD process with Fe catalysts was used to synthesize MWNTs in this work [74, 75]. Three-layered substrates, Fe (1 nm) / SiO_2 (100 nm) / Si, were prepared using the following techniques. First, an electron-beam evaporator was used to deposit a 1-nm thick Fe film on a SiO_2/Si wafer. This Fe film was oxidized to create iron oxide nano-islands, and then reduced by flowing 500 SCCM of H_2 at 750°C during the synthesis process of MWNT. Next, the Fe/SiO_2/Si substrates were used for the MWNT growth, utilizing previously reported top-growth mechanism [75]. The MWNT array was synthesized by a thermal CVD in a horizontal 2-in EasyTubeTM (ET1000, FirstNano) furnace. The growth conditions were 500 SCCM of H_2 flow, 700 SCCM of C_2H_4 flow, and a 750 °C growth temperature. The synthesizing process was performed for 5 minutes and the fabricated MWNTs were characterized by environmental scanning electron microscopy (ESEM). The characterization result showed that the fabricated MWNTs had a dimension of 20 nm in diameter and 3-5 μm in length.

For applying our technique to assemble SWNTs, the vertical array type of SWNTs grown by a CVD process was purchased from FirstNano (Ronkonkoma, NY). The characterization results by Raman spectroscopy and SEM image showed that the synthesized SWNT had a diameter of 1 to 2 nm and a length of around 50 μm. After dispersing the surfactant solution, the length of the SWNT was reduced to an average length of 3 μm because of mechanical breakdowns during the sonication process.

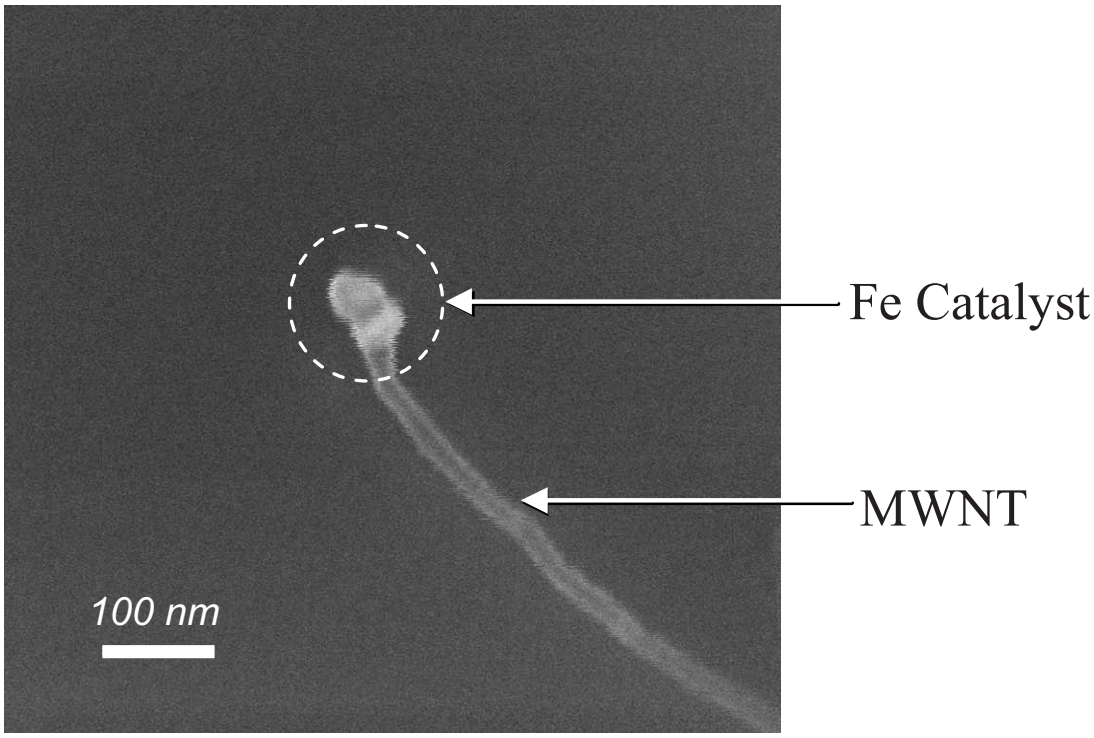

(a)

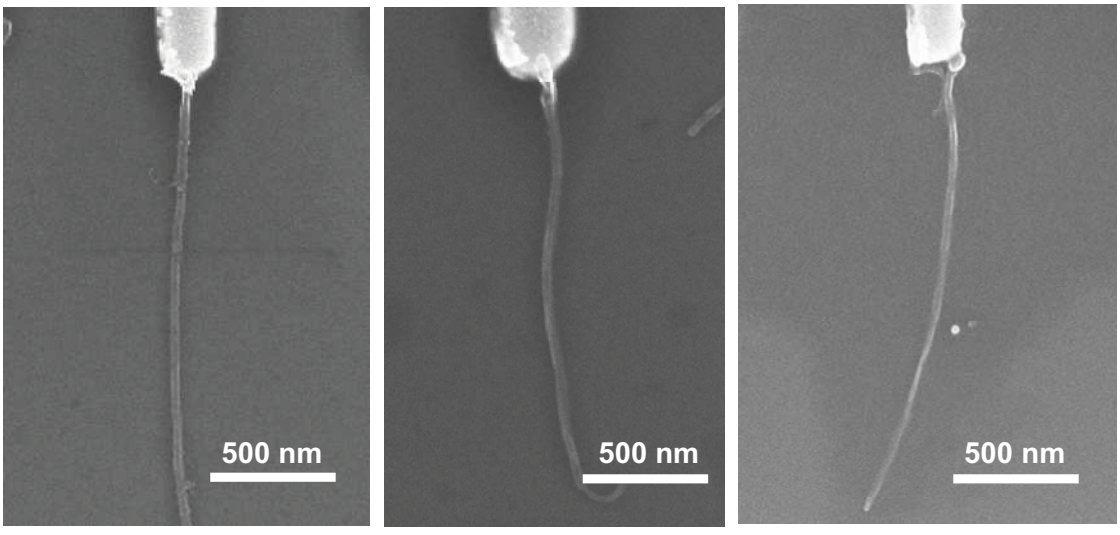

(b)

Figure 2.3 SEM images of (a) residual Fe catalyst at the end of MWNT and (b) individually assembled MWNT at the edge of 200 nm wide Ni pattern by magnetically attracting the residual Fe catalyst.

2.3.2 Fabrication of electrodes with Ni patterns

To position the CNT precisely, a nano-scale Ni pattern was fabricated by e-beam lithography. The magnetic force induced on the Ni pattern by an external magnetic field is proportional to the gradient of the magnetic field. Since the highest gradient of magnetic field over the Ni pattern occurs at its edge, a strong magnetic force is generated at the edge of the Ni pattern. Additionally, once the CNT has been attached to the Ni pattern, the edge of the Ni pattern is covered by the attached CNT, preventing the assembly of multiple CNTs at each Ni pattern. For this purpose, a small cross-sectional area of Ni (200 nm wide and 100 nm thick) was designed and fabricated to assemble a single CNT at each Ni pattern. With this approach, the individual CNT can be precisely assembled on the desired electrode point. Figure 2.3 shows scanning electron microscope (SEM) images of individually assembled MWNTs using the assembly method developed in this work.

The e-beam lithography was utilized to fabricate a Gold (Au)/Titanium (Ti) electrode, which was precisely aligned with the Ni pattern. Because CNTs were captured at the edge of the Ni pattern, the Ni pattern should be patterned at target position of CNT assembly. In order to precisely assemble the CNT on the Au/Ti electrode, the alignment of the Ni pattern was achieved by the multilayer process of e-beam lithography. For this procedure, the Au/Ti electrode was first patterned with the alignment mark for the fabrication of the Ni pattern. After the e-beam exposure and development of the PMMA, the Au/Ti deposited sequentially with a thickness of 100 nm and 10 nm, respectively. Following lift-off, in order to finalize the patterning of the Au/Ti electrode, the second e-beam lithography was performed for the patterning of Ni. In this step, the Ni pattern was

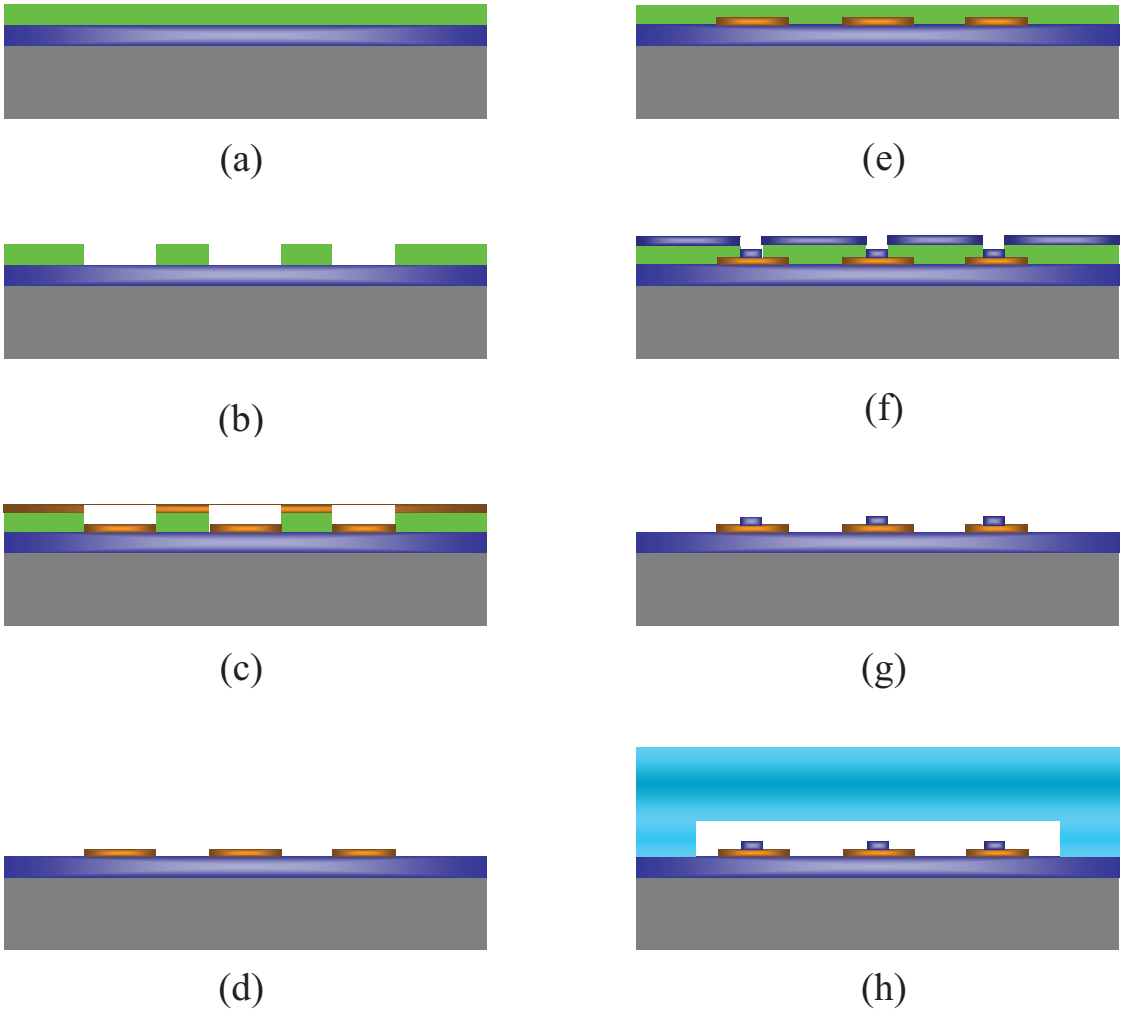

Figure 2.4 Fabrication procedures of Ni patterns on Au/Ti electrodes and PDMS microchannel: (a) PMMA spin coating on SiO_2/Si substrate; (b) E-beam Lithography; (c) Au/Ti deposition; (d) Lift-off; (e) 2nd PMMA spin coating; (f) E-beam Lithography and Ni deposition; (g) 2nd Lift-off; and (h) PDMS microchannel covering.

precisely aligned with the Au/Ti electrode through the use of the alignment mark fabricated at the first e-beam lithography. After e-beam exposure and developing, 100 nm of Ni was patterned on the Au/Ti electrode.

2.4 EXPERIMENT DETAILS

2.4.1 Dispersion and magnetic filtration of CNTs

In this suggested method, the filtration of the CNT solution is a critical step to avoid the attachment of metal impurities to the Ni pattern. After the synthesis and dispersion of CNTs in a surfactant solution, the solution contained many metal impurities, which were typically unused catalysts from the synthesis process [72]. Due to their ferromagnetic property, these impure Fe catalysts were also attracted to the Ni patterns by the same mechanism that attracted the CNT-catalyst complex, as shown in Figure 2.7 (a).

There are many methods available for purifying CNTs, such as acid refluxing and centrifugation. Even though acid treatments are widely used and effectively remove all the metal impurities, the acid causes the formation of defects or functional groups on the surface of the CNT [76]. Also, the magnetic filtration of Fe catalysts was reported previously, but the CNTs with residual Fe catalysts were also filtered out in that method, thus making it incompatible with our assembly process [77].

For the selective removal of the metal impurities that were not attached to CNTs, a new filtration procedure was developed in this work. First, the grown CNTs were dispersed in an insufficient volume of surfactant solution (a mixture of 1 wt% SDBS

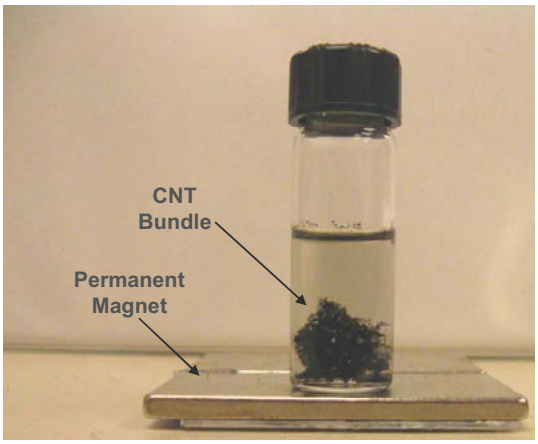

(a)

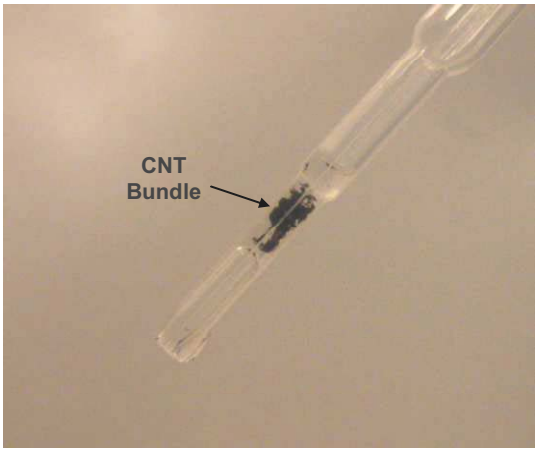

(b)

(c)

Figure 2.5 Procedures to filter out metal impurities: (a) Place on the magnet to magnetically separate the metal impurities; (b) Pipette the separated bundles of CNT from metal impurities; and (c) Full dispersion of CNT bundles in solution.

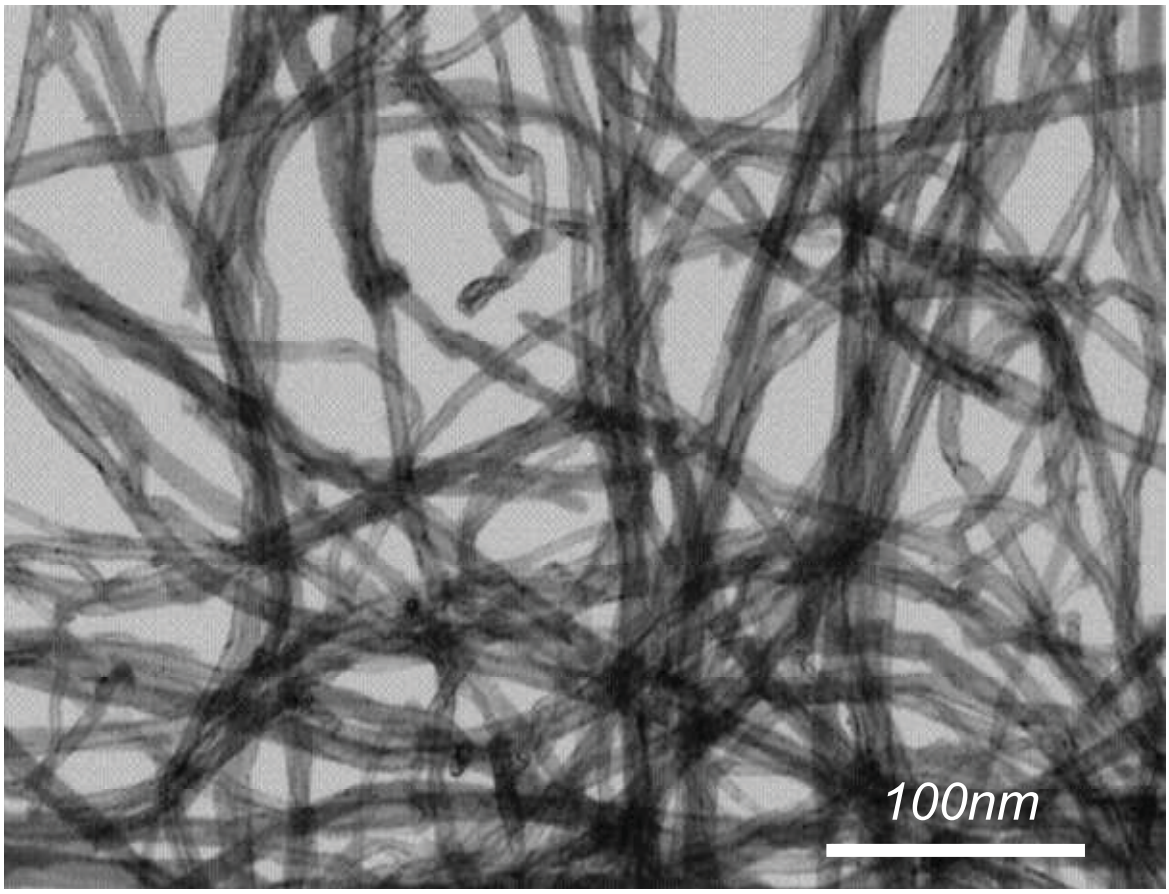

Figure 2.6 ESEM image of dispersed CNT in the solution of 0.5 wt% Tween 20 in DI water.

(sodium dodecylbenzenesulfonate, Sigma-Aldrich Co.) in DI water) [78, 79], and the sonicated solution was placed on the magnet for one week. Because the volume of surfactant solution was not enough for full dispersion, the CNTs became aggregated again and generated bundles over time. Since the CNT bundles had much larger surface areas than the metal impurities, the fluidic resistance of the CNT bundles restricted their movement in the solution. As a result, the CNTs were entangled together and formed bundles, while the metal impurities were magnetically attracted and precipitated at the bottom. The bundles of CNTs were carefully extracted from the solution with a pipette without agitating the container. The extracted CNT bundles were then sonicated again in

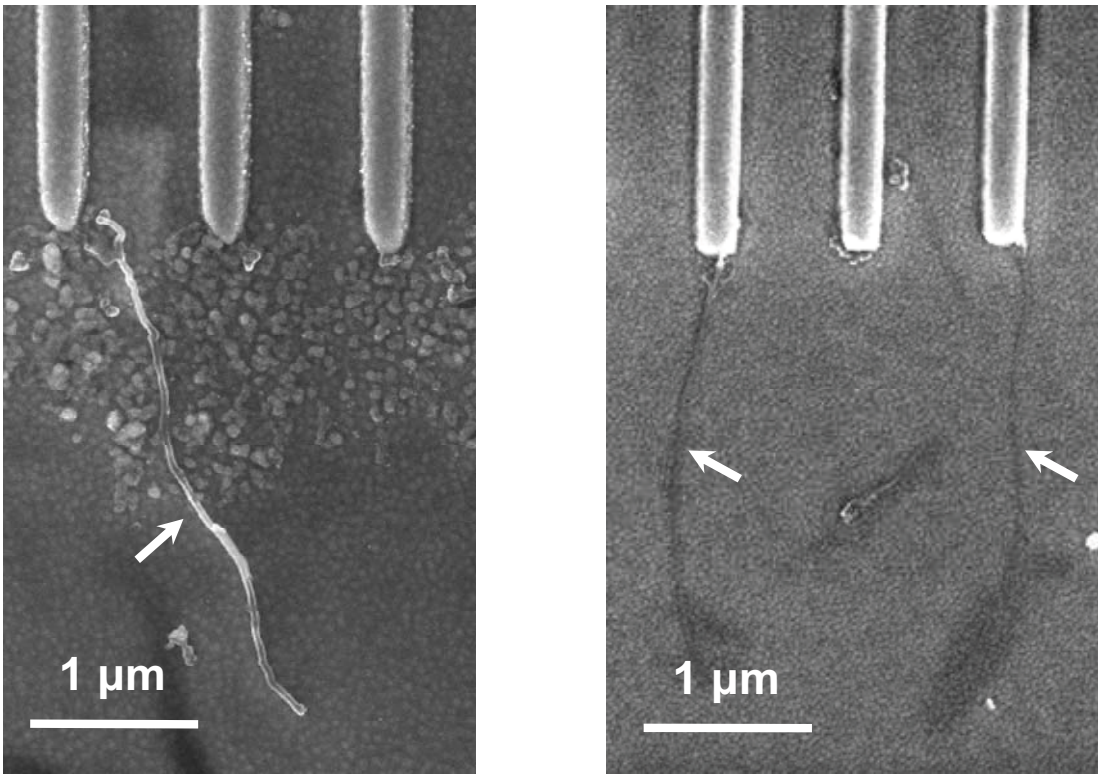

(a) (b)

Figure 2.7 (a) Assembled MWNTs without filtration and (b) with filtration for the removal of metal impurities.

an appropriate volume of surfactant solution for full dispersion. Following this filtration process, the assembly procedure resulted in the capture of CNTs without impurities at the edge of the Ni pattern, as depicted in Figure 2.7 (b).

2.4.2 CNT flow using PDMS microchannels

For the fabrication of the microchannel, soft lithography with poly(dimethylsiloxane) (PDMS, Essex Group Corp.) on a thick-film photoresist (AZ 4620, AZ Electronic Materials USA Corp.) pattern was completed. Patterns approximately 20 μm thick were fabricated on a mirror-finished silicon wafer and used as

a mold for casting with the PDMS elastomer. The PDMS microchannel has a dimension of 20 μm high by 2 mm wide, and was used to guide the CNT solution to the electrode pattern on the SiO_2/Si substrate. Since the PDMS microchannel had to be detached from the substrate in order to characterize the device after the alignment of CNTs, a permanent bond between the PDMS and SiO_2, normally achieved by oxygen plasma treatment, was not performed for this work. Without plasma treatment, the PDMS microchannel was attached to the SiO_2/Si wafer and showed no leakage of the solution containing dispersed CNTs during assembly. Under the external magnetic field of 0.7 Tesla, 10 μl of a well-dispersed CNT solution flowed through the microchannel with a flow velocity 4.2 mm/sec. After the flowing of the CNT solution, the PDMS microchannel was detached from the substrate for subsequent SEM imaging and electrical analysis.

After the solution was removed from the microchannel, the external magnet was maintained to prevent the CNTs from detaching from the Ni pattern while drying. The drying process caused the CNTs to adhere to the substrate surface by Van der Waals force, thus the CNTs remained stably attached even after they were submerged in an ultrasonic bath. As a result, this assembly technique does not need any post-processing to attach the assembled CNTs to the electrode by an additional metal deposition, which would require a precise alignment step and would also have the potential to introduce unwanted impurities. Even though there was no additional metal deposition to hold the CNT on the electrode, the CNT was stable and showed a good electrical contact with the Au/Ti electrode.

2.5 ELECTRICAL CHARACTERIZATION

Figure 2.8 (a) shows an SEM image of an assembled MWNT on the Au/Ti electrode using the new assembly method. The rectangular Ni patterns were fabricated on the Au/Ti electrode by e-beam lithography. The measured current-voltage characteristics for the assembled MWNT are presented in Figure 2.8 (b). Corresponding to the previous reports in which MWNTs usually possess metallic properties [80, 81], the result shows a linear relationship between the current and the voltage, demonstrating good ohmic contact between the electrode and the MWNT. To reduce contact resistance, the MWNT assembled electrode was annealed at 120 °C for 24 hours. The measured resistance before annealing was 40 kΩ to 100 kΩ, and it was reduced to around 30 kΩ after annealing. Compared with previous reports, this value of resistance is relatively low and does not require additional metal deposition on the assembled MWNT to reduce the contact resistance [80].

The SWNT was also assembled on an electrode using the proposed technique as shown in Figure 2.9 (a). In contrast with the results from the assembly of MWNT, some Fe impurities also attached at the Ni pattern despite the use of the same filtration step described above. To avoid the attachment of these metal impurities, an advanced filtration step for SWNTs is still under investigation. Since the catalyst size of the SWNT is smaller than that of the MWNT, a slower flow rate of 0.4 mm/sec was applied, while the other conditions were kept the same as those used for the assembly of the MWNT. To reduce the contact resistance and ensure a stable electrical response, the assembled SWNT was annealed by rapid thermal processing (RTP, AG Associates, Inc.) with N_2 flowing at 350 °C for 5 min. Because the assembled SWNT showed a very

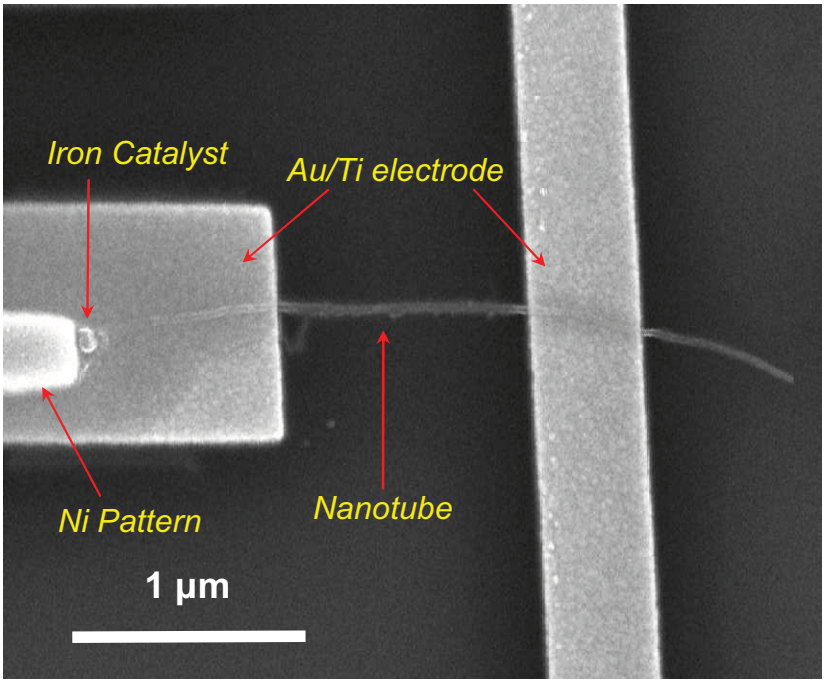

(a)

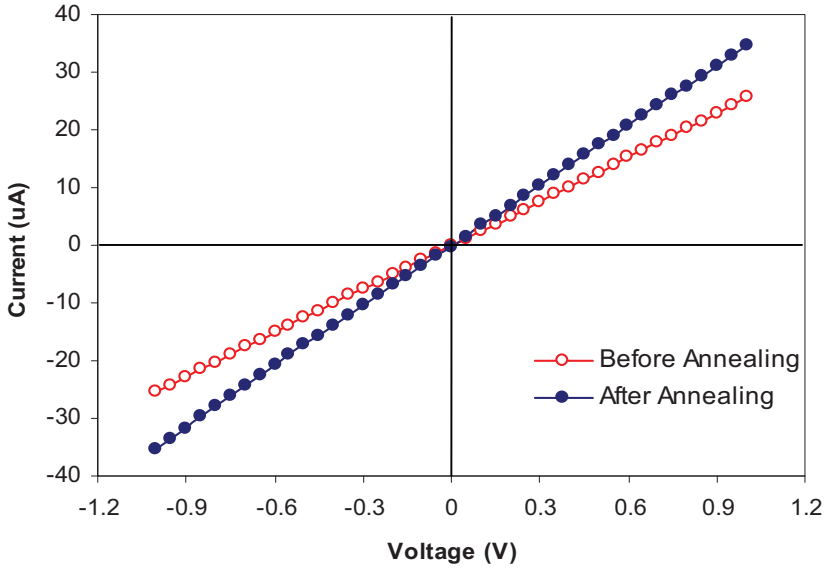

(b)

Figure 2.8 Assembled MWNT: (a) SEM image and (b) I-V curve for the aligned MWNT on Au/Ti electrode. The linear electrical response for MWNT shows stable ohmic contact. After annealing, the resistance of individually assembled MWNT on Au/Ti electrodes was reduced from 39 kΩ to 29 kΩ.

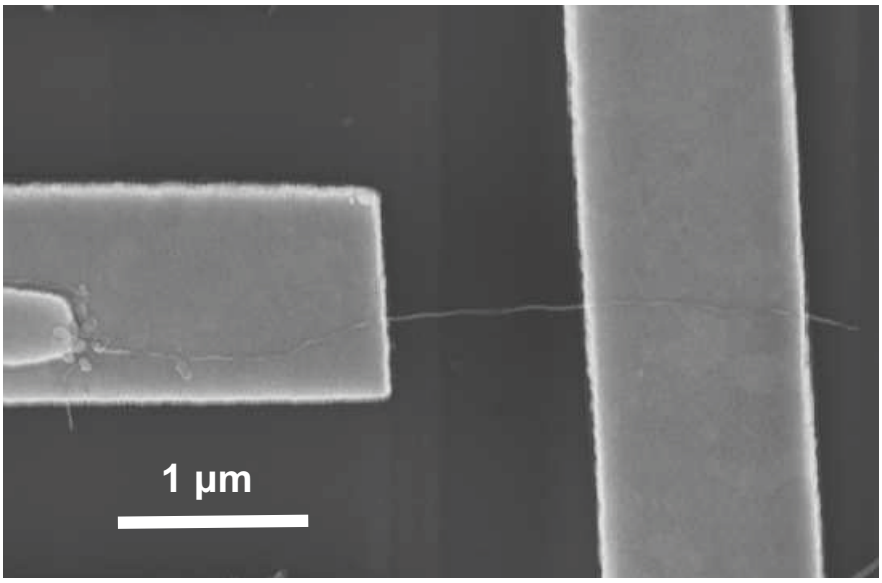

(a)

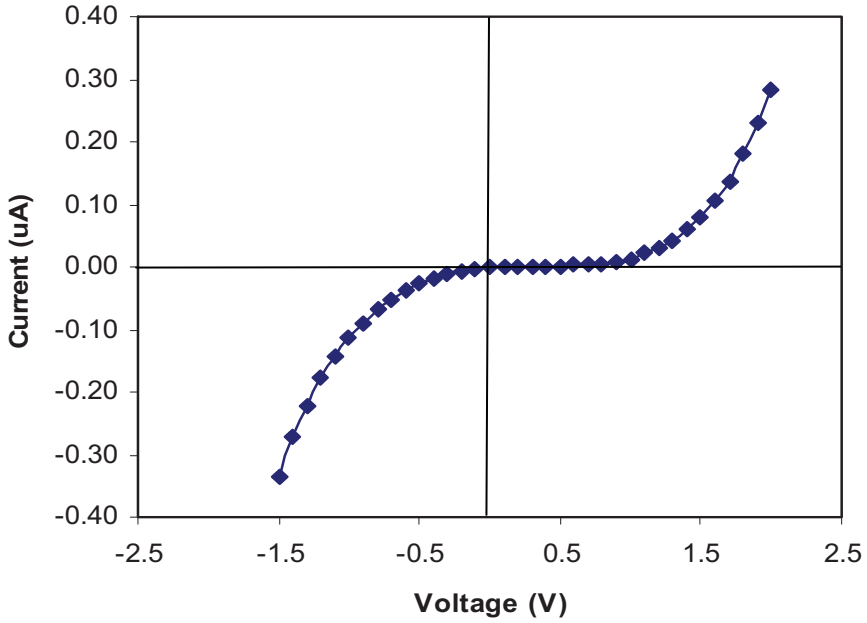

(b)

Figure 2.9 Assembled SWNT: (a) SEM image and (b) I-V curve for the assembled SWNT. The electrical response shows non-linear schottky contact, indicating the semiconducting property of the assembled SWNT.

unstable electrical response before annealing, the electrical characteristics were measured after annealing the SWNT, as plotted in Figure 2.9 (b). The result shows a non-linear response of back-to-back schottky junction, showing that the assembled SWNT is a semiconducting CNT [82]. Therefore, the suggested method was also successfully applied for the self-assembly of the semiconducting SWNT.

2.6 CONCLUSION

In conclusion, a new self-assembly technique for CNT has been proposed and successfully demonstrated in this work. By magnetically attracting the residual ferromagnetic catalyst, CNTs were assembled at the edge of Ni patterns and aligned along the flow direction. Both the metallic MWNT and the semiconducting SWNT were assembled on electrodes with stable electrical responses. The assembly technique demonstrated in this work requires only simple procedures without any pre-treatment or post-processing on the CNT. Furthermore, this method can provide the design flexibility of a CNT integrated circuit with high precision. In this regard, the new assembly technique demonstrated in this work can envisage the practical applications of CNTs to nanobiosensors or nanoelectronic devices.

CHAPTER 3

A THEORETICAL ANALYSIS FOR THE FLUIDIC AND MAGNETIC SELF-ASSEMBLY OF CARBON NANOTUBES

3.1 A SIMULATION MODEL OF CNTS

In this study, a theoretical analysis of CNT assembly has been performed to optimize the fluid velocity and the magnetic force. Figure 3.1 shows the simulation model for the theoretical analysis. The length of CNT was simply modeled as 3 μm, which was the average length of the CNTs experimented in this work. The SEM analysis showed that the average diameter of the catalyst was approximately 20 nm for SWNTs and 50 nm for MWNTs. In order to avoid the complexity arising from the single-domain

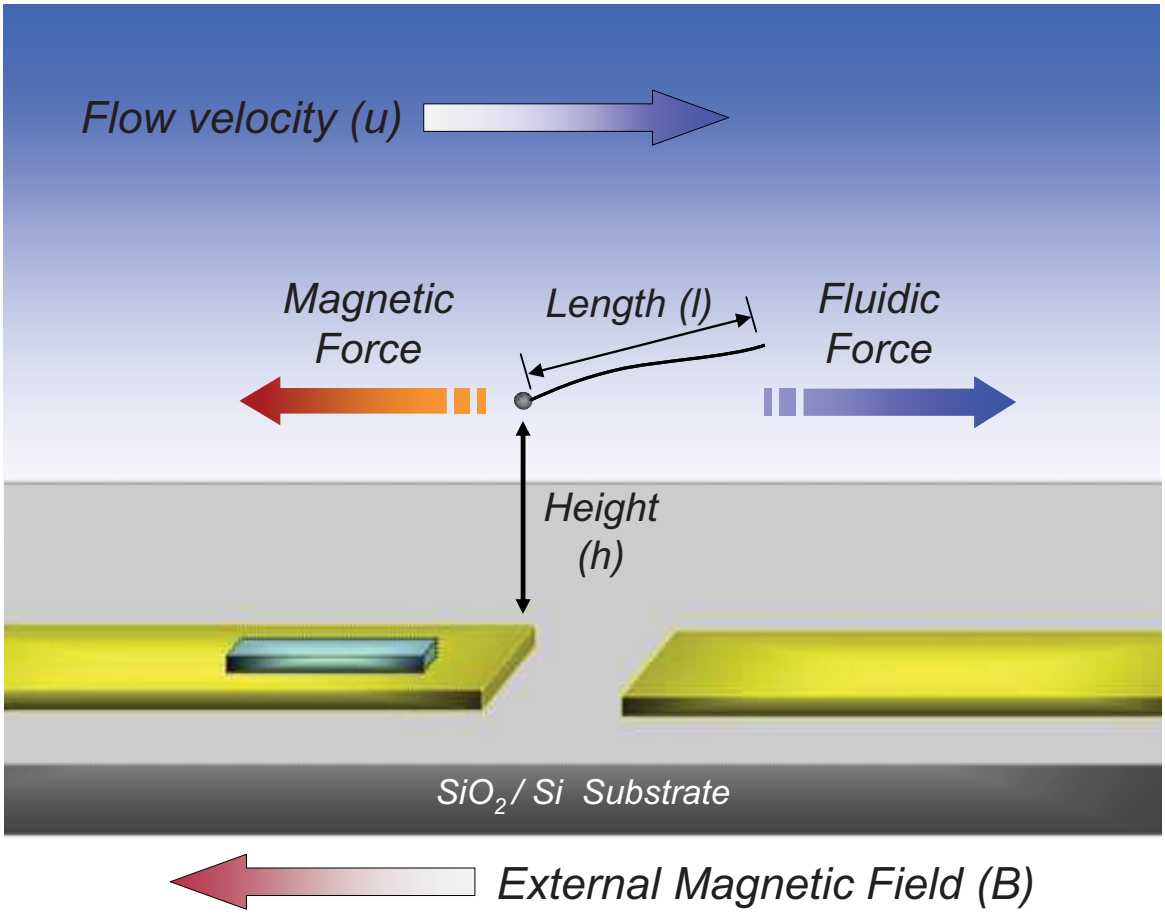

Figure 3.1 Theoretic model for the magnetic and fluidic analysis of CNT assembly. To simplify the analysis, the CNT was modeled to have 3 μm length and 50 nm diameter of catalyst, which were the average values for the experimented MWNTs.

effect of ferromagnetic material [83], the theoretical model was confined to the analysis of MWNTs with a Fe catalyst of 50 nm in diameter.

3.2 THEORETICAL ANALYSIS OF CNT ASSEMBLY

3.2.1 Magnetic simulation

The magnetic force, which is applied to the Fe catalyst of CNTs by the Ni pattern, can be described in Equation (1)

$$F = (m \cdot \nabla)B \tag{1}$$

, where m is magnetic momentum of the Fe catalyst and B is the magnetic field induced by the Ni pattern [84]. Because the magnetic momentum of the Fe catalyst is constant for all directions, the magnetic force is linearly proportional to the gradient of the magnetic field.

For the characterization of the magnetic force applied to the Fe catalyst, the magnetic momentum of the Fe nanoparticle with a diameter of 50 nm (m =~6x10−17 A m^2) was used [85, 86]. A magnetic simulation (MagNet, Infolytica, Inc.) was performed to analyze the magnetic force induced on the Ni pattern. Ni structures with different dimensions (0.2 μm, 0.5 μm, 1 μm, and 2 μm in length) and a fixed width and thickness of 0.2 μm and 0.1 μm, respectively, were simulated. A uniform external magnetic field of 0.7 Tesla was applied to the longitudinal direction of the Ni pattern.

Figure 3.2 (a) shows the simulation result for the magnetic field around the 1μm long Ni pattern under an external magnetic field of 0.7 T. The contour lines, which represent lines of equal magnetic fields, are very dense at the edge of the Ni pattern. This indicates that the localized and high gradient of the magnetic field occurs at the edge of

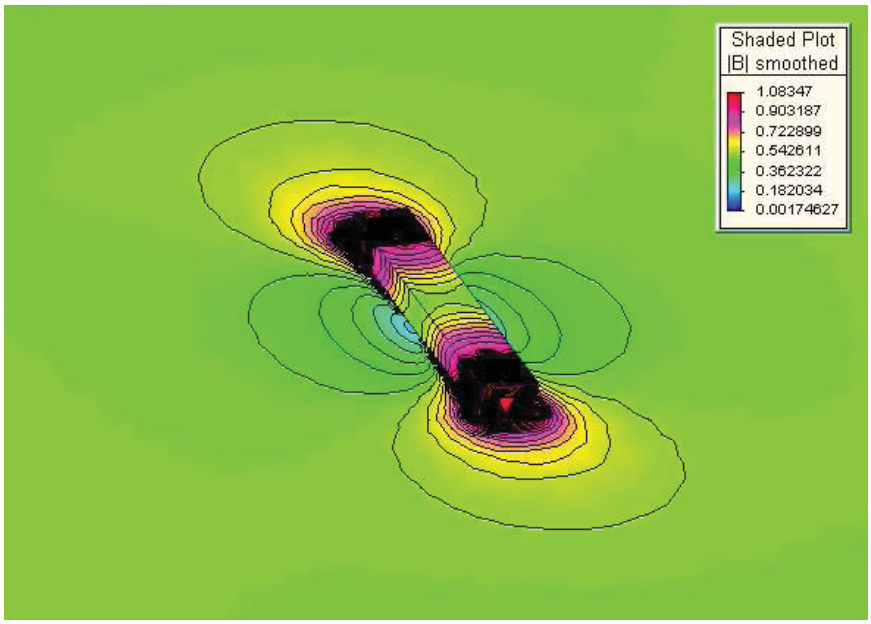

(a)

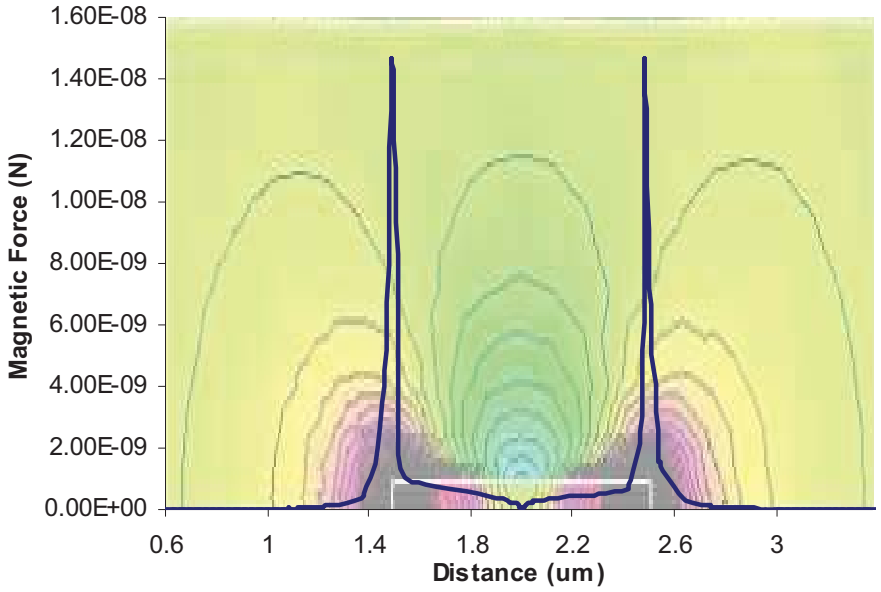

(b)

Figure 3.2 Magnetic simulation result under external magnetic field of 0.7 T: (a) Contour lines representing lines of equal magnetic field around Ni pattern. (b) Induced magnetic field around the 1μm long Ni pattern. The result displays the high magnetic field generated at the edge of Ni pattern.

the Ni pattern. With this simulation result of the magnetic field, the magnetic force is calculated by Eq. (1) and plotted in Figure 3.2 (b), which displays the magnetic force applied to the Fe catalyst along the longitudinal direction of the Ni pattern. The result shows that the magnetic force attracting the catalyst is localized at both ends of the Ni pattern, so the CNTs would be assembled at these positions. The magnetic force was also simulated as a function of the height above the Ni pattern, as shown in Figure 3.3. The result shows that the magnetic force rapidly decreases as the height is increased, and that the longer Ni pattern generates a greater magnetic force.

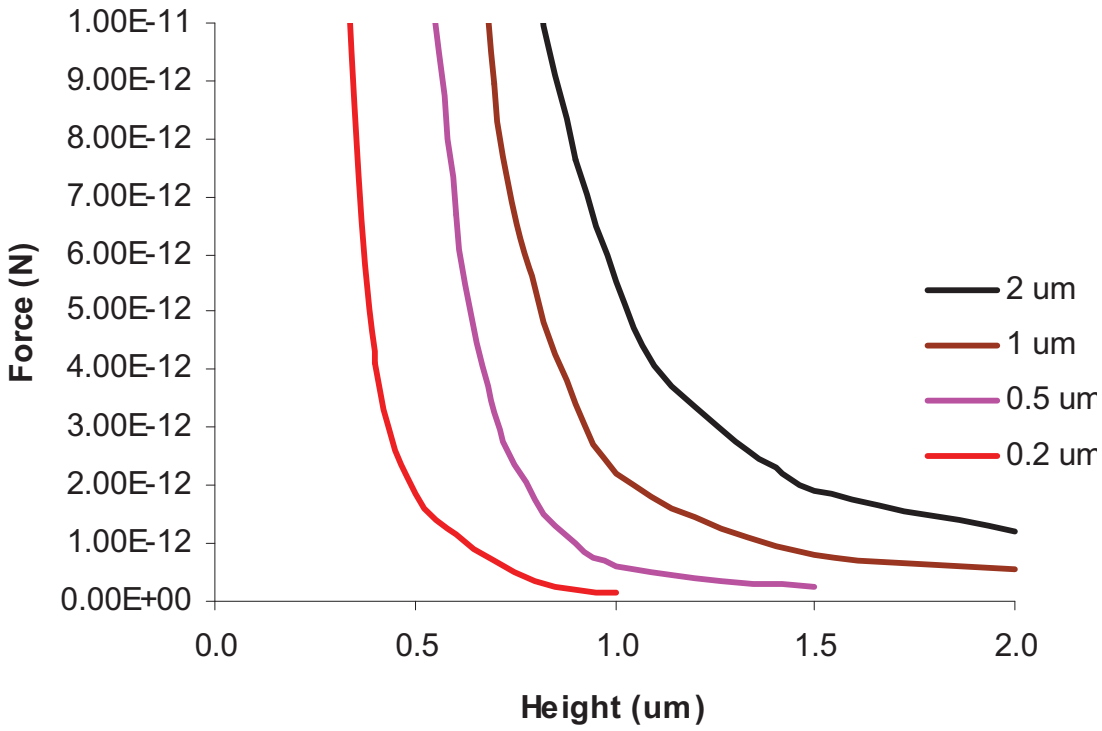

Figure 3.3 Simulated magnetic forces as a function of height above the Ni pattern for various pattern lengths (0.2 μm, 0.5 μm, 1 μm, and 2 μm).

3.2.2 Fluidic simulation

The slender body theory was applied to analyze the fluidic shear force on the surface of CNTs [87, 88]. The slender body theory gives the drag force (F) on a CNT parallel to the axis of a flow as described in Equation (2)

$$F \approx \frac{2\pi\mu l u}{\ln(l/r)} \tag{2}$$

, where μ ($\approx$ 0.001 N s/m^2) is the viscosity of a 1 wt% SDBS solution, u is the flow velocity, l is the length of the CNT, and r is the radius of the CNT. Due to the large ratio of length and radius, the constant term in the denominator is ignored. To analyze the fluidic shear force, the flow velocity (u) according to the height is simulated by CFD-ACE+ (ESI-CFD, Inc.). In this simulation, an experimented microchannel 20 μm high and 2 mm wide was designed, and the result is plotted in Figure 3.4 (a). With this designed microchannel, various flow velocities were simulated to characterize the fluidic shear force applied to the CNT. After calculating the profile of the flow velocity inside the microchannel, the velocity profile was utilized to calculate the fluidic force with Eq (2). By applying the values of a 3 μm length and 20 nm diameter, which were the dimensions of the simplified model of the CNT, the fluidic force acting on the CNT at a flow velocity of 4.2 mm/min was simulated according to the height of the microchannel, as plotted in Figure 3.4 (b).

3.2.3 Critical height

The simulated magnetic force and the fluidic shear force were used to determine the critical height at which the fluidic shear force was the same as the attractive magnetic

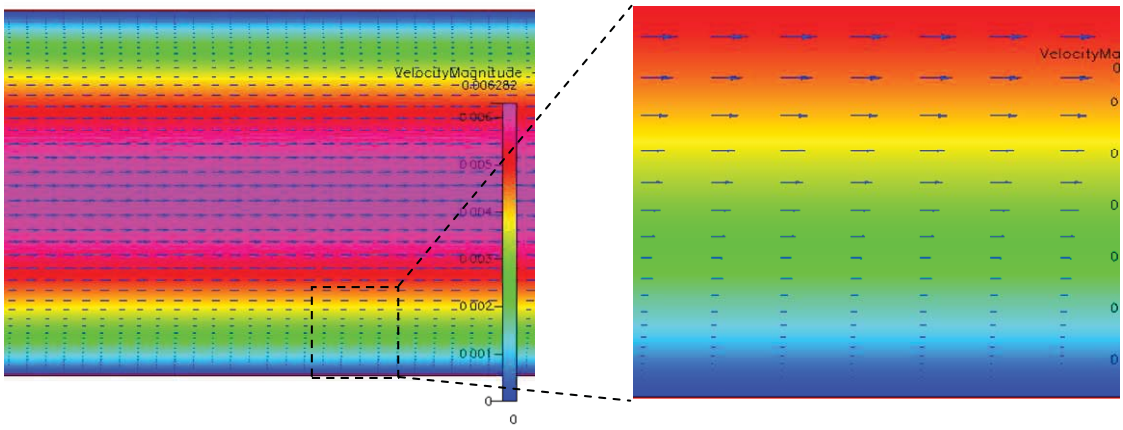

(a)

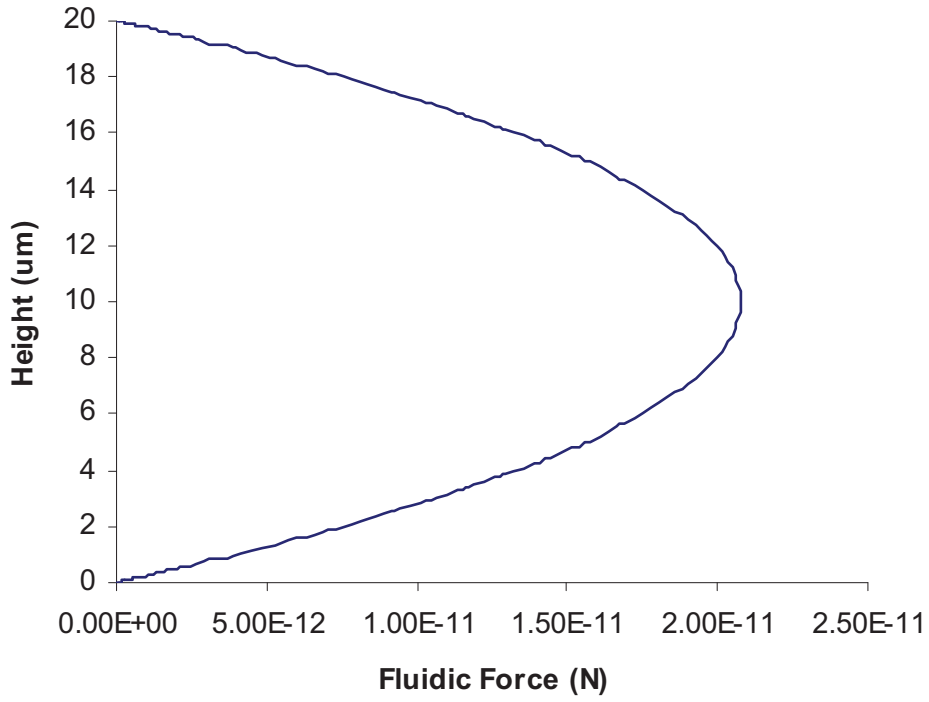

(b)

Figure 3.4 Fluidic simulation by CFD-ACE+: (a) Cut view of simulated flow velocity in a microchannel (20 μm thickness and 2 mm width); and (b) Fluidic force to the CNT according to the height at the flow velocity of 4.2 mm/sec. The slender-body theory was applied to simulate the flow velocity inside a microchannel.

force for capturing CNTs. As illustrated in Figure 3.5, the CNTs are captured at positions in which the magnetic force is stronger than the fluidic force, which occurs below the critical height. On the other hand, CNTs flow away at positions where the fluidic force is higher than the magnetic force, which occurs above the critical height. Another important result involves the size of the Ni patterns. The simulation result shows that as the Ni pattern becomes longer, the induced magnetic force increases. Consequently, the critical height is also increased, thus the longer Ni pattern captures more CNTs and increases the number of attached CNTs.

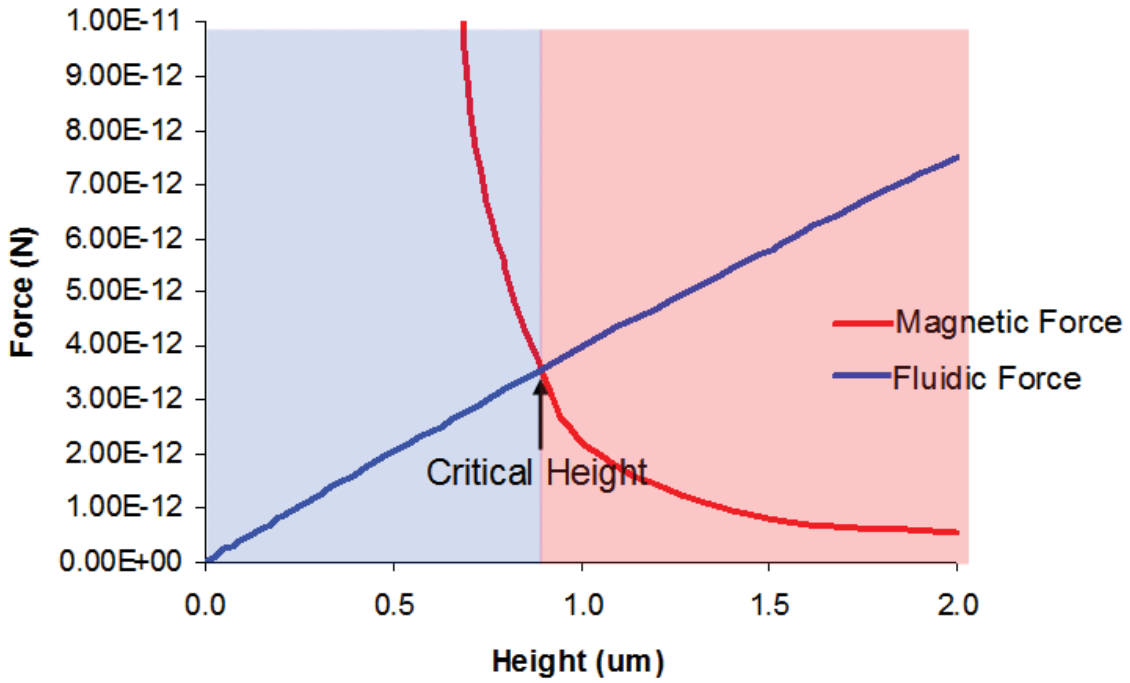

Figure 3.5 The simulated magnetic force and the fluidic shear force as a function of height above the Ni pattern. The critical height for capturing CNTs can be determined where the magnetic force is equal to the fluidic shear force.

3.3 COMPARISON WITH EXPERIMENTAL RESULTS

The number of attached CNTs is calculated from the simulated result of critical height. For this calculation, an effective zone is defined as an area where the CNTs are attracted to the Ni pattern by a higher magnetic force than the fluidic force. The effective zone is simply calculated as an area of a half circle with a radius of the critical height. A portion of the effective zone in the cross-sectional area of the microchannel is multiplied by the total volume of the solution that has flowed through the microchannel. This results in a flown volume of CNT solution passing through the effective zone, which is the effective volume of the CNT solution to be captured at the Ni pattern. Finally, this effective volume of flown solution is multiplied by the density of the CNT in the solution, leading to the calculated number of attached CNTs at the Ni pattern. From this analysis, the attached number of CNTs is plotted according to the flow velocity, Figure 3.6 (a), and the magnetic force, Figure 3.7 (a).

Compared to the simulation result, the number of assembled CNTs was experimentally quantified to characterize the assembly efficiency, in terms of magnetic force and flow velocity. Figure 3.6 (b) shows the experimental analysis of magnetic force by counting the number of attached CNTs at 100 Ni patterns that have different lengths of 0.2 μm, 0.5 μm, 1 μm and 2 μm with a fixed width of 0.2 μm and thickness of 0.l μm. The result shows that increasing the length of the Ni patterns allows the capture of more CNTs, which agrees with the result obtained from simulation as shown in Figure 3.6 (a).

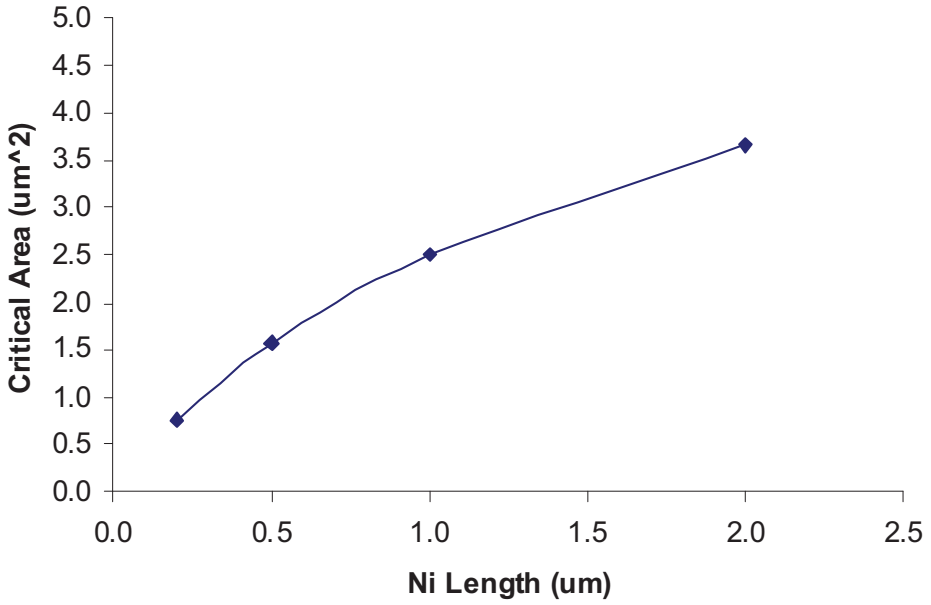

(a)

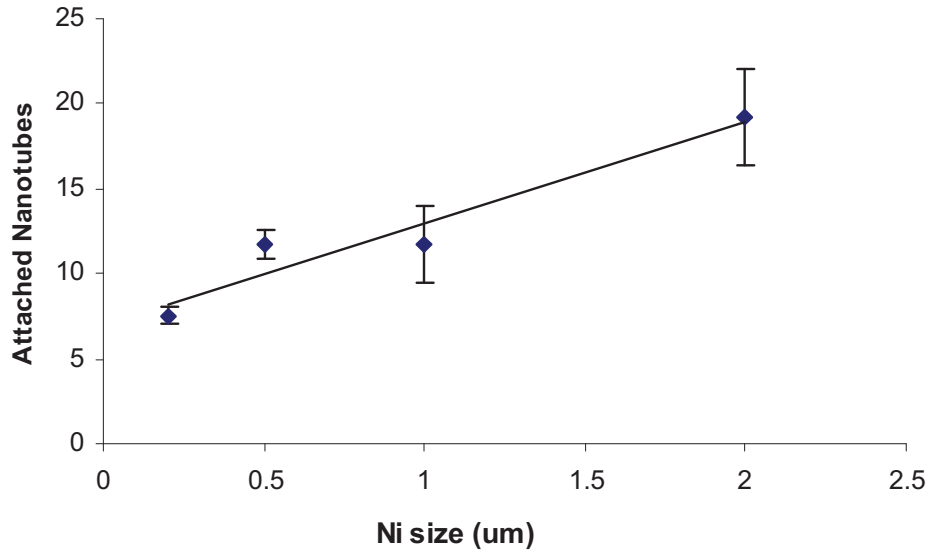

(b)

Figure 3.6 Number of attached CNTs at different lengths of 25 Ni patterns using flow velocity of 4.2 mm/sec: (a) Simulation result and (b) Experimental result.

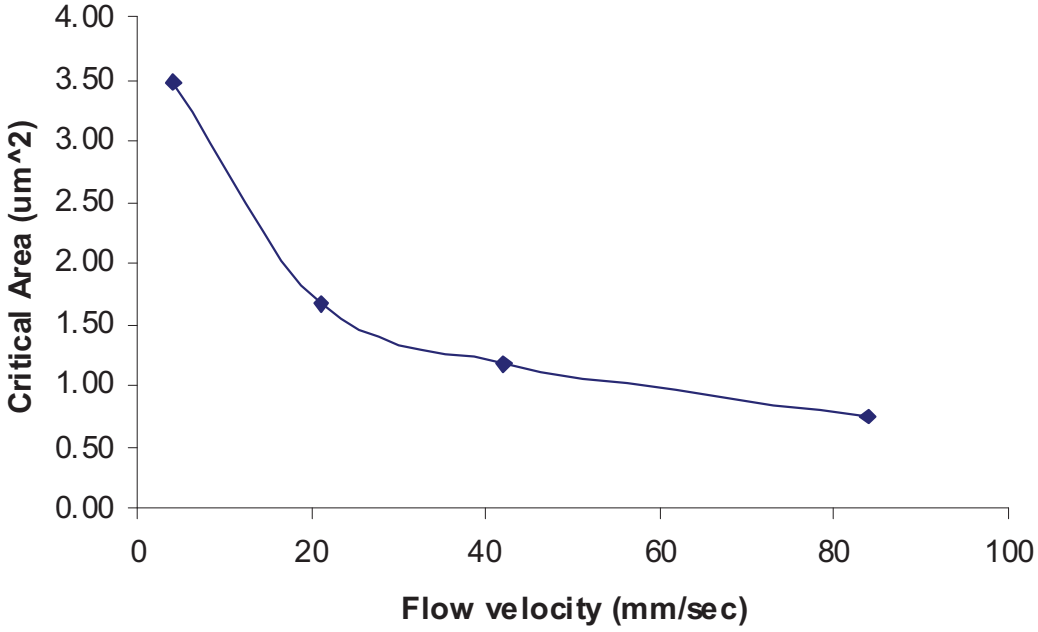

(a)

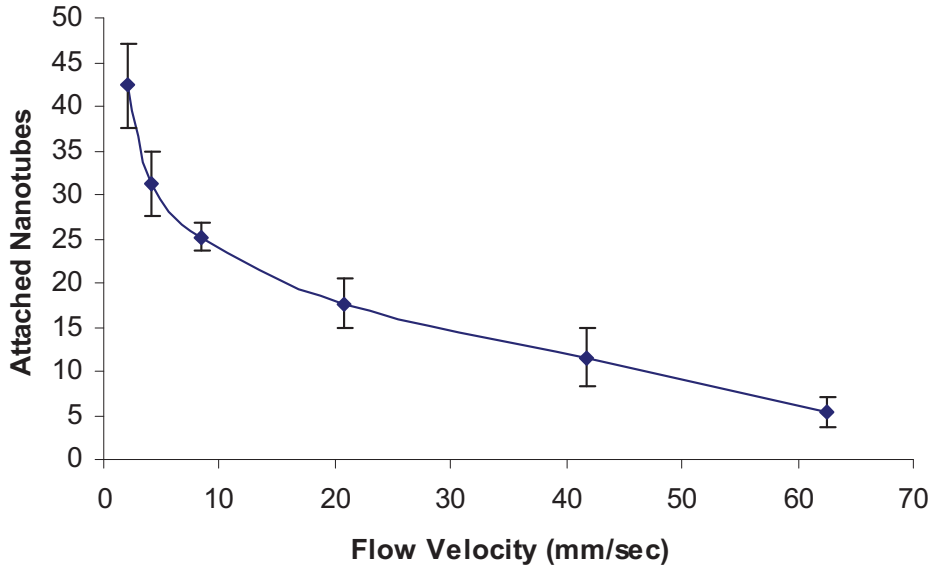

(b)

Figure 3.7 Number of attached CNTs at 25 Ni patterns with 2 μm length as a function of flow velocity: (a) Simulation result and (b) Experimental result.

Additionally, the effect of the flow rate on the quantity and alignment of the assembled CNTs was characterized. To investigate the fluidic effect, the number of CNTs attached at 25 Ni patterns with a 2 μm length was quantified and the results are shown in Figure 3.7 (b). The result shows that higher flow rates caused a reduction in the number of attached CNTs. Likewise, when the flow rate was lower, an increased number of CNTs were assembled on Ni patterns. Because fluidic shear force on the CNT is proportional to the velocity of the surrounding flow, the number of assembled CNTs is inversely proportional to the flow velocity.

The experimental result also showed that a higher flow rate results in a better alignment of the assembled CNTs to the flow direction. Because a higher flow rate applied a higher fluidic shear force to the CNT, the alignment direction of the CNT by surrounding flow is improved at a high flow rate. Therefore, while the flow rate was lowered as more CNTs were captured by the magnetic force, the alignment along the direction of the flow became poor. On the other hand, higher flow rates resulted in a reduced number of CNTs assembled on the Ni contact.

3.4 Optimized Self-Assembly of CNTs

As a result of these analyses, a flow velocity of 4.2 mm/sec was selected to optimize the capture and alignment of CNTs along the flow direction. Additionally, this flow velocity minimized the multiple assembly of the CNTs at a single Ni pattern, and approximately 80 % of the Ni patterns were assembled with a CNT.

To show the feasibility of a complex nanotube-assembled circuit, a sequential array of assembled MWNTs with a high-density interval of 2 μm was achieved, as shown

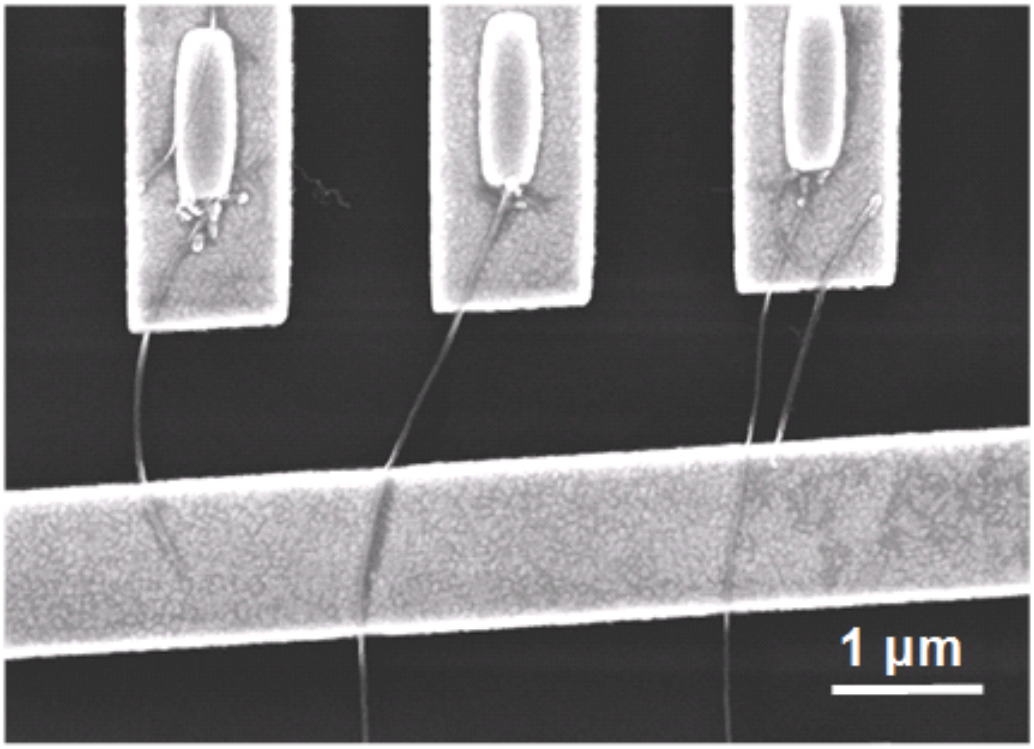

(a)

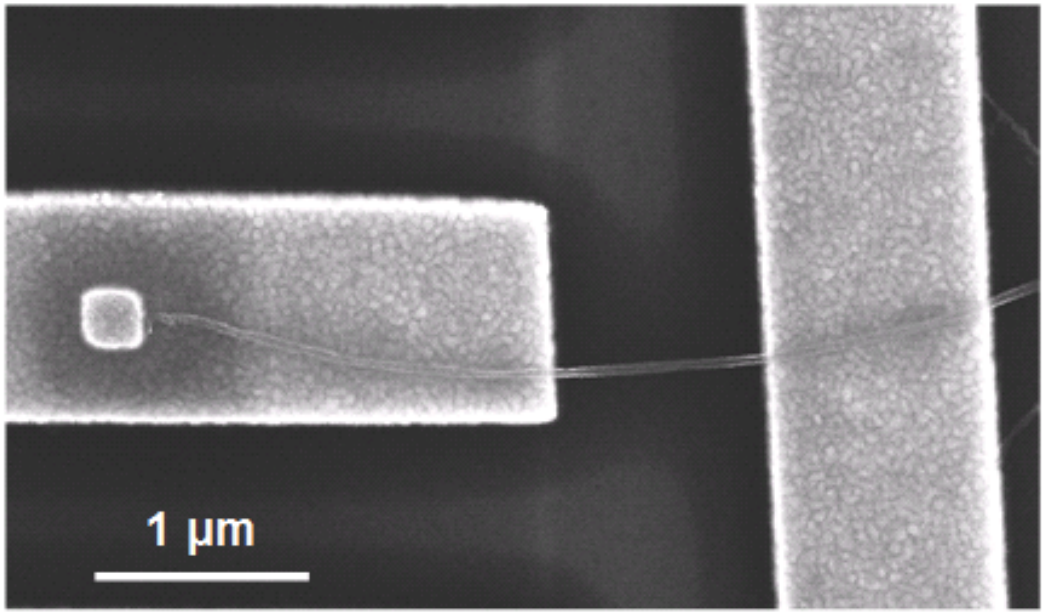

(b)

Figure 3.8 (a) SEM image of sequentially aligned MWNTs array with 2 μm interval and (b) Small dot-type Ni pattern for the assembly of nanotube.

in

Figure 3.8 (a). Ni patterns with dimensions of 200 nm in width and 1 μm in length were patterned on the Au/Ti electrodes by e-beam lithography. The Ni patterns and electrodes were designed to provide 1 μm contact length to each nanotube. The precise assembly of multiple nanotubes shows the feasibility of this technique for the creation of densely assembled nanotube devices.

As shown in the result of magnetic simulation, the concentrated magnetic force occurs at two ends of the Ni pattern. Thereby, the catalyst of nanotube usually attached at these two points. To locate the nanotube at the single target site, the use of a small Ni pattern (200nm by 200 nm, 100 nm thick) was tried for the assembly of the individual nanotube, as shown in Figure 3.8 (b). For the application of a large-scale integration of CNT circuitry, this small dot-pattern of Ni would be very desirable.

3.5 CONCLUSION

In this chapter, a theoretical and experimental characterization was performed to optimize the fluidic and magnetic conditions necessary for the self-assembly of CNTs. Using the average sizes of CNTs in experiments, the CNT was theoretically modeled to simulate the magnetic force and the fluidic force. Based on the simulated results, the critical height for capturing CNTs was calculated. The theoretical results were well matched with the experimental results, showing that a successful analysis was achieved in this work.

CHAPTER 4

SELF-ALIGNED MULTILAYER ELECTRODES WITH NANOGAPS FOR THE FLUIDIC AND MAGNETIC ASSEMBLY OF CARBON NANOTUBES

4.1 INTRODUCTION

Nanoscale components such as nanoparticles, nanowires and carbon nanotubes (CNTs) have shown tremendous potential for applications in electronics, biosensors, and optical devices [89]. In particular, CNTs have their advantages over the other nano-materials in terms of their strong mechanical properties [4, 90], extremely high sensitivity [56, 91], ballistic charge transport [8, 9, 92] and carrying high current density [10,11]. However, the integration of CNTs with electrical connections has been considered as one of the major obstacles which prevent to apply the superior CNT properties to a practical device [65, 66]. Additionally, the fabrication of nanoscale gaps (nanogaps) between electrodes is another challenging issue to achieve the reliable fabrication of CNT-assembled devices [93]. Since a sonication process for dispersing CNTs in a solution results in a tremendous partitioning of CNTs, the average length of dispersed CNTs is usually reduced to a submicrometer range [36-38]. As a result, the development of nanogap electrode is very desirable to ensure the successful connection of the submicrometer length of CNT between two electrodes.

Significant efforts have been made to develop a large-scale fabrication of CNT-assembled functional devices. Depending on the number of assembled CNTs, these works can be categorized into two types of implementation, which are a thin film network assembly of CNTs and an individual assembly of CNTs. The approach with a few layers or a single layer of CNT film has attained a strong advantage of mass-fabrication due to a compatibility with CMOS processes [21,22]. However, the random orientation of the CNT network may causes the loss of the superior electrical property of CNTs such as fast electron mobility and high transconductance. Although a horizontally aligned CNT

network makes up for these weaknesses, the synthesis of aligned CNT network should be processed on a sapphire or quartz substrate, which requires transferring the grown CNTs to a proper substrate through the expensive procedure of thick gold film deposition [23, 24]. In the case of individual CNT assembly, the excellent properties of CNTs can be fully exploited, and the cost of implemented device is low due to a small quantity of CNTs. To achieve the precise assembly of the individual CNTs, various approaches have been explored utilizing dielectrophoretic force [25,26], chemical template [27], and magnetic force [28]. However, there are still large demands for the development of simple assembly technique without modification of CNTs and connection of electrical power to each electrode.

Previously, we demonstrated the precise fluidic assembly of individual CNTs by magnetically capturing residual Fe catalyst [94]. In this technique, while the solution containing CNTs flows over a Ni-patterned electrode, the residual Fe catalyst at the one end of the CNT is magnetically attracted to the Ni pattern, which induces magnetic force under an external magnetic field. Then, a fluidic shear force from the surrounding flow aligns the CNT along the flow direction. This assembly technique does not require a pretreatment of the CNTs, so the full functionality of pristine CNTs can be attained. Also, compared with the dielectrophoretic (DEP) assembly of CNTs [32,93], it is not necessary to connect an external power source to the electrodes, and the geometrical shape of the electrode is not required for the concentration of the electric field at the end of electrodes. Furthermore, this technique does not have a preference for a metallic CNT over a semiconducting CNT, and thus, multiple transistors only using the semiconducting CNTs can be built after filtration of the metallic CNTs [35, 68]. However, this method requires

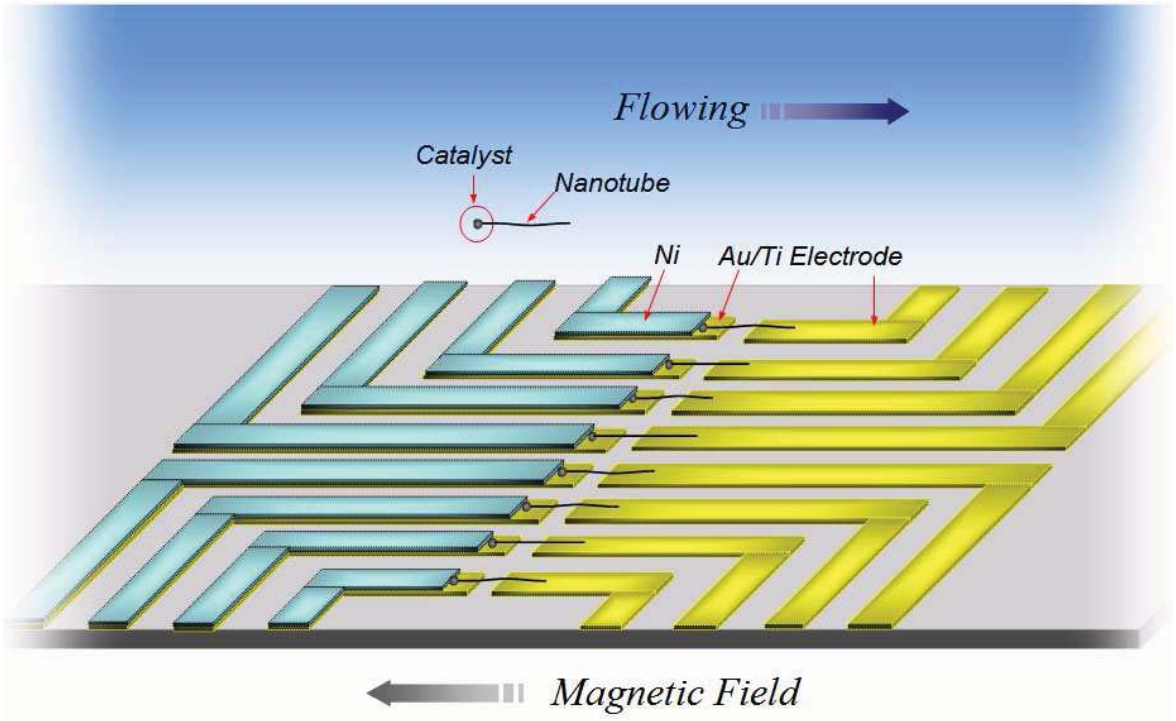

Figure 4.1 Illustration of fluidic self-assembly of CNTs by magnetic attraction on a residual iron catalyst. A self-aligned Ni pattern on the nanogap electrode induces magnetic force under an external magnetic field and localizes the placement of CNT between two electrodes.

an expensive fabrication process using E-beam lithography to achieve a nanogap between electrodes and a precise alignment between Ni and Au/Ti electrodes.

In order to overcome these difficulties, we have explored and developed a new approach to fabricate self-aligned electrodes using optical lithography for the magnetic and fluidic self-assembly of CNTs as illustrated in Figure 4.1. The developed technique allows precise alignment between Ni and the Au/Ti electrode with nanoscale dimensions by the self-aligning method. Furthermore, this method can be completed using i-line optical lithography (365 nm wavelength of UV light source) with Shipley photoresist, which is usually available from most clean room facilities. As a result, this approach

enables an inexpensive and simple process to fabricate the nanogap electrode, leading to an effective self-assembly of CNTs for the mass production of functional nanodevices.

4.2 PRINCIPLES

In this work, a precisely controlled undercut was adopted to fabricate the self-aligned pattern and the nanogap electrode as described in Figure 4.2. During the isotropic wet-etching of the metal layer, the undercut is generated underneath a lithographically patterned photoresist. After the formation of the undercut during the metal etching, the photoresist on the undercut-etched metal layer is preserved until a directional deposition of a second metal layer by E-beam evaporation. Due to the undercut of the first etched metal layer, the directional deposition of the second metal layer produces a small gap between the first etched layer and the second deposited layer [95]. As a result, the nanogap electrode can be fabricated with this simple approach, and the length of the gap between the electrodes can be controlled by adjusting the etching time of the first patterned metal layer.

This method of controlled undercut and metallization is extended to achieve the self-aligned multilayer electrode with nanogaps for the self-assembly of CNTs. After depositing multiple metal layers, the undercut-etching is completed with selective metal etchants for each metal layer. The selective etching for each metal layer is controlled to produce the designed gap between layers, which results in the aligned pattern on the electrode with nanoscale dimensions. Then, the final metal deposition on the masked photoresist is performed, and finally the small gap of electrodes with the aligned pattern is achieved with nanoscale precision. In this procedure of self-alignment, the aligned

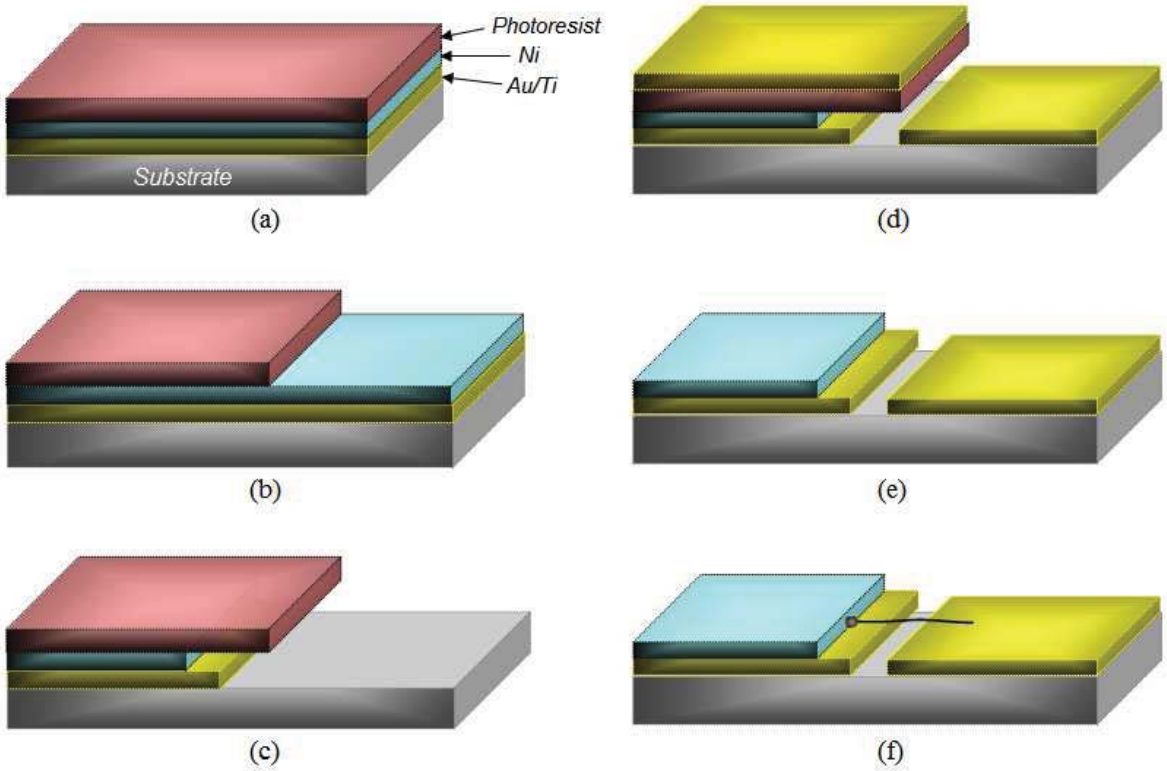

Figure 4.2 Fabrication procedures: (a) Spin-coating photoresist on Ni/Au/Ti deposited SiO_2/Si substrate; (b) Photoresist patterning; (c) Undercut etching of Ni and Au/Ti; (d) 2nd Au/Ti deposition; (e) Lift-off the upper layer on the photoresist; and (f) Fluidic self-assembly of CNT by magnetic attraction on a residual iron catalyst

distance between each pattern is precisely adjusted by the controlled undercut. Consequently, the nanoscale alignment is simply achieved by controlling the etching time for the undercut without any complex or difficult aligning procedures.

4.3 DESIGN AND FABRICATION

To fabricate a functional nanogap electrode with this technique, Ni and Au/Ti layers have been selected to implement a precise self-assembly of CNTs on the electrode.

To make a self-aligned Ni pattern on the electrode, the Ni layer was deposited on the Au/Ti layer and then each layer was etched with the generation of undercut. After the second deposition of Au/Ti, the subsequent lift-off process finalized the fabrication of the functional nanogap electrode for the CNT assembly. The aligned Ni layer was utilized to induce the magnetic force under an external magnetic field, and attracted the residual Fe catalyst at one end of the CNT. Then, the captured CNT at the edge of the Ni layer was assembled on the Au/Ti electrode in the flow direction due to the fluidic shear force. Considering the submicrometer size of the CNT, the Ni layer was patterned to have a nanoscale distance from the gap of the Au/Ti electrodes, allowing the assembled CNT to bridge two Au/Ti electrodes.

To achieve a smooth and uniform edge on the undercut, photoresist patterning was carefully carried out. Hard baking of the photoresist resulted in the generation of a non-uniform undercut and long exposure yielded a rough sidewall of patterned photoresist. As a result, each step for photoresist patterning needed to be properly processed. The photoresist of Shipley 1818 (S1818; Rohm and Haas Electronic Materials, LLC.) was spin-coated on the substrate at 4000 rpm for 30 seconds, followed by soft baking inside an oven at 90°C for 20 minutes. After exposing it to 365 nm of UV wavelength for 10 seconds with an intensity of 8.5 mW/cm^2, the photoresist was developed in a 1:5 mixture of M-351 and DI water for 90 seconds. A hard baking step of S1818 was not performed in our procedures because the undercut etched patterns had a rough edge after hard baking.

Detailed procedures for the suggested fabrication are described in Figure 4.2. First, Ti (10 nm), Au (50 nm) and Ni (100 nm) were sequentially deposited on a SiO_2/Si

substrate. Standard optical lithography with a medium-quality mask, which had a minimum feature size of 10 μm, was processed. With the patterned photoresist, the Ni layer was etched at room temperature by the etchant, which was a mixture of nitric acid (HNO_3), acetic acid (CH_3COOH) and DI water with a ratio of 1:1:1. After the first etching of the Ni layer, gold etching was performed at 50 °C with a mixed solution of iodine (40 g), potassium iodine (10 g) and DI water (400 ml). The second Ni etching was completed for the fabrication of the Au/Ti contact area by increasing the undercut of the Ni layer at the Ni/Au/Ti electrode. Followed by the formation of these controlled undercuts, a second metal layer of Au/Ti (50 nm/ 10 nm) was directionally deposited by e-beam evaporation, finally achieving the gap between the first etched layer and the second deposited metal. An SEM image of the fabricated nanogap electrodes is shown in Figure 4.3 (a). The resolution limit of this technique has been achieved at up to 250 nm in this work, and the etched edge of each layer had a roughness of 50 nm. To reduce the resolution limit and the roughness of the etched edges of the electrodes, various etching conditions could be tried in future work, using the optimized concentration, type, temperature, and stirring rate of the etchant. After this gap fabrication, five pairs of electrodes with self-aligned Ni were fabricated to implement an array of CNT-assembled electrodes, as shown in Figure 4.3 (b). Each electrode was 10 μm wide, and the self-aligned Ni pattern had dimensions of 500 μm in length, 10 μm in width and 0.1 μm in thickness on top of the Au/Ti electrodes.

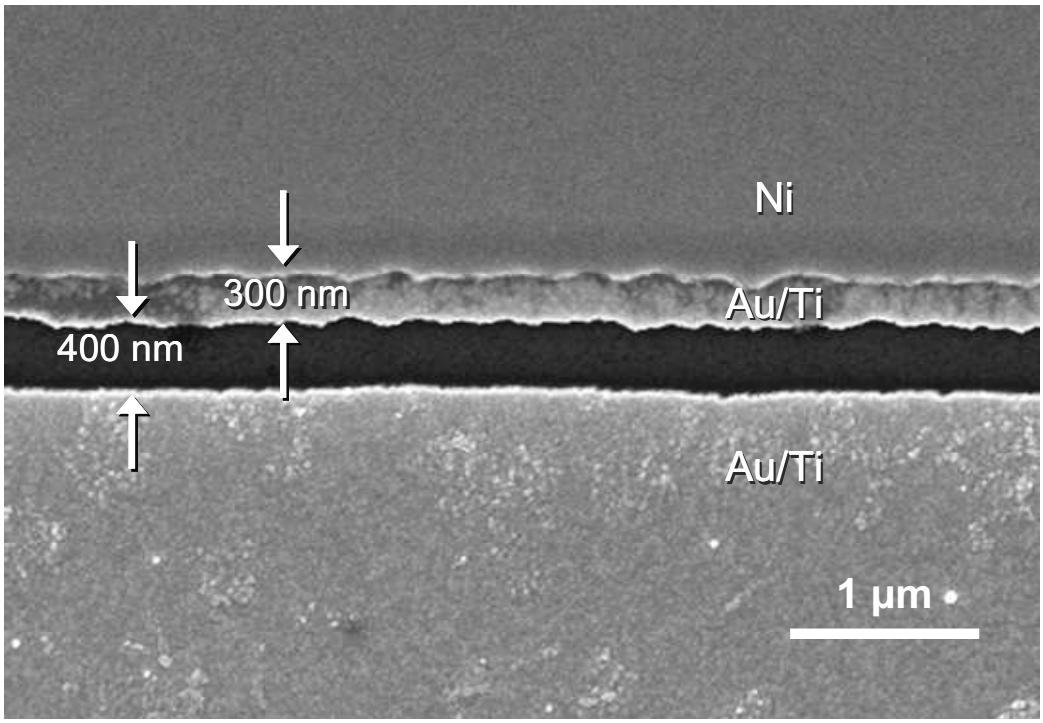

(a)

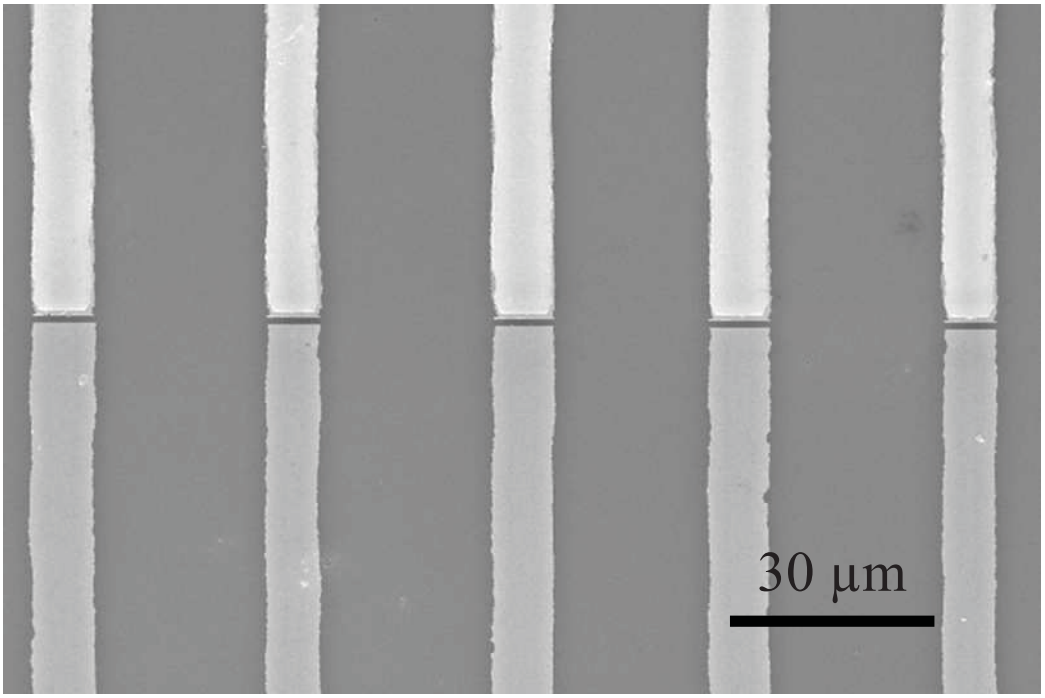

(b)

Figure 4.3 SEM images of (a) fabricated multi-layer nanogap electrode and (b) 5 pairs of electrodes.

4.4 EXPERIMENT DETAILS

The grown CNTs were dispersed in a surfactant solution, which was a mixture of 1 wt% Tween 20 (Sigma-Aldrich Co.) in DI water. In this dispersion process, bundles of CNTs in the surfactant solution were sonicated for 30 min in an ultrasonic bath (Branson Ultrasonics Corp.). To filter out metal impurities, CNT arrays were dispersed in an insufficient volume of surfactant solution for 30 minutes. Due to the lack of surfactant to cover the CNT surface, the dispersed CNTs gradually regenerated bundles over the course of time. Consequently, when the solution with dispersed CNTs was placed on a magnet, the metal impurities magnetically precipitated to the bottom of the container, and the bundles of CNTs were selectively separated with the impurities [94]. After placing the CNT solution on the magnet for one week, the bundle of CNTs were carefully

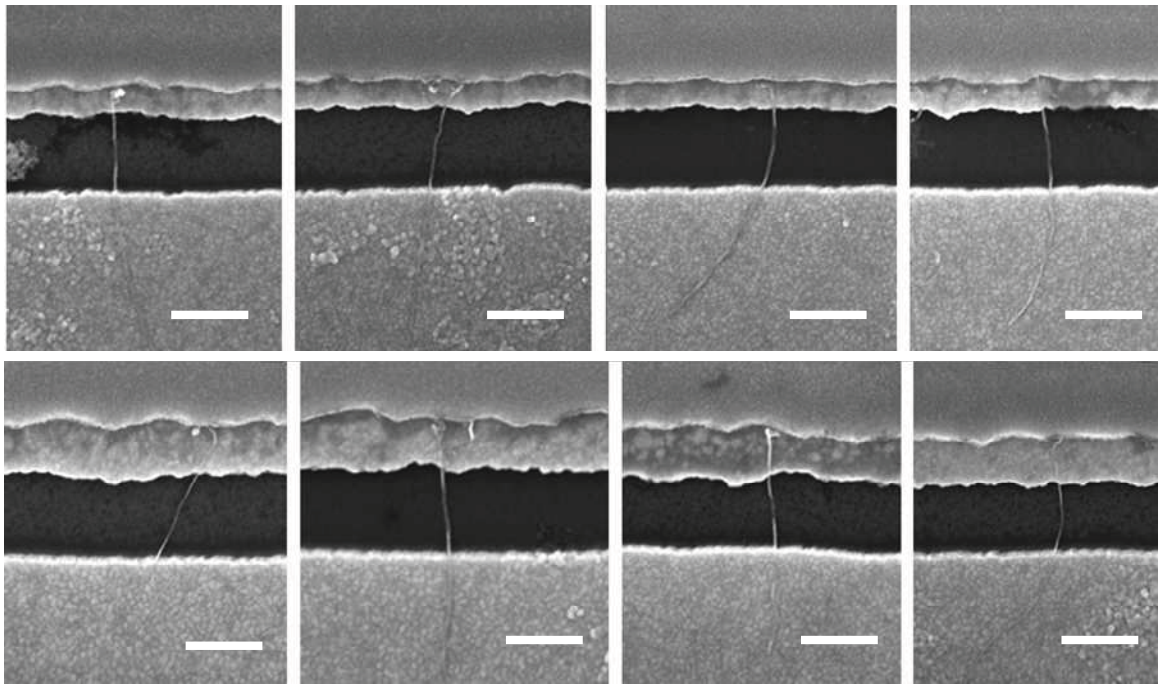

Figure 4.4 SEM image of assembled CNT between multilayer nanogap (500 nm scale bar).

pipetted and dispersed again in a sufficient volume of surfactant solution. A microchannel 20 μm thick and 2 mm wide was fabricated by soft lithography using PDMS on the mold of the photoresist (AZ 4620). After the assembly of the CNT on the electrode, the PDMS microchannel was detached from the substrate for SEM detection and electrical characterization.

Once the solution containing the dispersed CNTs was introduced to the Ni self-aligned electrodes, the substrate was dried at room temperature under the external magnetic field, which prevented a possible detachment of the CNT while drying. When the CNT solution flowed through the microchannel, an external magnetic field of 0.7 T was applied to the Ni patterns. A flow rate of 4.2 mm/sec was selected for magnetically capturing the Fe catalyst with the appropriate fluidic alignment of CNTs. Figure 4.4 shows SEM images of assembled CNTs at the edge of the Ni pattern on Au/Ti electrodes by the developed technique.

4.5 RESULTS AND DISCUSSION

4.5.1. Magnetic field analysis

During the assembly procedures for the CNT, the Fe catalyst at the end of the CNT is locally captured at the edge of the Ni pattern, because the induced magnetic force by the Ni pattern is strongly generated at the edge by a high gradient magnetic field. The induced magnetic force by the Ni pattern is represented as

$$F = (m \cdot \nabla)B \tag{1}$$

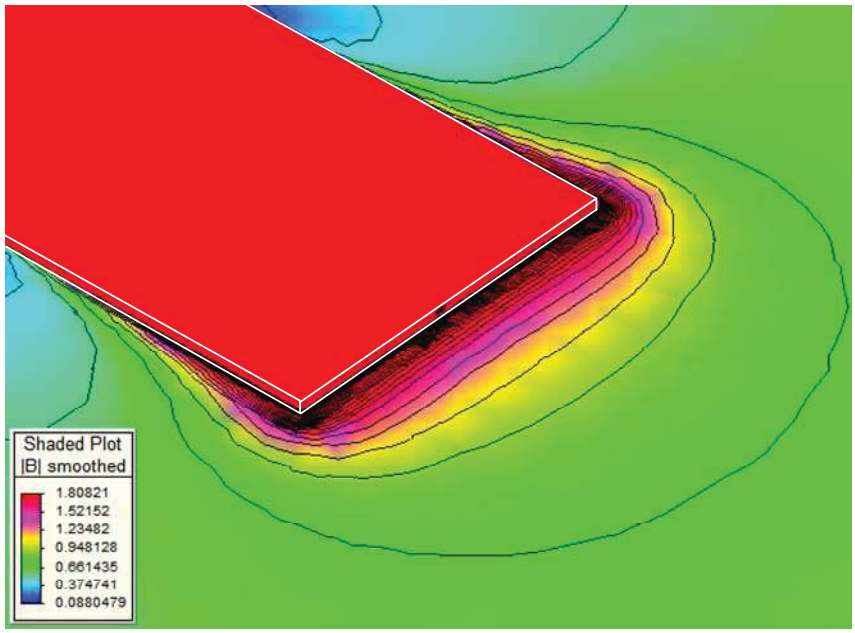

(a)

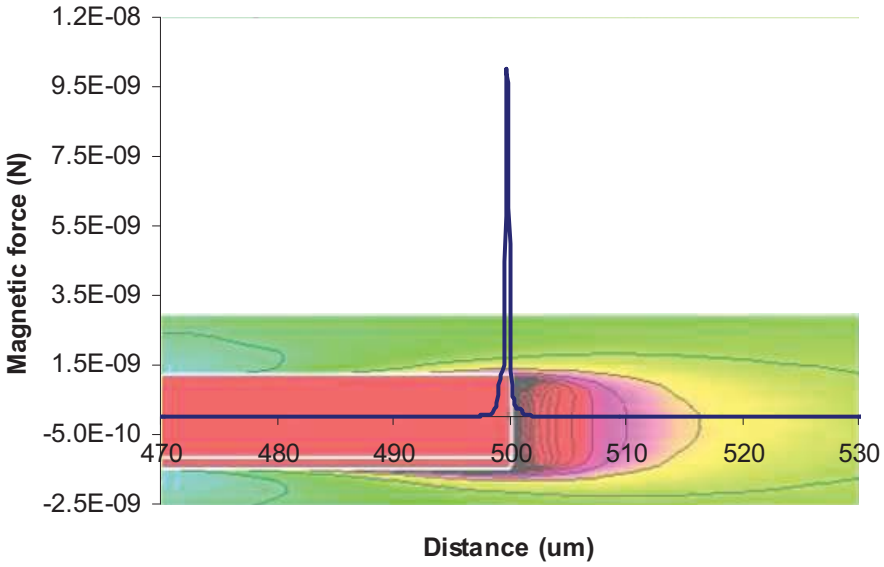

(b)

Figure 4.5 FEM simulation of magnetic field at the edge of Ni pattern (10 μm width, 500 μm length and 0.1 μm thickness) under the external magnetic field of 0.7 Tesla: (a) Magnetic field distribution; and (b) Localized peak of magnetic force at the edge of Ni pattern.

,where m is a magnetic momentum ($A \cdot m^2$) of the Fe catalyst and B is the magnetic field (Tesla) around the Ni pattern [84]. As shown in this equation, the magnetic force is linearly proportional to the gradient of the magnetic field. With the same dimensions of the experimented Ni pattern, FEM simulation (MagNet, Infolytica Inc.) was performed under the external magnetic field of 0.7 Tesla for the characterization of the induced magnetic force at the Ni pattern. Figure 4.5 (a) shows that the contour lines of the magnetic field is very dense at the edge of the Ni, representing the high gradient of the magnetic field. Due to this gradient profile of the magnetic field, the high magnetic force is locally generated at the edge of the Ni pattern as plotted in Figure 4.5 (b). As a result, the Fe catalyst of the CNT is magnetically captured only at the end of the Ni where the magnetic force has a peak value.

Due to this localized placement of the CNT, the distance from the edge of the Ni layer to the electrode and the gap between the electrodes are important factors for achieving the successful assembly of CNTs between two electrodes. If the Ni pattern is distant from the gap of electrodes, the assembled CNT will not successfully bridge the electrode gap. Additionally, if the gap between the electrodes is larger than the length of the CNT, the assembled CNTs cannot cross over two electrodes. For these reasons, the patterning of the Ni pattern and the gap of the electrode need to be designed to have a proper length by considering the average length of CNTs. Due to the shortening of CNTs to a submicrometer length during the dispersion process, the nanoscale distance from the edge of the Ni layer to the electrode gap and the nanogap between two electrodes were designed and fabricated to successfully assemble CNTs.

4.5.2. Self-aligned multilayer electrodes

To create this self-aligned Ni pattern on the electrode and adjust the gap between electrodes with nanoscale precision, the time-dependant generation of the undercut for Ni and Au was carefully monitored and characterized as plotted in Figure 4.6 (a) and (b), respectively. The generation rate of the undercut was dominated by the mass transport of etching molecules to the metal layer, because molecular transport is geometrically restricted by the patterned photoresist on the metal layer. There were three phases of the undercut-etching rate as the etching time increased [96]. As the etching first started, there was no or very little, generation of the undercut. During the second phase, the undercut was rapidly increased with a constant slope, where the precise control of undercut generation was necessary. As the undercut generation was increased, the generation rate slowed down in the third phase.

Fick's first law of diffusion was adopted to explain these rate changes in undercut generation, according to the etching time. From Fick's first law, the diffusion flux (J) is defined as

$$J = -D\frac{\partial \phi}{\partial x} \qquad \text{(Eq. 3.1)}$$

, where D is the diffusion coefficient (m^2/s), Φ is the concentration of etching molecule (mol/m^3), and x is the diffusion length (m). For the first period, most of the etching molecules in the etchant are consumed away as soon as they contact the patterned open area of the metal layer. Due to the rapid consumption of etching molecules, the concentration of active etching molecules is low, which reaches to the metal film under the photoresist. As a result, the reduced concentration (low Φ) of etchant results in a very slow undercut generation in the first phase. After the metal layer in the open area is

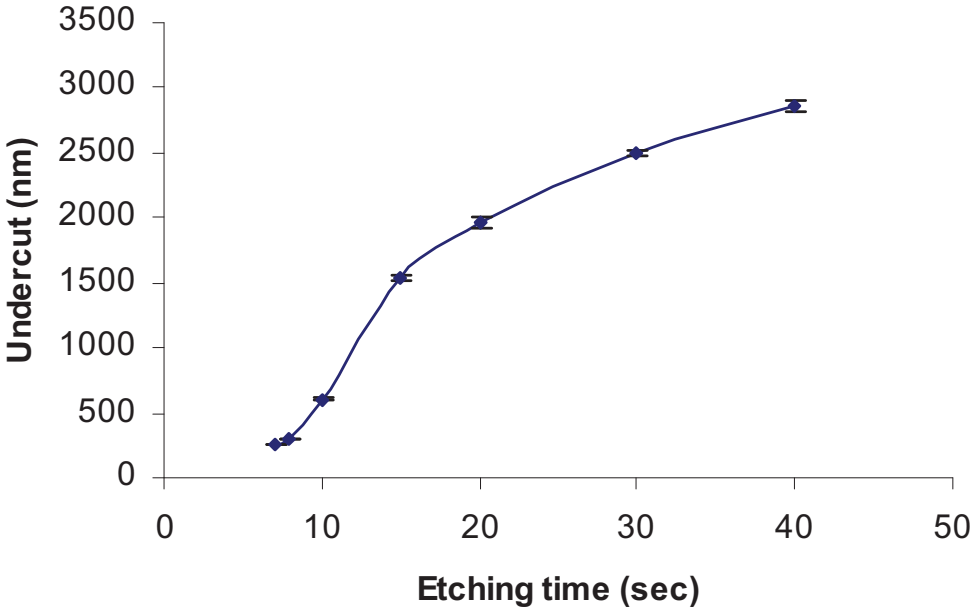

(a)

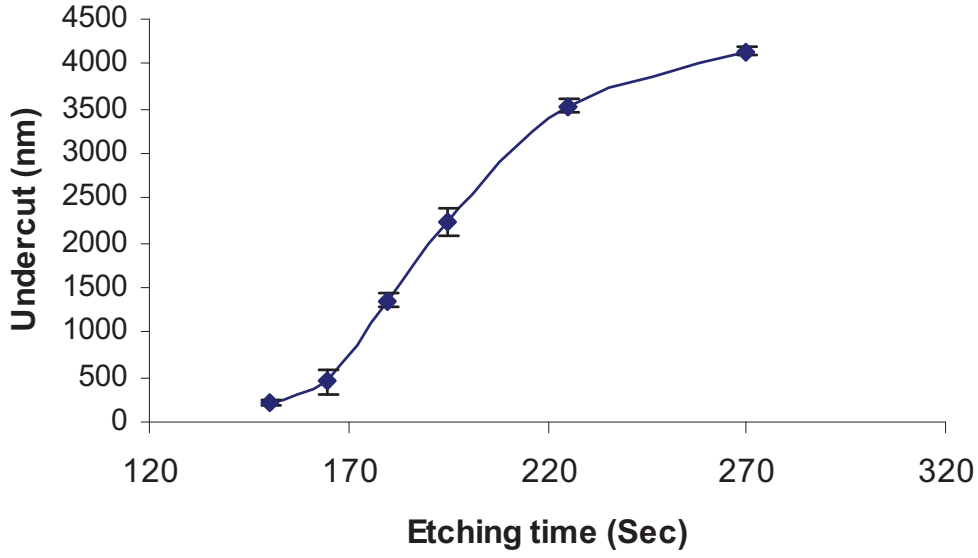

(b)

Figure 4.6 Undercut generation of (a) Ni and (b) Au according to etching time. There are three phases for the generation rate of undercut due to the mass-transport limited process.

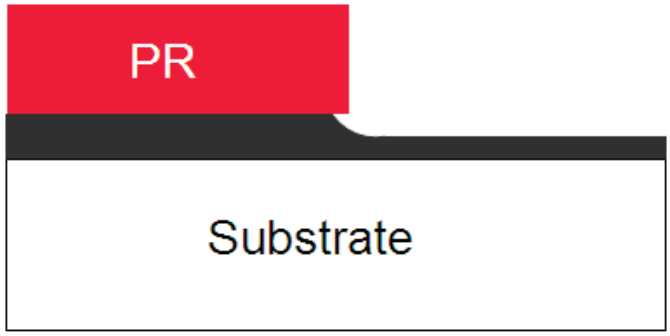

(a)

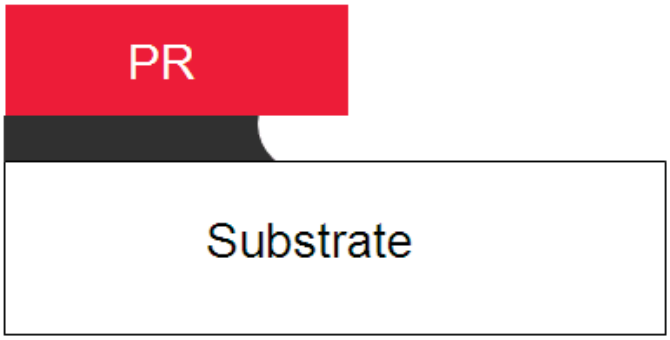

(b)

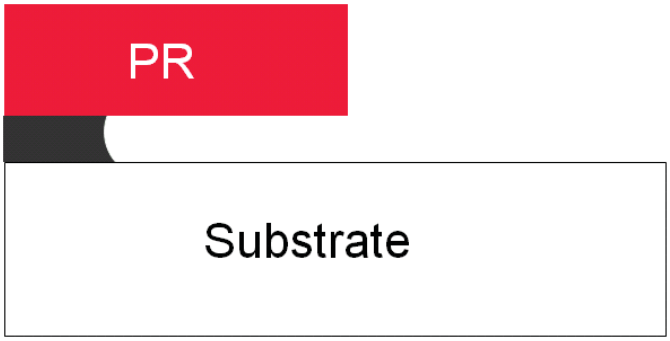

(c)

Figure 4.7 Three phases of undercut generation according to the etching time: (a) First phase of open area etching; (b) Second phase of rapid generation of undercut; and (c) third phase of limited mass-transport of etching molecule.

etched out, the undercut rapidly increases because the consumption of the active etching molecules stopped in the open area of the metal layer. Therefore, concentrated etchant (high Φ) massively diffuses under the photoresist. In this second phase, the length of the undercut should be carefully controlled by monitoring the etching time. Finally, the mass-transport of etching molecules is limited by the spatial restriction of the narrow gap under the photoresist, which has the same thickness as the etched metal layer. This spatial restriction increases the diffusion length (x) of the active etching molecules to reach the metal layer under the photoresist. Thus, the undercut is slowly generated and finally saturated. Based on these characterizations of undercut generation according to etching time, nano-scale fabrication was accomplished by carefully monitoring the etching time. As a result, the nano-scale fabrication of gap (400 nm) and alignment distance (300 nm) was designed and successfully achieved in this work in order to assemble the sub-micron length of CNTs.

4.5.3. Characterization of CNT connections

The volume of flowed CNT solution affects the number of assembled CNTs and the yield of the successful connection of CNTs between electrodes. Based on the previous characterization of flow velocity, the flow velocity was fixed at 4.2 mm/sec [94]. Then, different amounts of CNT solution flowed on Ni patterns to characterize the number of assembled CNTs at the Ni pattern and the yield of CNT connections between electrodes. After the CNT solution flowed on the electrodes, the assembled CNTs at 5 Ni patterns were counted with respect to the flowed volumes of CNT, as shown in Figure 4.8 (a). The result shows that more CNTs are assembled on the electrode, as the increased

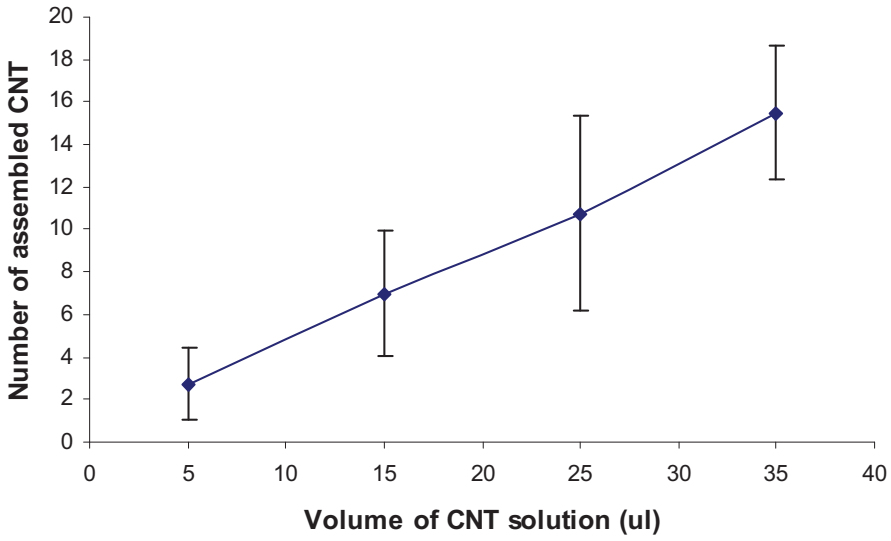

(a)

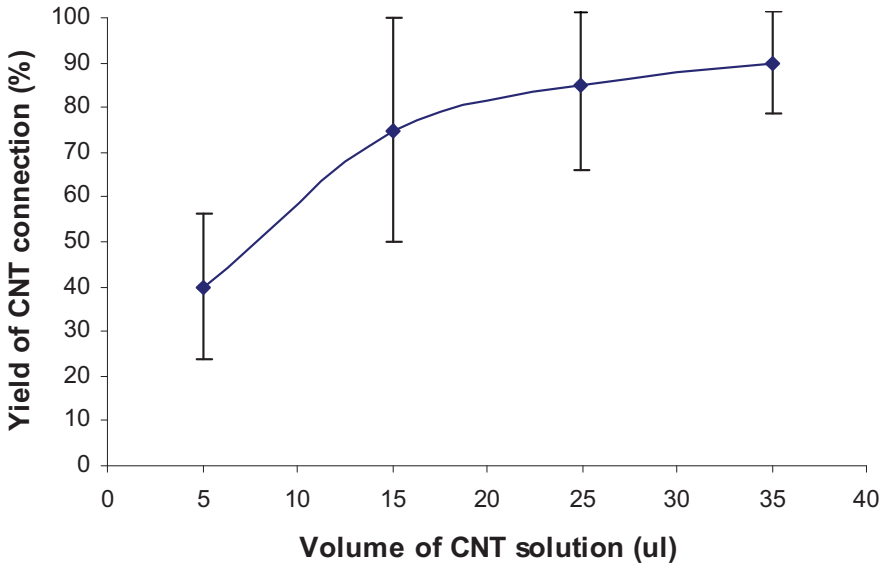

(b)

Figure 4.8 The effect of flowed volume of CNT solution: (a) The number of assembled CNT at 5 Ni patterns with respect to the volume of CNT solution; and (b) The yield of CNT connection between electrodes depending on the flowed volume of CNT solution.

volume of CNT solution flowed on the Ni patterns. Also, the yield of the CNT connection between electrodes was calculated for different volumes of CNT solution by counting the successful CNT connection between electrodes among the 5 pairs of electrodes. As shown in Figure 4.8 (b), the probability of a successful CNT connection is increased when larger volumes of CNT solution flow over the electrode. As a result, a large amount of CNT flow ensures the successful bridging of CNTs between the electrodes, but it also results in the assembly of multiple CNTs on a single electrode pair.

4.5.4. Electrical characterization

On the fabricated electrodes, both metallic MWNTs and semiconducting SWNTs were successfully assembled. Because the electrical response from the assembled CNTs was not stable before the annealing, the I-V characteristic were measured after the annealing procedure by a rapid thermal process (RTP; AG Associates, Inc.) at 350 °C with N_2 flowing for 5 min. This annealing step also reduced the contact resistance between the CNTs and the electrodes and resulted in a stable electrical response. After the annealing procedure, I-V measurements were performed for the electrical characterization of the assembled CNTs.

As plotted in Figure 4.9 (a), the measured electrical result for the assembled metallic MWNTs shows stable ohmic behavior. Figure 4.9 (b) shows a non-linear I-V response between the SWNT and the metal electrode, demonstrating that the assembled SWNT has a semiconducting property. Since the contact between a semiconductor and a metal forms a schottky junction, a back-to-back schottky diode is formed at the contacts between the SWNT and the electrodes.

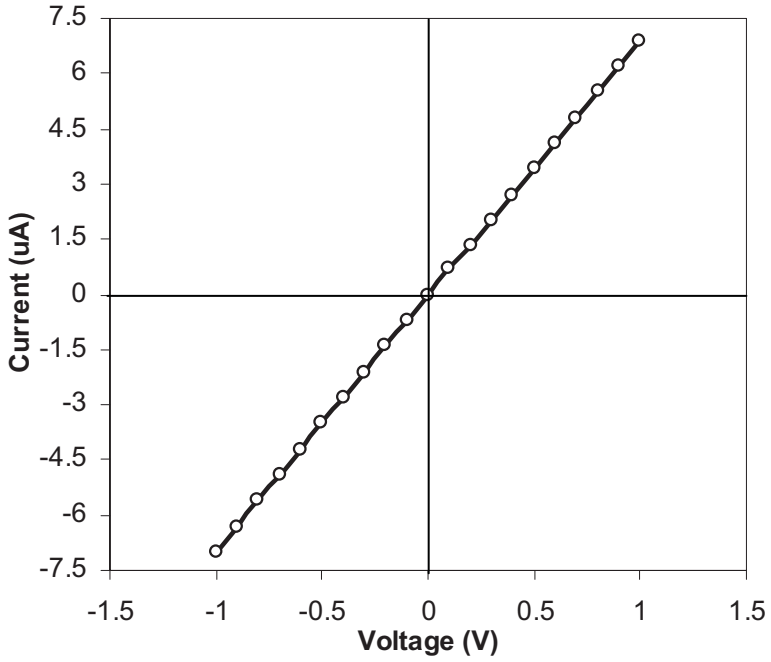

(a)

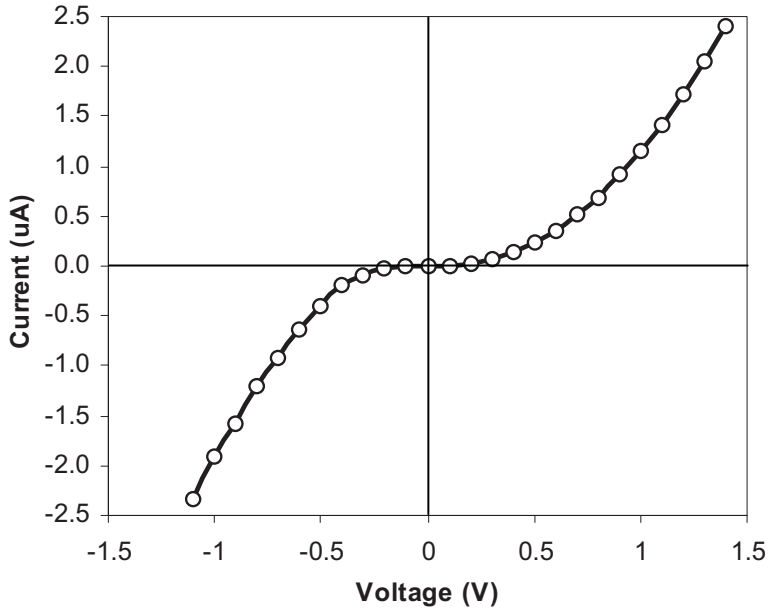

(b)

Figure 4.9 Measured I-V curve for the individually assembled (a) metallic MWNT and (b) semiconducting SWNT.

4.6 CONCLUSION

In conclusion, a functional nanogap electrode with a self-aligned Ni pattern was successfully fabricated and applied to an individual assembly of CNTs. The fabrication for the nanogap electrode and the assembly of CNTs were fully processed with simple, inexpensive and mass-producible techniques. The pristine CNTs were reliably assembled on the developed nanogap electrode, and they showed stable electrical responses for both metallic and semiconducting nanotubes. As a result, the suggested technique for CNT-assembled electrodes provides an easy and reliable way to implement functional nano-electronic or biosensing devices utilizing the excellent capabilities of CNTs.

CHAPTER 5

AN OPTICAL IMMUNOSENSOR USING CARBON NANOTUBES COATED WITH A PHOTOVOLTAIC POLYMER

5.1 INTRODUCTION

Over the recent decades, carbon nanotubes (CNTs) have been explored for highly sensitive sensors that detect various types of biomolecules such as cells, proteins, and DNA. [18, 19, 21] With the basic structure of the field effect transistor (FET) assembled with an ideal 1D structure of CNT, the charged molecules around the CNT modulate on an extremely narrow current path through the CNT. As a result, the CNT-based biosensors have achieved a highly sensitive detection of target proteins with the simple structure of a device. Additionally, the electrical sensing mechanism can be flexibly implemented with electric components, allowing a miniaturize-sized device and simple steps for measurement. In spite of these advances in the CNT-based biosensors, the realization of a practical biosensor with CNT for clinical diagnosis is still retarded, since the surface of CNT is still hard to be flexibly functionalized for a desired molecular selectivity. Because the FET-type CNT biosensors respond very sensitively to most surrounding charges [56, 97], it is difficult to selectively detect target molecules without interruptions from ions or non-specifically bound proteins in sample solutions.

To improve the selectivity of the CNT biosensor for target molecule, various efforts have been made through functionalizing the surface of CNTs with surfactants [19], proteins [62] and polymers [60, 61]. Particularly, polymers such as PEG (Polyethylene glycol) [60] and PEI (Polyethylenimine) [61] were utilized to completely coat the surface of the CNT, functionalizing it for the selective detection of target proteins. Even though these functionalization techniques of CNT significantly reduced the non-specific binding of proteins, the detection-limit of the functionalized CNT has not yet been proved to show the high sensitivity of CNT [98].

Furthermore, the disturbance from various ions in sample solutions is a more significant challenge for accomplishing a reliable biosensor than control of non-specifically bound proteins. Many reports have shown that the electrical properties of CNTs are easily changed by the interaction of the ionic molecules around CNT [56, 97]. Additionally, since the ionic molecules are much smaller than the proteins, it is more difficult to block the intervention of the ions than the non-specifically bound proteins. Human blood contains various ionic molecules as well as proteins, and therefore the isolation of CNT from these molecules is highly desired for the application of the CNT-assembled device to a clinical diagnosis. As a result, in order to implement a practical biosensor with CNTs, the reliable selectivity without the loss of sensitivity for target molecules has to be achieved.

In this work, an innovative mechanism for the CNT-based biosensor to realize a selective detection of target proteins has been proposed and developed while maintaining high sensitivity. To achieve an excellent selectivity as well as sensitivity, a new optical immunosensor based on CNTs which are covered with photovoltaic polymer, which works like a CNT-based photodetector, has been developed. Chemiluminescent-based immunoassay was directly performed on the CNT photodetector. When the light was produced from the chemiluminescent assay, the generated charges in the photovoltaic polymer were accumulated around the surface of CNT. Consequently, the immunosensor with the CNT photodetector works like an on-chip optical immunosensor. Also, since the CNT photodetector was insulated with Parylene, the noises from ionic molecules were completely blocked. With this configuration of the biosensor, cardiac biomarker (cTnT) could be successfully detected with an extremely low concentration of 12 pg/ml. Thus,

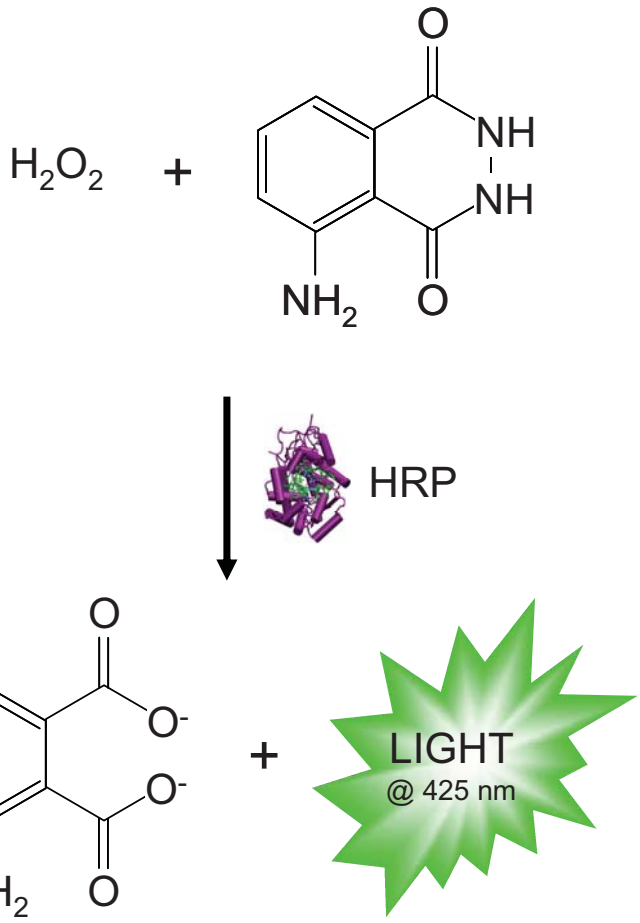

Figure 5.1 Chemiluminescent light generation during immunoassay by catalyzing reaction of HRP.

the FET-type CNT-based immunosensor for point-of-care (POC) clinical diagnostics has been realized for the detection of cardiac biomarkers, including other proteins and peptides.

5.2 PRINCIPLES

5.2.1 Chemiluminescent immunoassay

In order to achieve a high selectivity and sensitivity for target detection, the principle of the proposed biosensor consists of the generation of chemiluminescent light

and the detection of the chemiluminescent light by a CNT photodetector, which were fully performed in an on-chip platform. The commercially available protocol of enzyme-linked immunoassay (ELISA; Femtolight, Inc.) was utilized to generate the optical signal from the target molecule. In this assay, a chemiluminescent enzyme of horseradish peroxidase (HRP) was tagged to the secondary antibody, which could be selectively immobilized on the target antigen. The HRP catalyzes the conversion of an enzyme substrate (Luminol) into the product of a 3-aminophthalate, which decays to a lower energy state by emitting light as shown in Figure 5.1.

The chemiluminescent immunoassay is first performed by functionalizing a substrate with the capturing antibody. While the sample solution flows to the functionalized region, the target antigen in a sample is tethered by the capturing antibody. Because the chemiluminescent enzyme of HRP is conjugated with the secondary antibody, the capturing antibody and the secondary antibody are linked by the target antigen, finally cross-linking the HRP. When this linked HRP reacts with the enzyme substrate, the chemiluminescent light is generated. The intensity of this optical signal is proportional to the number of linked HRPs, which increases as the concentration of the target antigen increases. As a result, the target antigen can be detected through measuring the intensity of chemiluminescent light by the CNT photodetector.

5.2.2 On-chip optical sensing through photovoltaic-polymer coated CNTs

To achieve the on-chip signal sensing, the self-assembled carbon nanotube was coated with a photovoltaic polymer. Figure 5.2 shows a schematic drawing for the principle of light detection by the photovoltaic-polymer coated CNT. The photovoltaic

polymer of Poly(m-phenylenevinylene-co-2,5-dioctoxy-p-phenylenevinylene) (PmPV) produces electric dipoles under the incident light. Because a valence band of the PmPV is aligned with CNT, the holes in the produced electric dipoles are injected into the carbon nanotube, leaving the electrons in the vicinity of CNT [99]. As a result, the electric

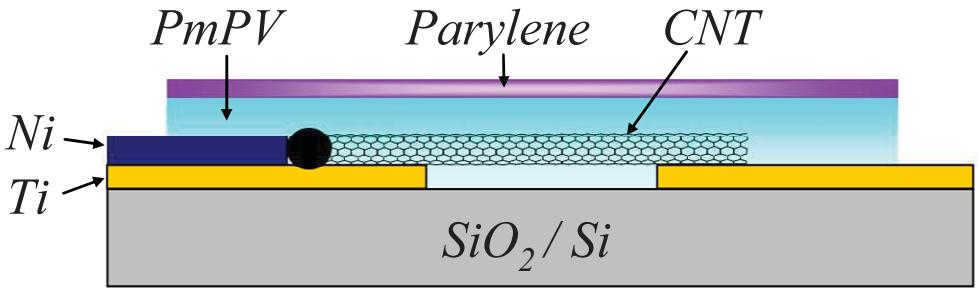

(a)

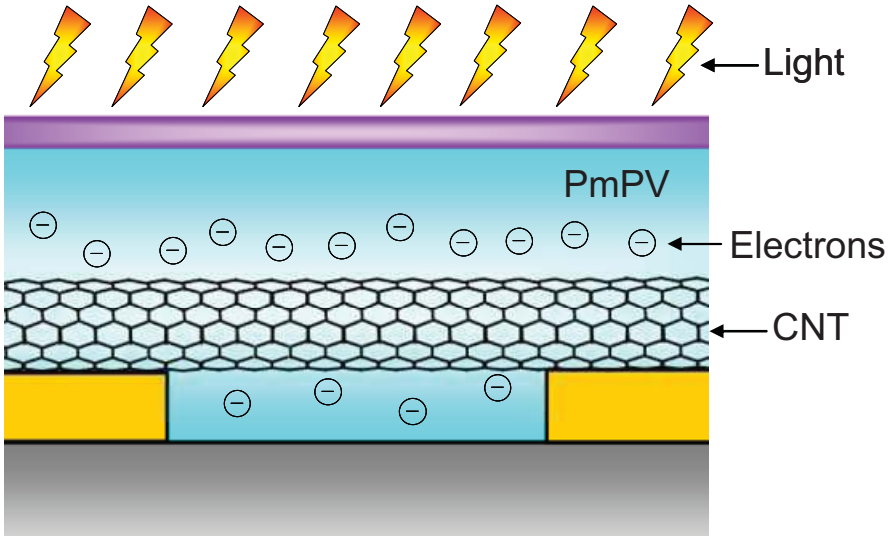

(b)

Figure 5.2 (a) Conceptual picture of CNT photodetector insulated with parylene and (b) Schematic illustration of charge generation in PmPV changing the conductivity of CNT.

charges of the surrounding electrons change the conductivity of CNT between the electrodes, leading the detection of light by measuring the conductivity of CNT. Additionally, the UV-VIS spectra of PmPV show the peak absorption at a wavelength of 450 nm. This specific absorption of wavelength is well matched with a wavelength of 430 nm produced by HRP. Thus, the optical response of PmPV-coated CNT leads the highly sensitive detection of biological molecules by chemiluminescent immunoassay.

5.2.3 Parylene insulation

The CNT-assembled electrode with PmPV coating is insulated with parylene to make a highly stable, selective and sensitive device in this work. Parylene has excellent properties such as optical transparency for a wide range of light wavelengths [100], which is very desirable for optical detection by CNT photodetectors. Also, its biocompatible and non-toxic material properties provide an excellent platform for protein immobilization, and thereby the capturing protein immobilized on the Parylene which serves as an intermediate moderator to provide protein-binding surface on the PmPV-coated CNT [101]. Finally, as an insulation layer, the parylene improved long-term stability of the fabricated device and completely prevents the disturbances from the ionic molecules, which greatly enhances the selectivity of CNT biosensors for highly accurate clinical diagnostics [102, 103].

5.3 DESIGN AND FABRICATION

The gap between the electrodes and the self-aligned Ni pattern were fabricated by a controlled undercut and metallization [104]. Utilizing a standard i-line optical

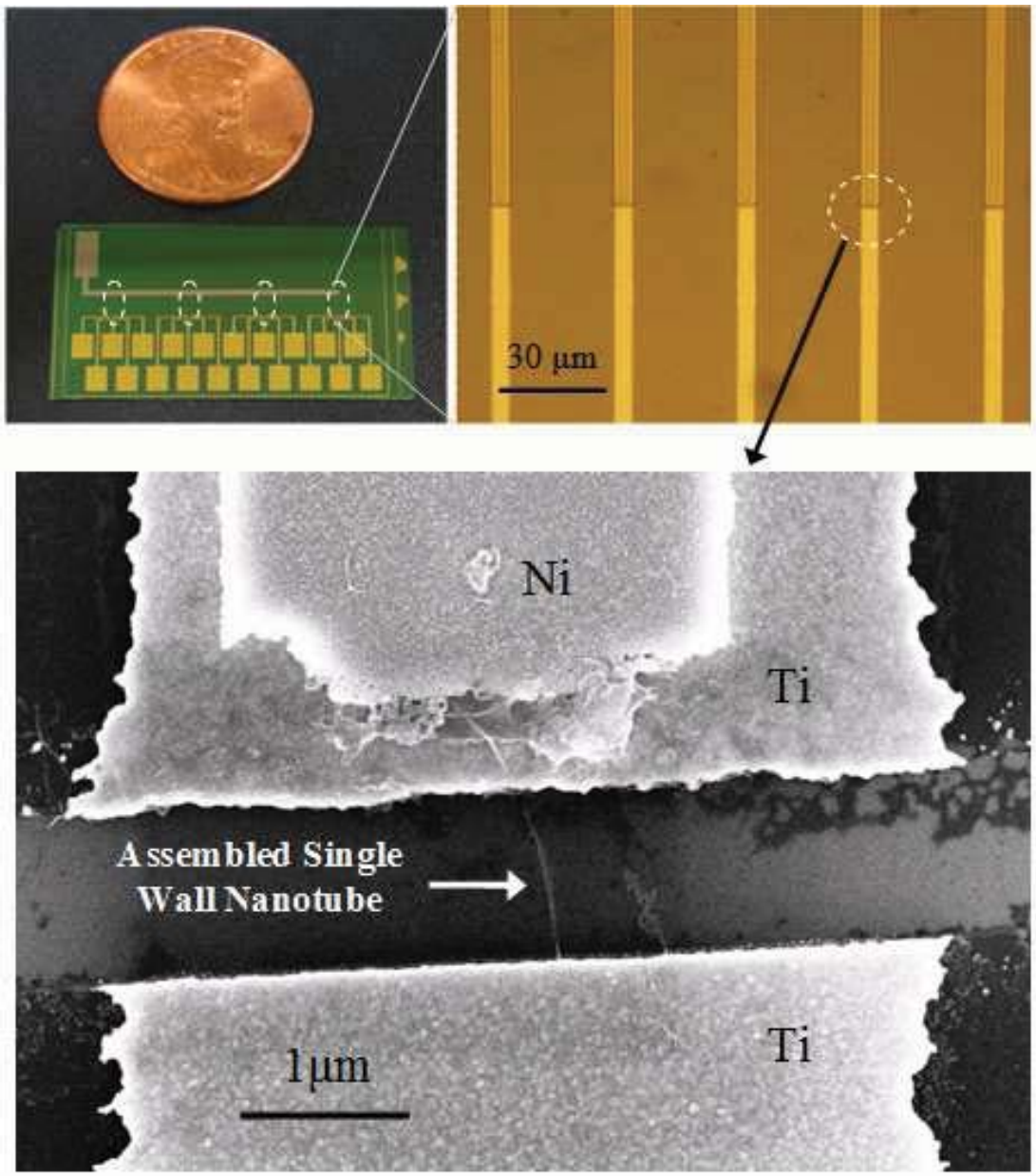

Figure 5.3 Picture of fabricated electrode. Sub-micron gap of electrode with self-aligned Ni pattern was fabricated by optical lithography. The Ni self-aligned electrode with nanogap was applied to self-assemble SWNT by magnetic capturing and fluidic alignment.

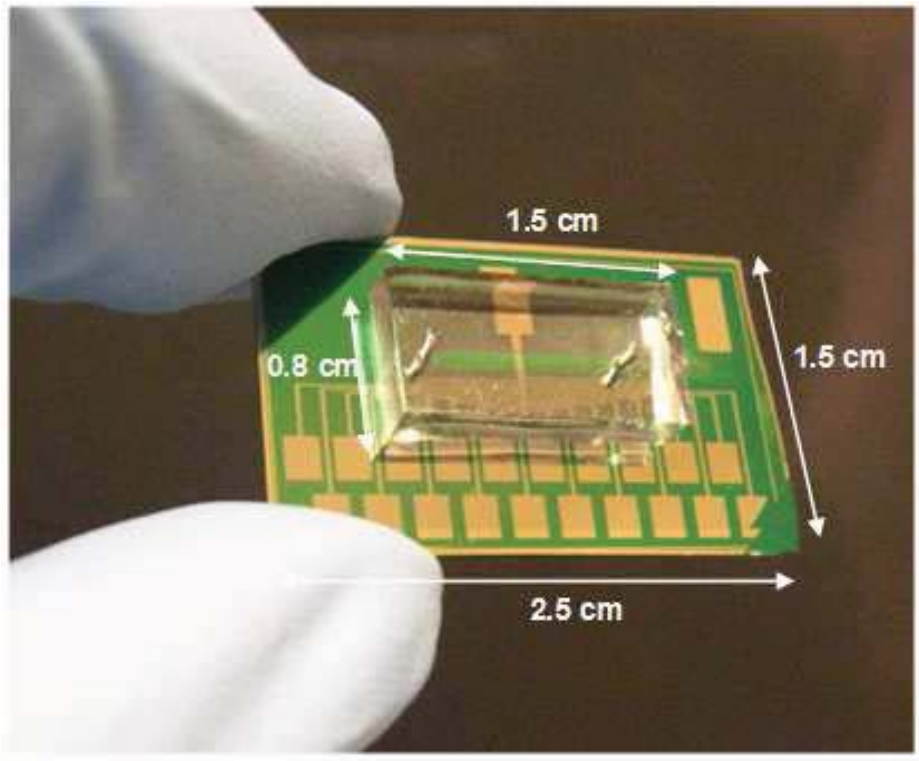

Figure 5.4 Attached PDMS microchannel on CNT photodetector for microfluidic control for the sequential steps of the chemiluminescent immunoassay.

lithography with 365 nm, the precise alignment of the Ni pattern on the electrode and the sub-micron sized gap between electrodes was successfully fabricated without complex alignment procedures. This fabrication technique realized an inexpensive fabrication of nano structures, suitable for a disposable type biosensor. As shown in Figure 5.3, the fabricated device has 20 pairs of electrodes with nano scale gap. Each electrode has a self-aligned Ni pattern to magnetically assemble the SWNT at the edge of Ni pattern.

To fabricate a microchannel with 20 μm thickness, a soft lithography with PDMS was performed using an AZ4620 photoresist. The regular bonding procedure of the oxygen plasma treatment is not processed to avoid the permanent bonding of PDMS to

the SiO_2 substrate. Without permanent bonding, the SWNT solution flowed through the microchannel without any leakage. After the self-assembly of SWNT, the PDMS microchannel was detached from the substrate for subsequent procedures.

The vertical-array type SWNT was purchased from FirstNano (FirstNano Inc., NY). The SWNT has a length of 60 μm and was synthesized by a water-assisted CVD process [74]. The SWNT array was sonicated in a 1 wt% mixture of DI water and Tween 20 for 30 minutes. After the SWNT solution was placed on the magnet for 24 hours to magnetically separate the metal impurities [94], the top half of the SWNT solution was carefully pipetted and utilized for device fabrication.

The SWNT was self-assembled at the Ni pattern by the previously developed method. External magnetic field (0.7 Tesla) was applied to the device while the dispersed SWNT flowed through the devices. Using the induced magnetic force, the Fe catalyst at the end of SWNT was captured at the edge of Ni pattern and aligned parallel to the flow direction. In order to flow the SWNT solution, the PDMS microchannel with a 20 μm height was attached on the device. After flowing 2 μl of the SWNT dispersed solution with a flow velocity of 4.2 mm/sec, 80% of the electrode was assembled with SWNTs.

The SWNT-assembled electrode was coated with a photovoltaic polymer by a drop-casting method [99]. The photovoltaic polymer of PmPV was dissolved in chloroform with a 1wt% concentration. After fully dissolving the PmPV, 1ul volume of PmPV in chloroform was pipetted and then carefully dropped on the assembled SWNT. By evaporating the chloroform at room temperature, the SWNT-assembled electrode was uniformly coated with PmPV.

The PmPV-coated device was insulated with Parylene by vaporized deposition (Parylene Coater). Raw parylene pellet (1.5 g) was deposited to attain a 2 μm thick parylene layer on the PmPV-coated SWNT. The parylene was coated on the whole device with a uniform thickness. After parylene was deposited on the device, oxygen plasma etching (Technique RIE) was performed to etch out the parylene at contact electrodes that were connected to the measuring equipment [105]. Because the photoresist is also etched during the oxygen plasma, a thick photoresist of AZ 4620 was patterned on the device with a thickness of 20 μm to protect the sensing area. After etching out the parylene at contact electrode, the photoresist was rinsed by acetone, methanol and DI water.

5.4 EXPERIMENT DETAILS

5.4.1 Equipment setup

To reduce the loss of chemiluminescent light, on-chip detection was achieved by performing the immunoassay directly on the parylene-insulated CNT photodetector. For this purpose, the microchannel with a 20 μm height was attached as shown in Figure 5.4. The electrical characterization for the CNT coated with the photovoltaic polymer was performed by wiring the contact electrode of the fabricated device to the Picoammeter (Keith 780, Keithly Inc.). For the detection of chemiluminescent light, the wired device was shielded by a black box which blocks external light during optical measurement. Also, a flexible silicone tube was utilized to connect the microchannel to the syringe pump outside of the shielding box. Thus, the equipment for the electrical measurement and the flow control could be implemented outside of the black box. The black box was

covered with the conductive foil, and blocking electrical noise and optical interruptions from external light during the signal measurement.

5.4.2. Chemiluminescent immunoassay

Standard steps of chemiluminescent immunoassay were carried inside the microchannel for the detection of cTnT protein as illustrated in Figure 5.5. To flow the reagents through the attached PDMS microchannel and to prevent the microchannel from leaking, suction pressure was applied to the outlet by applying high pressure inside the microchannel. After connecting the flow tubes to the inlet and outlet of the microchannel, the captured antibody (Abcam, Inc.) was injected into the microchannel and immobilized for 15 minutes. After washing out the microchannel by flowing DI water, PBS (Protein Blocking Solution; Fisher, Inc.) was applied to the microchannel for preventing the non-specific binding of proteins. Following these steps for the functionalization of the microchannel, the sample containing the target antigen was applied and immobilized for 3 minutes. After washing the microchannel with DI water, the HRP conjugated secondary antibody was flowed into the microchannel and stayed for 3 minutes. With the washing of DI water, the black box cover was closed for the optical measurement. Then, the HRP substrate was applied to the microchannel and the chemiluminescent light was detected by measuring the conductivity change of the PmPV coated CNT.

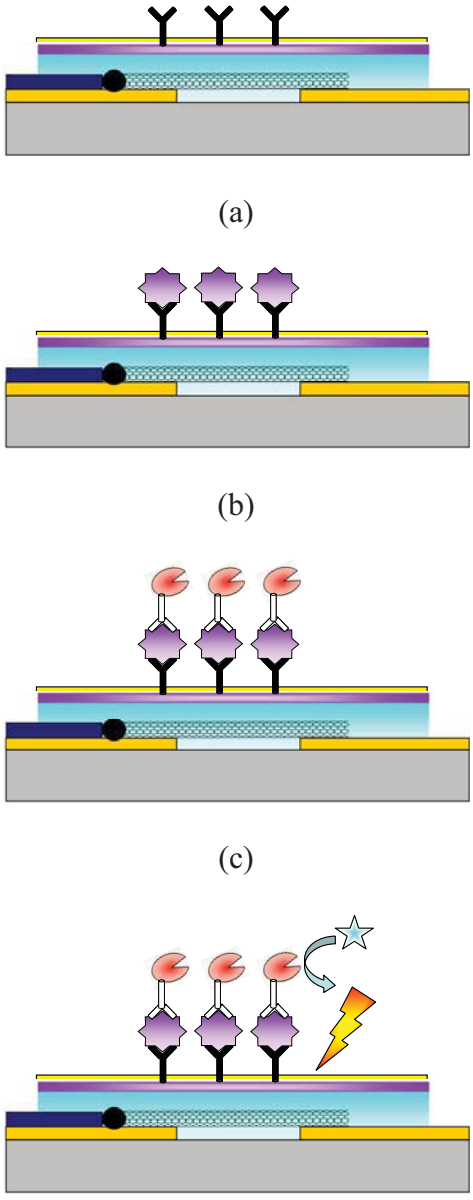

Figure 5.5 Attached PDMS microchannel on CNT photodetector for the sequences of chemiluminescent immunoassay inside the microchannel. (a) Immobilizing 1st antibody on the surface of the parylene coated CNT photodetector, (b) Capturing target protein (cTnT) from the sample, (c) Immobilizing the HRP conjugated 2nd antibody on cTnT, and (d) Chemiluminescent reaction with the substrate solution by the enzyme of HRP.

5.5 RESULTS AND DISCUSSION

5.5.1 Electrical characterization

The electrical characterization is performed for the CNT-assembled electrode and the PmPV-coated electrode without CNTs as plotted in Figure 5.6 (a). The PmPV coated electrode without CNTs did not show any response for the incident light with no changes of conductivity. Also, the conductivity change of bare CNTs without PmPV coatings were not detected for the incident light. These results show that the electrical response for the incident light is mainly attributed to the interaction between PmPV and CNTs. Figure 5.6 (b) shows the electrical response under the incident light, where the light has a 365 nm wavelength and 8.4 mW/cm^2 intensity. The PmPV-coated CNT changed its conductivity in response to the incident light as the generated charges in PmPV surrounded the assembled CNT.

The conductivity change is also measured with respect to the intensity of the incident light as plotted in Figure 5.7 (a). This measurement performed under the UV light with a wavelength of 365 nm. As shown in the results, the increased intensity of the incident light results in a larger change of conductivity for the CNT coated with PmPV. The change of conductivity, which changes depending on light intensity, implies that more charges in the photovoltaic polymer are generated as the intensity of light is increased. In this sense, as the chemiluminescent light is increased according to the concentration of antigen, the conductivity change is also increased from the PmPV-coated CNT. As a result, the implemented CNT optical sensor can be successfully applied to detect the amount of chemiluminescent light.

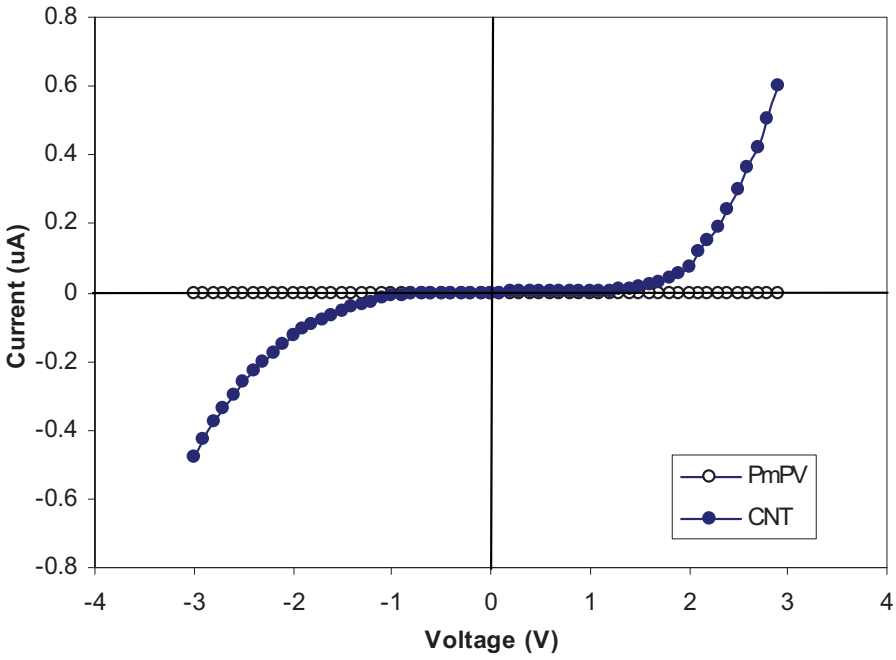

(a)

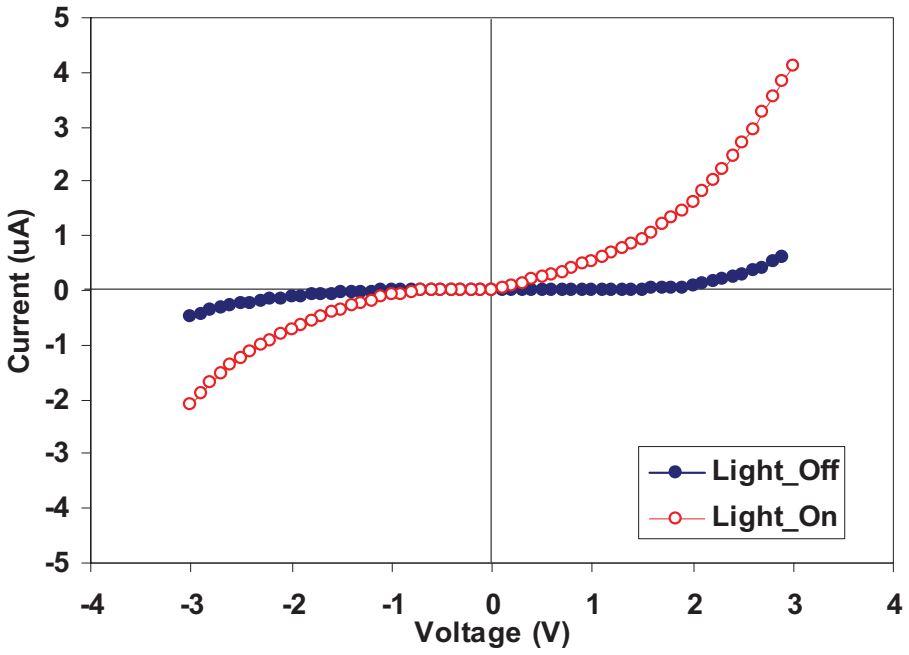

(b)

Figure 5.6 (a) I-V curve from bare CNT and PmPV, (b) Conductivity change for CNT coated with PmPV under the incident light.

Because the intensity of the chemiluminescent light was very weak, an optimization of the electrical condition was required to improve the detection limit for the developed CNT immunosensor. For this purpose, the drain-source voltage (V_{ds}) of the device was characterized to increase the signal change ($\Delta I / I = \frac{(I_{on} - I_{off})}{I_{off}}$) from the device as plotted in Figure 5.7 (b). Previous reports show that the signal from CNT FET sensors could be maximized at the sub-threshold regime [106]. Our characterization result also agrees that the optimized range of drain-source voltage could be chosen in the sub-threshold regime. Additionally, if the current level of output is too low in spite of the largest change of conductivity, it was hard to measure the signal from base noise-level. Considering this signal conditioning, 0.5 V of the drain-source voltage (V_{ds}) was selected to maximize the output signal in our measurements.

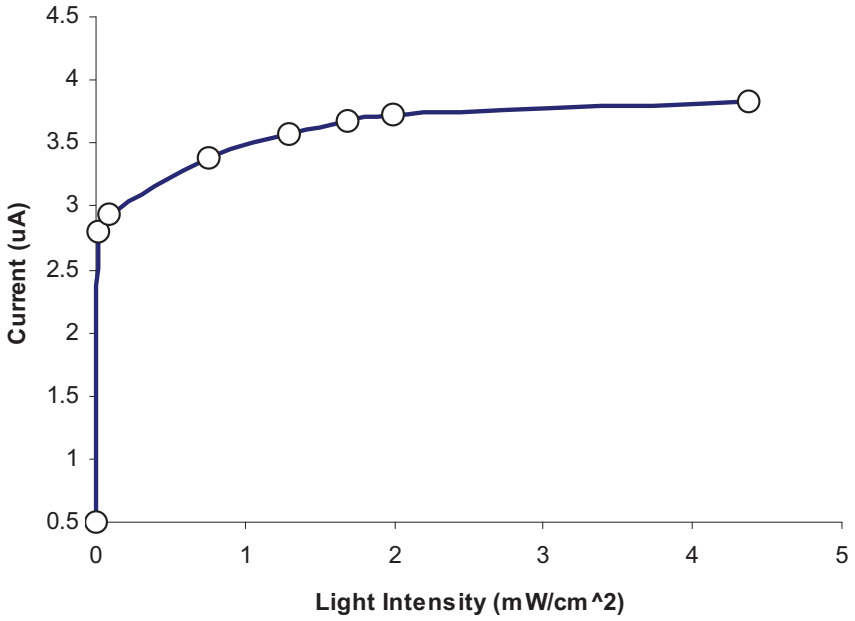

(a)

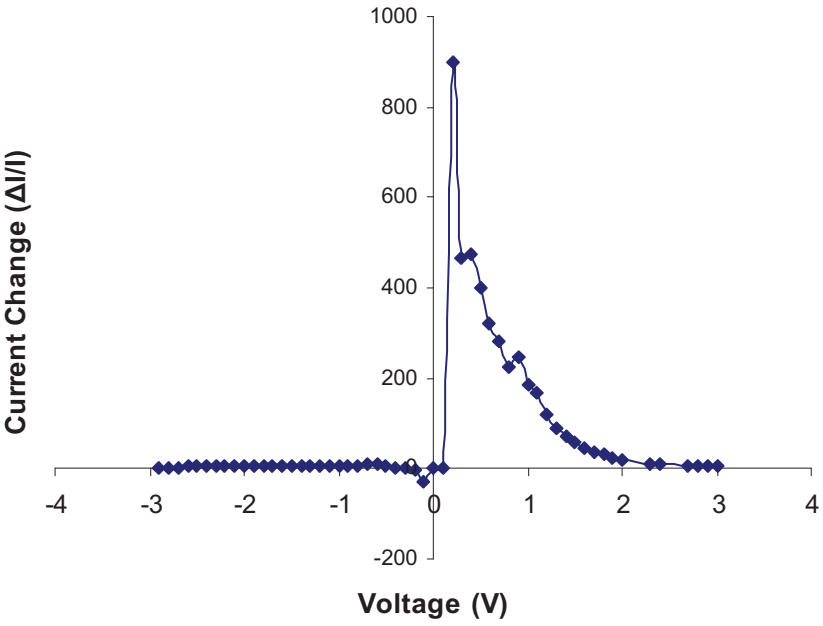

(b)

Figure 5.7 (a) Drain-source current change according to the intensity of incident light and (b) Characterization of V_{ds} for maximum output.

5.5.2 Chemiluminescent light detection

Figure 5.8 shows the conductivity change for different concentrations of the target antigen of cTnT. Because cTnT provides the cross-linking site in the procedures of ELISA, the intensity of chemiluminescent light by HRP is proportional to the concentration of cTnT. In this experiment, cTnT with a concentration of 12 pg/ml is detected by the CNT photodetector. The limit of detection achieved by this on-chip detection is two orders of magnitude lower than the one by the off-chip detection, which was a standard setup for current detection using chemiluminescent immunoassay, measuring the optical signal outside the chip. Compared with the result from the off-chip

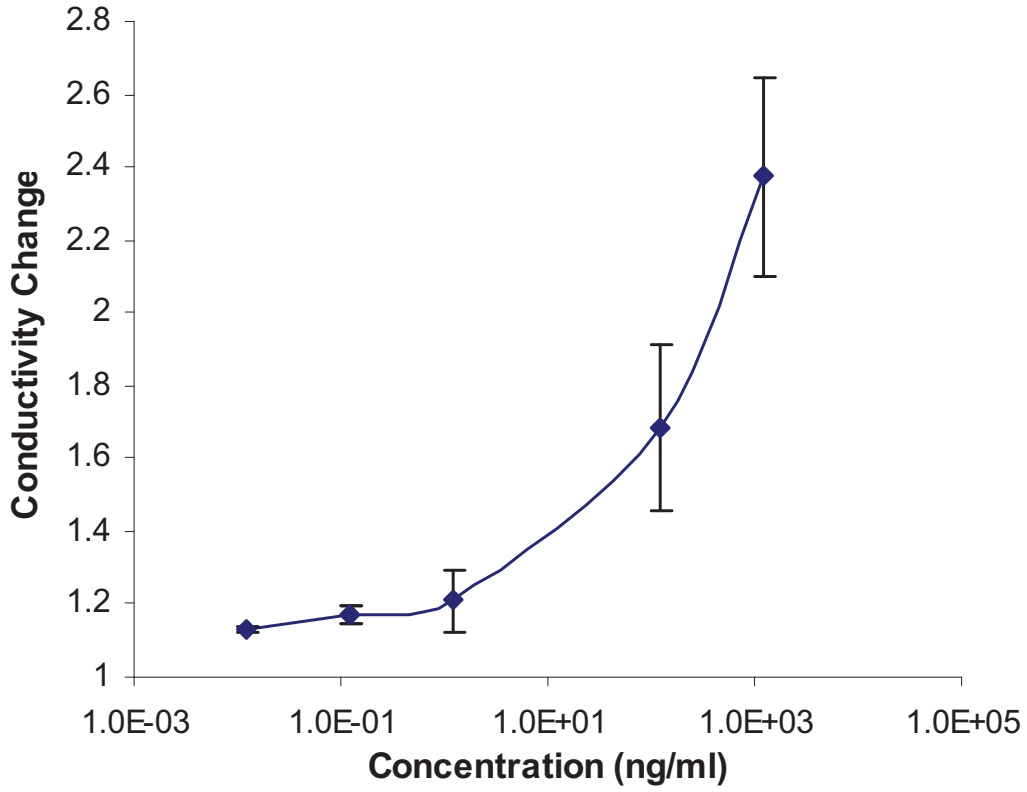

Figure 5.8 Conductivity change of photovoltaic polymer coated SWNT according to the concentration of cTnT

detection, this high performance was attributed to the direct on-chip detection of chemiluminescent light, which minimized the loss of light by scattering through the substrate in case of the off-chip detection. For this on-chip detection, a thin film of transparent parylene was utilized to enable the reaction of chemiluminescence directly above the CNT photodetector. Furthermore, the parylene film successfully blocked the effect of charges in the sample solution, achieving a stable signal during the electrical measurement.

The sensitivity achieved in this optical immunosensor also resulted from the superior functionality of the CNT coated with PmPV. Since all the atoms of CNT make direct contact with the surrounding photovoltaic polymer, a highly sensitive response to the optical signal is accomplished from the generation of negative charges in PmPV. Additionally, the matched optical spectra between PmPV and chemiluminescent light reduce the interruption of external light and maximize the signal change for the chemiluminescent light by HRP.

5.6 CONCLUSION

In this work, a highly sensitive and selective CNT biosensor was developed using the photovoltaic-polymer coated CNT and successfully detected 12 pg/ml of cTnT. The developed optical immunosensor was developed for clinical diagnosis at low cost. In spite of this inexpensive method of fabrication, superior functionality was achieved utilizing CNTs. Also, the fabricated device was electrically insulated by the Parylene, which greatly enhanced the selectivity of the CNT-based biosensor and provided an excellent platform for protein immunoassay. Furthermore, since the CNT photodetector

was directly contacted to the site of chemiluminescent assay, the loss of optical signal was extremely low while scattering through the substrate. As a result, this biosensor can be applied to low-cost POCT devices, achieving highly specific and sensitive optical detection.

CHAPTER 6

CONCLUSIONS

6.1 Summary of Research

In this work, a new mass-producible nanofabrication process for nanodevices using self-assembled CNTs has been proposed, designed, fabricated and successfully characterized; additionally, the process has been applied for the realization of a functional optical nanobiosensor (i.e., photovoltaic immunosensor) as a demonstration vehicle. For this purpose, first, a new method for the self-assembly of CNTs was proposed and fully characterized. Second, a new nano-scale alignment and gap fabrication by optical lithography was developed and characterized for the electrodes to assemble CNTs. Finally, a new photovoltaic nanobiosensor was developed and characterized as an optical immunosensor for detecting a cardiac biomarker (cTnT) with a concentration of 12 pg/ml.

A new method for precisely assembling CNTs at a target position used the specific location of an Fe catalyst. Because the Fe catalyst was located at one end of each CNT after CVD synthesis, individual CNTs could be magnetically captured using magnetic forces produced on the ferromagnetic Fe. Then, the surrounding flow controlling the captured CNT was aligned parallel to the flow direction by fluidic shear force. To optimize the conditions of this magnetic and fluidic assembly of CNTs, a theoretical analysis was performed with the simulation softwares of MagNet and CFD-ACE+. For the experimental characterization, the number of assembled CNTs at Ni patterns was counted in terms of the various flow velocities and the different sizes of Ni patterns. Through these characterizations, the simulation results were compared with the experimental results, showing a good agreement. Electrical analysis was also performed for the assembled CNTs. In consistence with previous works, the assembled MWNTs showed a metallic property with a stable ohmic contact to the metal electrode. For the

assembled SWNT, a non-linear I-V response was measured from a schottky junction between the SWNT and the electrode, which showed that the assembled SWNT had a semiconducting property.

For this assembly method, Ni was precisely patterned on the Au/Ti electrode to magnetically capture the individual CNTs. Furthermore, the gap between electrodes needs to be on a nano scale, because the average length of CNTs is easily reduced to a sub-micron range while the CNT array is dispersed in a solution by sonication. The multilayer process of E-beam lithography was utilized to fabricate the Ni aligned Au/Ti electrode. However, it took a long time with complex alignment steps. To overcome the difficulty of electrode fabrication for CNT assembly, a new fabrication technique was developed for the precise alignment of Ni and the patterning of nanogap electrodes with a low-cost process. With this suggested method, the nano-scale alignment and patterning was easily achieved by a standard optical lithography.

The principle for this technique utilized a generated undercut during isotropic wet-etching, followed by a directional deposition of the subsequent metal layer. This procedure produced a nanoscale gap between the undercut etched metal layer and the secondly deposited metal layer. Through this simple approach a nano-scale gap and alignment was successfully achieved without any expensive procedures. The generation of an undercut according to the etching time was carefully monitored to control the gap between electrodes. The fabricated electrodes were successfully developed and characterized and then applied to the assembly of semiconducting and metallic SWNTs.

Then, the SWNT-assembled device was applied for the on-chip optical immunosensor. Because all of the atoms in the SWNT were exposed to the surrounding

environment, CNT biosensors were realized with an extremely high sensitivity. However, charging molecules such as ions and non-specifically bound proteins also affect the electrical properties of CNTs. So, there has been a great demand for the improvement of the selectivity of CNT sensors to apply to clinical diagnostics.

In order to achieve these desires, the CNT biosensor was implemented by optically detecting light from target proteins. Thus, the optical sensor was developed by coating the SWNT with a photovoltaic polymer. When the SWNT is coated with the photovoltaic polymer PmPV, the SWNT changes its conductivity under the incident light because of the charge generation in PmPV. After the implementation of the CNT optical sensor, parylene was deposited on the whole device for high selectivity. The biocompatibility of parylene also was helpful for capturing proteins to be immobilized on the CNT optical sensor. After attaching the PDMS microchannel on the parylene insulated device, a chemiluminescent immunoassay was performed inside the microchannel. Because the thin film of the parylene had excellent optical transparency, the light signal generated from chemiluminescent immunoassay was fully transmitted to the CNT optical sensor. Thus, the target protein was selectively detected during the immunoassay and the light signal was sensitively measured by the CNT optical sensor. With the CNT optical immunosensor, 12 pg/ml of cTnT was successfully detected, showing the highly selective and sensitive performance of fabricated device.

In conclusion, novel techniques for practically implementing the CNT-assembled device have been proposed and fully explored in this research. In a mass-producible manner, CNTs were self-assembled on the functional nanogap electrode by the developed techniques. As an application of this CNT biosensor, a highly selective and sensitive

optical immunosensor was realized on the functional CNT-device to detect the cardiac biomarker cTnT.

6.2 Research Contributions

The major contribution of this research is its introduction and demonstration of a mass-producible, self-assembled CNT method for CNT-based nanodevices. To the best of my knowledge, this is the first time that the specific location of the Fe catalyst has been used as a control point to assemble CNTs. Also, the self-assembly approach of this technique enables the massive integration of CNTs precisely at the target position, leading to the exploitation of the full functionality of the pristine CNT without an external power connection for the assembly.

Additionally, this research suggests a mass-producible technique for the functional nanogap electrode. The novel fabrication of the self-aligned nanogap electrode is fully processed by standard optical lithography without any delicate alignment procedures, which is highly desirable for the mass-production of nano-devices. Also, the fabrication is fully processed by inexpensive procedures with basic lithographic equipment, achieving a low-cost production of functional nano-devices.

Another innovative contribution made by this study is the proposal and realization of a new mechanism for detecting biological species by the CNT sensor. To overcome the major issue of selectivity in CNT biosensors, an on-chip chemiluminescent immunoassay was performed on the parylene-insulated CNT optical sensor. Due to the parylene insulation, the noise from ions and unwanted proteins were perfectly prevented

in this detection scheme. As a result, high selectivity as well as sensitivity was attained in the developed CNT biosensor.

6.3 Suggestions for Future Work

A low-cost fabrication of a highly selective and sensitive CNT immunosensor has been investigated in this work. The research is scoped from the basic step of CNT assembly to the final application of a functional biosensor. However, there are several tasks still desired as a future work.

First, the process for the CNT assembly should be scaled up to the wafer-level production of CNT-assembled devices. In our assembly procedure, a PDMS microchannel was utilized to precisely control the flow rate and volume of the CNT solution. To achieve wafer-level assembly of CNTs, macro-scale flow control needs to be utilized under the strong external magnetic field.

Second, the self-aligned multilayer nanogap electrode can be applied to assemble the other nano-materials such as nano particles and nano wires. These materials can be modified to have Fe or Ni at one end as a catalyst during their growing process. In this case, these nano-materials can also be assembled on the developed functional nanogap electrode with the same procedures developed in this work.

Third, the CNT optical biosensor should be improved further, in order to minimize the complex procedures of immunoassay by smart microfluidic networks. There are various microfluidic components and techniques available to automatically control the reagents in a microchannel. For this reason, the sensitive and selective nano-biosensor developed in this work should be further researched, in order to be combined

with microfluidic technologies. This future work would develop rapid and precise clinical diagnostics on a handheld device.

Finally, the developed techniques to assemble CNTs between the electrodes can be expanded to implement the device assembled with various types of nano-material. Nanotechnology has been researched intensively to implement a functional device with high performance and low cost. However, only the proof concept and its potentials have been reported. The research in this work can contribute to developing a mass-producible technique for the assembly of nano-materials to make a practical device. Also, the CNT-assembled device can be applied to implement various functional devices utilizing the superior properties of CNT.

7. REFERENCES

[1] A. P. Graham, G. S. Duesberg, W. Hoenlein, F. Kreupl, M. Liebau, R. Martin, B. Rajasekharan, W. Pamler, R. Seidel, W. Steinhoegl and E. Unger, "How do carbon nanotubes fit into the semiconductor roadmap?" *Applied Physics A: Materials Science and Processing,* vol. 80, pp. 1141-1151, 2005.

[2] W. Hoenlein, F. Kreupl, G. S. Duesberg, A. P. Graham, M. Liebau, R. Seidel and E. Unger, "Carbon nanotubes for microelectronics: Status and future prospects," *Materials Science and Engineering C,* vol. 23, pp. 663-669, 2003.

[3] J. W. G. Wildöer, L. C. Venema, A. G. Rinzler, R. E. Smalley and C. Dekker, "Electronic structure of atomically resolved carbon nanotubes," *Nature,* vol. 391, pp. 59-62, 1998.

[4] M. -. Yu, B. S. Files, S. Arepalli and R. S. Ruoff, "Tensile loading of ropes of single wall carbon nanotubes and their mechanical properties," *Phys. Rev. Lett.,* vol. 84, pp. 5552-5555, 2000.

[5] D. A. Walters, L. M. Ericson, M. J. Casavant, J. Liu, D. T. Colbert, K. A. Smith and R. E. Smalley, "Elastic strain of freely suspended single-wall carbon nanotube ropes," *Appl. Phys. Lett.,* vol. 74, pp. 3803-3805, 1999.

[6] M. -. Yu, O. Lourie, M. J. Dyer, K. Moloni, T. F. Kelly and R. S. Ruoff, "Strength and breaking mechanism of multiwalled carbon nanotubes under tensile load," *Science,* vol. 287, pp. 637-640, 2000.

[7] M. S. Dresselhaus, G. Dresselhaus and R. Saito, "Physical Properties of Carbon Nanotubes," *Phil. Trans. R. Soc. Lond. A,* vol. 362, pp. 2065, 2002.

[8] C. T. White and T. N. Todorov, "Carbon nanotubes as long ballistic conductors," *Nature,* vol. 393, pp. 240-241, 1998.

[9] A. Javey, J. Guo, Q. Wang, M. Lundstrom and H. Dai, "Ballistic carbon nanotube field-effect transistors," *Nature,* vol. 424, pp. 654-657; 654, 08-07. 2003.

[10] P. L. McEuen, M. S. Fuhrer and H. Park, "Single-walled carbon nanotube electronics," *IEEE Transactions on Nanotechnology,* vol. 1, pp. 78-84, 2002.

[11] B. Q. Wei, R. Vajtai and P. M. Ajayan, "Reliability and current carrying capacity of carbon nanotubes," *App. Phy. Lett.,* vol. 79, pp. 1172-1174, August 20. 2001.

[12] Z. Yao, C. L. Kane and C. Dekker, "High-field electrical transport in single-wall carbon nanotubes," *Phys. Rev. Lett.,* vol. 84, 2000.

[13] C. Rutherglen, D. Jain and P. Burke, "Nanotube electronics for radio frequency applications," *Nature Nanotechnology,* vol. 4, pp. 811-819, 2009.

[14] S. Li, Z. Yu, S. -. Yen, W. C. Tang and P. J. Burke, "Carbon nanotube transistor operation at 2.6 GHz," *Nano Letters,* vol. 4, pp. 753-756, 2004.

[15] S. N. Kim, J. F. Rusling and F. Papadimitrakopoulos, "Carbon nanotubes for electronic and electrochemical detection of biomolecules," *Adv Mater,* vol. 19, pp. 3214-3228, 2007.

[16] D. R. Kauffman and A. Star, "Carbon nanotube gas and vapor sensors," *Angewandte Chemie - International Edition,* vol. 47, pp. 6550-6570, 2008.

[17] G. Gruner, "Carbon nanotube transistors for biosensing applications," *Analytical and Bioanalytical Chemistry,* vol. 384, pp. 322-335, 2006.

[18] B. Panchapakesan, G. Cesarone, S. Liu, K. Teker and E. Wickstrom, "Single-wall carbon nanotubes with adsorbed antibodies detect live breast cancer cells," *Nanobiotechnology,* vol. 1, pp. 353-360, 2005.

[19] R. J. Chen, S. Bangsaruntip, K. A. Drouvalakis, N. Wong Shi Kam, M. Shim, Y. Li, W. Kim, P. J. Utz and H. Dai, "Noncovalent functionalization of carbon nanotubes for

highly specific electronic biosensors," *Proc. Natl. Acad. Sci. U. S. A.,* vol. 100, pp. 4984-4989, 2003.

[20] K. Bradley, M. Briman, A. Star and G. Gruner, "Charge Transfer from Adsorbed Proteins," *Nano Letters,* vol. 4, pp. 253-256, 2004.

[21] A. Star, E. Tu, J. Niemann, J. -. P. Gabriel, C. S. Joiner and C. Valcke, "Label-free detection of DNA hybridization using carbon nanotube network field-effect transistors," *Proc. Natl. Acad. Sci. U. S. A.,* vol. 103, pp. 921-926, 2006.

[22] B. L. Allen, P. D. Kichambare and A. Star, "Carbon nanotube field-effect-transistor-based biosensors," *Adv Mater,* vol. 19, pp. 1439-1451, 2007.

[23] S. G. Rao, L. Huang, W. Setyawan and S. Hong, "Large-scale assembly of carbon nanotubes," *Nature,* vol. 425, pp. 36-37, 2003.

[24] C. Klinke, J. B. Hannon, A. Afzali and P. Avouris, "Field-effect transistors assembled from functionalized carbon nanotubes," *Nano Letters,* vol. 6, pp. 906-910, 2006.

[25] G. S. Tulevski, J. Hannon, A. Afzali, Z. Chen, P. Avouris and C. R. Kagan, "Chemically assisted directed assembly of carbon nanotubes for the fabrication of large-scale device arrays," *J. Am. Chem. Soc.,* vol. 129, pp. 11964-11968, 2007.

[26] D. P. Long, J. L. Lazorcik and R. Shashidhar, "Magnetically directed self-assembly of carbon nanotube devices," *Adv Mater,* vol. 16, pp. 814-819, 2004.

[27] S. Niyogi, C. Hangarter, R. M. Thamankar, Y. -. Chiang, R. Kawakami, N. V. Myung and R. C. Haddon, "Magnetically assembled multiwalled carbon nanotubes on ferromagnetic contacts," *J Phys Chem B,* vol. 108, pp. 19818-19824, 2004.

[28] Y. Y. Wei and G. Eres, "Directed assembly of carbon nanotube electronic circuits," *Appl. Phys. Lett.,* vol. 76, pp. 3759-3761, 2000.

[29] Y. -. Tseng, K. Phoa, D. Carlton and J. Bokor, "Effect of diameter variation in a large set of carbon nanotube transistors," *Nano Letters,* vol. 6, pp. 1364-1368, 2006.

[30] N. R. Franklin, Q. Wang, T. W. Tombler, A. Javey, M. Shim and H. Dai, "Integration of suspended carbon nanotube arrays into electronic devices and electromechanical systems," *Appl. Phys. Lett.,* vol. 81, pp. 913, 2002.

[31] J. Chung, K. -. Lee, J. Lee and R. S. Ruoff, "Toward Large-Scale Integration of Carbon Nanotubes," *Langmuir,* vol. 20, pp. 3011-3017, 2004.

[32] R. Krupke, F. Hennrich, H. B. Weber, M. M. Kappes and H. v. Löhneysen, "Simultaneous deposition of metallic bundles of single-walled carbon nanotubes using ac-dielectrophoresis," *Nano Lett.,* vol. 3, pp. 1019-1023, 2003.

[33] A. Vijayaraghavan, S. Blatt, D. Weissenberger, M. Oron-Carl, F. Hennrich, D. Gerthsen, H. Hahn and R. Krupke, "Ultra-large-scale directed assembly of single-walled carbon nanotube devices," *Nano Letters,* vol. 7, pp. 1556-1560, 2007.

[34] R. Krupke, F. Hennrich, H. V. Löhneysen and M. M. Kappes, "Separation of metallic from semiconducting single-walled carbon nanotubes," *Science,* vol. 301, pp. 344-347, 2003.

[35] D. H. Shin, J. E. Kim, H. C. Shim, J. W. Song, J. H. Yoon, J. Kim, S. Jeong, J. Kang, S. Baik and C. S. Han, "Continuous extraction of highly pure metallic single-walled carbon nanotubes in a microfluidic channel," *Nano Lett.,* vol. 8, pp. 4380-4385, 2008.

[36] M. Zheng, A. Jagota, E. D. Semke, B. A. Diner, R. S. McLean, S. R. Lustig, R. E. Richardson and N. G. Tassi, "DNA-assisted dispersion and separation of carbon nanotubes," *Nature Materials,* vol. 2, pp. 338-342, 2003.

[37] M. F. Islam, E. Rojas, D. M. Bergey, A. T. Johnson and A. G. Yodh, "High weight fraction surfactant solubilization of single-wall carbon nanotubes in water," *Nano Lett.,* vol. 3, pp. 269-273, 2003.

[38] J. I. Paredes and M. Burghard, "Dispersions of individual single-walled carbon nanotubes of high length," *Langmuir,* vol. 20, pp. 5149-5152, 2004.

[39] S. J. Tans, A. R. M. Verschueren and C. Dekker, "Room-temperature transistor based on a single carbon nanotube," *Nature,* vol. 393, pp. 49-52, 1998.

[40] A. Bachtold, P. Hadley, T. Nakanishi and C. Dekker, "Logic circuits with carbon nanotube transistors," *Science,* vol. 294, pp. 1317-1320, 2001.

[41] Y. -. Lin, J. Appenzeller and P. Avouris, "Ambipolar-to-unipolar conversion of carbon nanotube transistors by gate structure engineering," *Nano Letters,* vol. 4, pp. 947-950, 2004.

[42] Z. Chen, J. Appenzeller, J. Knoch, Y. -. Lin and P. Avouris, "The role of metal-nanotube contact in the performance of carbon nanotube field-effect transistors," *Nano Letters,* vol. 5, pp. 1497-1502, 2005.

[43] P. Van Gerwen, W. Laureyn, W. Laureys, G. Huyberechts, M. Op De Beeck, K. Baert, J. Suls, W. Sansen, P. Jacobs, L. Hermans and R. Mertens, "Nanoscaled interdigitated electrode arrays for biochemical sensors," *Sensors and Actuators, B: Chemical,* vol. 49, pp. 73-80, 1998.

[44] A. E. Cohen and R. R. Kunz, "Large-area interdigitated array microelectrodes for electrochemical sensing," *Sensors and Actuators, B: Chemical,* vol. 62, pp. 23-29, 2000.

[45] J. P. Silverman, "X-ray lithography: Status, challenges, and outlook for 0.13 μm," *Journal of Vacuum Science and Technology B: Microelectronics and Nanometer Structures,* vol. 15, pp. 2117-2124, 1997.

[46] B. D. Gates, Q. Xu, J. C. Love, D. B. Wolfe and G. M. Whitesides, "Unconventional nanofabrication," *Annual Review of Materials Research,* vol. 34, pp. 339-372, 2004.

[47] S. Y. Chou, P. R. Krauss and P. J. Renstrom, "Imprint lithography with 25-nanometer resolution," *Science,* vol. 272, pp. 85-87, 1996.

[48] T. Matsuo and M. Esashi, "Methods of isfet fabrication," *Sensors and Actuators,* vol. 1, pp. 77-96, 1981.

[49] P. L. H. M. Cobben, R. J. M. Egberink, J. G. Borner, P. Bergveld, W. Verboom and D. N. Reinhoudt, "Transduction of selective recognition of heavy metal ions by chemically modified field effect transistors (CHEMFETs)," *J. Am. Chem. Soc.,* vol. 114, pp. 10573-10582, 1992.

[50] J. Bausells, J. Carrabina, A. Errachid and A. Merlos, "Ion-sensitive field-effect transistors fabricated in a commercial CMOS technology," *Sensors and Actuators, B: Chemical,* vol. 57, pp. 56-62, 1999.

[51] D. M. Wilson, S. Hoyt, J. Janata, K. Booksh and L. Obando, "Chemical sensors for portable, handheld field instruments," *IEEE Sensors Journal,* vol. 1, pp. 256-274, 2001.

[52] A. K. Wanekaya, W. Chen, N. V. Myung and A. Mulchandani, "Nanowire-based electrochemical biosensors," *Electroanalysis,* vol. 18, pp. 533-550, 2006.

[53] F. Patolsky, G. Zheng and C. M. Lieber, "Nanowire-based biosensors," *Anal. Chem.,* vol. 78, pp. 4260-4269, 2006.

[54] J. Hu, T. W. Odom and C. M. Lieber, "Chemistry and physics in one dimension: Synthesis and properties of nanowires and nanotubes," *Acc. Chem. Res.,* vol. 32, pp. 435-445, 1999.

[55] C. Li, M. Curreli, H. Lin, B. Lei, F. N. Ishikawa, R. Datar, R. J. Cote, M. E. Thompson and C. Zhou, "Complementary detection of prostate-specific antigen using In 2O3 nanowires and carbon nanotubes," *J. Am. Chem. Soc.,* vol. 127, pp. 12484-12485, 2005.

[56] P. G. Collins, K. Bradley, M. Ishigami and A. Zettl, "Extreme oxygen sensitivity of electronic properties of carbon nanotubes," *Science,* vol. 287, pp. 1801-1804, 2000.

[57] J. Kong, N. R. Franklin, C. Zhou, M. G. Chapline, S. Peng, K. Cho and H. Dai, "Nanotube molecular wires as chemical sensors," *Science,* vol. 287, pp. 622-625, 2000.

[58] P. Avouris, M. Freitag and V. Perebeinos, "Carbon-nanotube photonics and optoelectronics," *Nature Photonics,* vol. 2, pp. 341-350, 2008.

[59] X. Tang, S. Bansaruntip, N. Nakayama, E. Yenilmez, Y. -. Chang and Q. Wang, "Carbon nanotube DNA sensor and sensing mechanism," *Nano Letters,* vol. 6, pp. 1632-1636, 2006.

[60] A. Star, J. -. P. Gabriel, K. Bradley and G. Grüner, "Electronic detection of specific protein binding using nanotube FET devices," *Nano Letters,* vol. 3, pp. 459-463, 2003.

[61] M. Shim, N. W. S. Kam, R. J. Chen, Y. Li and H. Dai, "Functionalization of Carbon Nanotubes for Biocompatibility and Biomolecular Recognition," *Nano Letters,* vol. 2, pp. 285-288, 2002.

[62] J. P. Kim, B. Y. Lee, J. Lee, S. Hong and S. J. Sim, "Enhancement of sensitivity and specificity by surface modification of carbon nanotubes in diagnosis of prostate cancer based on carbon nanotube field effect transistors," *Biosensors and Bioelectronics,* vol. 24, pp. 3372-3378, 2009.

[63] S. Iijima, "Helical microtubules of graphitic carbon," *Nature,* vol. 354, pp. 56-58, 1991.

[64] H. Dai, "Carbon nanotubes: Opportunities and challenges," *Surf. Sci.,* vol. 500, pp. 218-241, 2002.

[65] L. Dai, A. Patil, X. Gong, Z. Guo, L. Liu, Y. Liu and D. Zhu, "Aligned Nanotubes," *Chem. Phys. Chem.,* vol. 4, pp. 1150-1169; 1150, 2003.

[66] Y. Yan, M. B. Chan-Park and Q. Zhang, "Advances in carbon-nanotube assembly," *Small,* vol. 3, pp. 24-42, 2007.

[67] M. Lee, K. Y. Baik, M. Noah, Y. -. Kwon, J. -. Lee and S. Hong, "Nanowire and nanotube transistors for lab-on-a-chip applications," *Lab on a Chip - Miniaturisation for Chemistry and Biology,* vol. 9, pp. 2267-2280, 2009.

[68] R. Krupke, F. Hennrich, H. v. Löhneysen and M. M. Kappes, "Separation of metallic from semiconducting single-walled carbon nanotubes," *Science,* vol. 301, pp. 344-347, 2003.

[69] C. Journet, W. K. Maser, P. Bernier, A. Loiseau, M. Lamy de la Chapelle, S. Lefrant, P. Deniard, R. Lee and J. E. Fischer, "Large-scale production of single-walled carbon nanotubes by the electric-arc technique," *Nature,* vol. 388, pp. 756-758, 1997.

[70] Z. F. Ren and Z. P. Huang, "Synthesis of large arrays of well-aligned carbon nanotubes on glass," *Science,* vol. 282, pp. 1105-1107, 1998.

[71] T. W. Ebbesen and P. M. Ajayan, "Large-scale synthesis of carbon nanotubes," *Nature,* vol. 358, pp. 220-222, 1992.

[72] M. Terrones, "Science and Technology of the Twenty-First Century: Synthesis, Properties, and Applications of Carbon Nanotubes," *Annual Review of Materials Research,* vol. 33, pp. 419-501, 2003.

[73] M. D. Lay, J. P. Novak and E. S. Snow, "Simple route to large-scale ordered arrays of liquid-deposited carbon nanotubes," *Nano Letters,* vol. 4, pp. 603-606, 2004.

[74] K. Hata, D. N. Futaba, K. Mizuno, T. Namai, M. Yumura and S. Iijima, "Water-assisted highly efficient synthesis of impurity-free single-walled carbon nanotubes," *Science,* vol. 306, pp. 1362-1364, 2004.

[75] Y. Yun, V. Shanov, Y. Tu, S. Subramaniam and M. J. Schulz, "Growth mechanism of long aligned multiwall carbon nanotube arrays by water-assisted chemical vapor deposition," *J. Phys. Chem. B,* vol. 110, pp. 23920-23925, 2006.

[76] S. R. C. Vivekchand, R. Jayakanth, A. Govindaraj and C. N. R. Rao, "The problem of purifying single-walled carbon nanotubes," *Small,* vol. 1, pp. 920-923, 2005.

[77] L. Thién-Nga, K. Hernadi, E. Ljubovic, S. Garaj and L. Forró, "Mechanical Purification of Single-Walled Carbon Nanotube Bundles from Catalytic Particles," *Nano Letters,* vol. 2, pp. 1349-1352, 2002.

[78] M. F. Islam, E. Rojas, D. M. Bergey, A. T. Johnson and A. G. Yodh, "High weight fraction surfactant solubilization of single-wall carbon nanotubes in water," *Nano Letters,* vol. 3, pp. 269-273, 2003.

[79] V. C. Moore, M. S. Strano, E. H. Haroz, R. H. Hauge, R. E. Smalley, J. Schmidt and Y. Talmon, "Individually Suspended Single-Walled Carbon Nanotubes in Various Surfactants," *Nano Letters,* vol. 3, pp. 1379-1382, 2003.

[80] F. Wakaya, K. Katayama and K. Gamo, "Contact resistance of multiwall carbon nanotubes," *Microelectronic Engineering,* vol. 67-68, pp. 853-857, 2003.

[81] Q. Ngo, D. Petranovic, S. Krishnan, A. M. Cassell, Q. Ye, J. Li, M. Meyyappan and C. Y. Yang, "Electron transport through metal-multiwall carbon nanotube interfaces," *IEEE Transactions on Nanotechnology,* vol. 3, pp. 311-317, 2004.

[82] S. M. Sze, *Semiconductor Devices: Physics and Technology, 2nd Edition.* New York, USA: Wiley, John & Sons, Inc., 2001,

[83] A. K. Gupta and M. Gupta, "Synthesis and surface engineering of iron oxide nanoparticles for biomedical applications," *Biomaterials,* vol. 26, pp. 3995-4021, 2005.

[84] Q. A. Pankhurst, J. Connolly, S. K. Jones and J. Dobson, "Applications of magnetic nanoparticles in biomedicine," *J. Phys. D: Appl. Phys.,* vol. 36, 2003.

[85] R. B. Frankel, R. P. Blakemore and R. S. Wolfe, "Magnetite in freshwater magnetotactic bacteria," *Science,* vol. 203, pp. 1355-1356, 1979.

[86] H. K. Kim, S. H. Hong, S. W. Hwang, J. S. Hwang, D. Ahn, S. Seong and T. H. Park, "Magnetic capture of a single magnetic nanoparticle using nanoelectromagnets," *J. Appl. Phys.,* vol. 98, pp. 1-4, 2005.

[87] R. G. Cox, "The motion of long slender bodies in a viscous fluid. Part 1. General Theory," *J. Fluid Mech.,* vol. 44, pp. 791-810, 1970.

[88] G. K. Batchelor, "Slender-body theory for particles of arbitrary cross-section in Stokes flow," *J. Fluid Mech.,* vol. 44, pp. 419-440, 1970.

[89] K. J. Klabunde, *Nanoscale Materials in Chemistry.* New York, USA: Wiley, John & Sons, Inc., 2001,

[90] M. M. J. Treacy, T. W. Ebbesen and J. M. Gibson, "Exceptionally high Young's modulus observed for individual carbon nanotubes," *Nature,* vol. 381, pp. 678-680, 1996.

[91] J. Kong, N. R. Franklin, C. Zhou, M. G. Chapline, S. Peng, K. Cho and H. Dai, "Nanotube molecular wires as chemical sensors," *Science,* vol. 287, pp. 622-625, 2000.

[92] J. Kong, E. Yenilmez, T. W. Tombler, W. Kim, H. Dai, R. B. Laughlin, L. Liu, C. S. Jayanthi and S. Y. Wu, "Quantum interference and ballistic transmission in nanotube electron waveguides," *Phys. Rev. Lett.,* vol. 87, 2001.

[93] J. Chung and J. Lee, "Nanoscale gap fabrication and integration of carbon nanotubes by micromachining," *Sens Actuators A Phys,* vol. 104, pp. 229-235, 2003.

[94] J. S. Shim, Y. H. Yun, M. J. Rust, J. Do, V. Shanov, M. J. Schulz and C. H. Ahn, "The precise self-assembly of individual carbon nanotubes using magnetic capturing and fluidic alignment," *Nanotechnology,* vol. 20, 2009.

[95] J. C. Love, K. E. Paul and G. M. Whitesides, "Fabrication of nanometer-scale features by controlled isotropic wet chemical etching," *Adv. Mat.,* vol. 13, pp. 604-608, 2001.

[96] M. Datta, "Microfabrication by electrochemical metal removal," *IBM J. Res. Develop.,* vol. 42, pp. 655-669, 1998.

[97] Y. Cui, Q. Wei, H. Park and C. M. Lieber, "Nanowire nanosensors for highly sensitive and selective detection of biological and chemical species," *Science,* vol. 293, pp. 1289-1292, 2001.

[98] G. Zheng, F. Patolsky, Y. Cui, W. U. Wang and C. M. Lieber, "Multiplexed electrical detection of cancer markers with nanowire sensor arrays," *Nat. Biotechnol.,* vol. 23, pp. 1294-1301, 2005.

[99] A. Star, Y. Lu, K. Bradley and G. Grüner, "Nanotube optoelectronic memory devices," *Nano Letters,* vol. 4, pp. 1587-1591, 2004.

[100] Y. S. Jeong, B. Ratier, A. Moliton and L. Guyard, "UV-visible and infrared characterization of poly(p-xylylene) films for waveguide applications and OLED encapsulation," *Synth. Met.,* vol. 127, pp. 189-193, 2002.

[101] T. Y. Chang, V. G. Yadav, S. De Leo, A. Mohedas, B. Rajalingam, C. -. Chen, S. Selvarasah, M. R. Dokmeci and A. Khademhosseini, "Cell and protein compatibility of parylene-C surfaces," *Langmuir,* vol. 23, pp. 11718-11725, 2007.

[102] E. M. Schmidt, "Parylene as an electrode insulator: A review," *Journal of Electrophysiological Techniques,* vol. 10, pp. 19-29, 1983.

[103] G. E. Loeb, M. J. Bak, M. Salcman and E. M. Schmidt, "Parylene as a chronically stable, reproducible microelectrode insulator," *IEEE Transactions on Biomedical Engineering,* vol. 24, pp. 121-128, 1977.

[104] J. S. Shim, Y. -. Yun, W. Cho, V. Shanov, M. J. Schulz and C. H. Ahn, "Self aligned multi-layer electrodes with nano-gap for fluidic and magnetic assembly of carbon nanotubes," *NSTI Nanotech 2009*, pp. 8-11, 2009

[105] E. Meng, P. -. Li and Y. -. Tai, "Plasma removal of Parylene C," *J Micromech Microengineering,* vol. 18, 2008.

[106] I. Heller, J. Mãnnik, S. G. Lemay and C. Dekker, "Optimizing the signal-to-noise ratio for biosensing with carbon nanotube transistors," *Nano Letters,* vol. 9, pp. 377-382, 2009.

-

8. PUBLICATIONS

Journals

[1] **J. S Shim**, Y. Yun, M. J Rust, J. Do, V. Shanov, M. J. Schulz, and C. H. Ahn, "Precise self-assembly of individual carbon nanotube using magnetic capturing and fluidic alignment," Nanotechnology, vol. 20, pp. 325607-325613, 2009.

[2] **J. S. Shim**, Y. Yun, W. Cho, V. Shanov, M. J. Schulz and C. H. Ahn, "Self Aligned Multilayer Electrodes with Nano-Gap for Fluidic and Magnetic Assembly of Carbon Nanotubes," Langmuir, (In review)

[3] **J. S. Shim**, A. W. Browne, S. H. Lee, and C. H. Ahn, "An On-Chip Whole Blood/Plasma Separator With Colloidal Silica Bead-Packed Microchannel On COC Polymer," Biomedical Microdevices, 2010 (Accepted)

[4] [Review] Y. Yun, E. Eteshola, A. Bhattacharya, Z. Dong, **J. S. Shim**, L. Conforti, D. Kim, M. J. Schulz, C. H. Ahn, N. Watts, J. Sankar, and S. Sarin, "Tiny Medicine: Nanomaterial-Based Biosensors," Sensors, 9, pp. 9275-9299, 2009

[5] C. A. Currie, **J. S. Shim**, S. H. Lee, C. Ahn, P. A. Limbach, H. B. Halsall, W. R. Heineman, "Comparing polyelectrolyte multilayer-coated PMMA microfluidic devices and glass microchips for electrophoretic separations," Electrophoresis, 30, pp. 4245-4250, 2009

[6] Z. Zou, A. Jang, E. McKnight, P. Wu, J. Do, **J. S. Shim**, P. L. Bishop, and C. H. Ahn, "An On-Site Heavy Metal Analyzer with Polymer Lab-on-a-Chips for Continuous Sampling and Monitoring," IEEE Sensors Journal, 9, pp. 586-594, 2009.

Conferences

[7] **J. S. Shim**, Andrew W. Browne, and Chong H. Ahn, "An optical immunosensor using carbon nanotube coated with photovoltaic polymer," uTAS 2009, Jeju, Korea, November 1-5, 2009

[8] **J. S. Shim**, Y. Yun, W. Cho, V. Shanov, M. J. Schulz and C. H. Ahn, "Self Aligned Multi-Layer Electrodes with Nano-Gap for Fluidic and Magnetic Assembly of Carbon Nanotubes," Proceedings of NSTI Nanotech 2009, Arlington, TX, May 3-7, 2009

[9] **J. S. Shim**, A. W. Browne, S. H. Lee, and C. H. Ahn, "An On-Chip Whole Blood/Plasma Separator With Colloidal Silica Bead-Packed Microchannel On COC Polymer," uTAS 2008, San Diego, CA, October 12-16, 2008.

[10] **J. S. Shim**, M. J. Rust, and C. H. Ahn, "Interdigitated Array Electrodes with Nano Gaps Using Optical Lithography and Controlled Undercut Method," Arlington, TX, August 18-21, 2008.

[11] **J. S. Shim**, Y. Yun, M. J. Rust, J. Do, V. Shanov, M. J. Schulz, and C. H. Ahn, "High Precision Fluidic Alignment Of Carbon Nanotubes Using Magnetic Attraction On A Metal Catalyst," MEMS 2008, Tucson, AZ, January 13-17, 2008.

[12] **J. Sub Shim**, I. Nikcevic, M. J. Rust, A. A. S. Bhagat, W. R. Heineman, C. J. Seliskar, C. H. Ahn and I. Papautsky, "Simple Passive Micromixer Using Recombinant Multiple Flow Streams," Proc. of SPIE Vol. 6465, 64650Y, (2007).

[13] Y. Park, **J. S. Shim**, S. Park, D. Kwak, H. Ko, T. Song, W. Carr, D. Setiati, J. Buss, and D. Cho, "Feedback control for expanding range and improving linearity of microaccelerometers," 2004 International Conference on Control, Automation and Systems (ICCAS 2004), pp. 1706-1710, Bangkok, Thailand, Aug. 2004.